4

RESULTS AND DISCUSSION

Medicinal plants are crucial in research due to their natural products that can be utilized in the treatment of various diseases, such as diabetes, cancer and infections. Medicinal plants have been used in medicine for a long time and scientists are currently researching them to find safe and effective new medications. Medicinal plants are also crucial in the development of green synthesis of nanoparticles. Being natural, they are most likely to possess fewer side effects than chemical drugs. Research on medicinal plants assists in the integration of traditional knowledge with contemporary science to design improved methods of treatment for health issues (Manisha *et al*., 2025).

Phytochemicals in some plants of natural origin have been more of the focus in diabetes studies because they can aid in the modulation of blood glucose levels. The bioactive phytochemicals can stimulate insulin activity and reduce oxidative stress levels, two of the biggest hurdles in the treatment of diabetes. Plants therapies are easily accessible compared to synthetic drugs and are generally more acceptable. Scientists are, therefore, turning to traditional therapeutic knowledge more and more to identify new and effective therapeutic agents for diabetes based on empirical proof (Balkrishna *et al*., 2024).

Plant-based natural substances are gradually being identified as having the potential to be beneficial in the management of obesity. Some phytochemicals have proved to be beneficial in appetite suppression, lipid metabolism enhancement and blocking inflammation of excess weight. These characteristics are making these substances potential rivals in the creation of less harmful, more natural treatments against weight gain. Present research upholds the fact that treatments from plants can be helpful and gentle to the body and a supplement to conventional antiobesity medications (Alshammaa and Alshammaa, 2024).

Growing evidence for the use of medicinal plants as a safer and effective alternative to conventional drug therapy in diabetes and obesity has been established. In contrast to conventional medicines, which carry the threat of hypoglycemia, gastrointestinal disturbance and liver toxicity, traditional plant medicines act more subtly due to their bioactive

phytochemicals. When used together, these compounds act synergistically to control blood sugar, enhance insulin sensitivity and facilitate weight loss, acting on multiple pathways implicated in these multifactorial diseases. Thus, medicinal plants represent a promising, sustainable and holistic treatment for the management of metabolic disorders with a few side effects (Nair *et al*., 2024).

Boerhavia diffusa L. or Punarnava, is a plant commonly used in traditional healthcare systems due to its versatility for therapeutic applications. Plant leaves, stems and roots are used for medicinal applications. Plant roots are particularly renowned for their activities in ensuring liver function, anti-inflammatory and diuretic effects. Leaves, on the other hand, are renowned for their antioxidant and hypoglycemic activities. The wealth of bioactive compounds such as alkaloids, flavonoids and phenolics, *Boerhavia diffusa* L. was used in the treatment of diseases such as diabetes, obesity, liver disease and water retention (Gour, 2021).

Due to the therapeutic potential of *Boerhavia diffusa* L. the present research work was carried out to thoroughly study its antidiabetic and antiobesity activity using a whole-plant silver nanoparticles ethanolic extract of *Boerhavia diffusa* L. (EBdAgNPs). The experiment included four experimental phases to systematically compare its efficacy and the mechanism involved in its action.

Phase I comprises green synthesis of silver nanoparticles (AgNPs) from ethanolic extract of *Boerhavia diffusa* L. (*B. diffusa*) and their further extensive characterization towards determining their structure and physicochemical properties using a variety of analytical techniques.

Phase II involves the evaluation of *in vitro* antioxidant and antidiabetic activity of synthesized EBdAgNPs. Biochemical assays are used to examine their free radical scavenging activity, inhibitory activity towards enzymatic activity and control over the level of glucose.

Phase III is the *in vivo* antidiabetic and antiobesity efficacy evaluation of EBdAgNPs in albino rats. Biochemical parameters are estimated to assess the therapeutic efficacy of EBdAgNPs.

Phase IV explores the molecular mechanisms of the effects observed by identifying the expression of core metabolic genes, i.e., PPAR-α, PPAR-γ and RBP4, through the use of real-time quantitative PCR (RT-qPCR). The method provides informative data on gene-level changes after EBdAgNPs treatment.

PHASE I

The systematic work schedule diagrammed yields a reproducible and uniform method for phytochemical extraction from *Boerhavia diffusa* L. (*B. diffusa*), a plant that has been widely researched for its therapeutic application. The process began with the systematic harvesting of healthy plant material, which was a critical step that ensured uniformity of the bioactive constituents. The subsequent processing steps, including extensive washing, shade-drying and grinding, increased the stability and shelf life of the plant material while preserving the major phytocompounds. The ethanolic extraction step was particularly important, as ethanol had been reported to be effective in extracting a broad spectrum of phytochemicals, including flavonoids, phenolics and alkaloids, all of which were pivotal to various bioactivities. This extract served as a strong starting material for downstream operations such as the synthesis of nanoparticles and assays associated with antioxidant or antidiabetic activity. It was also noted that earlier studies had reported that the choice of solvent and the use of standardized extraction procedures played a major role in influencing the yield and functionality of the extract obtained, thereby emphasizing the need for methodological uniformity in herbal research. (Maheshwari *et al*., 2025).

4.1 Synthesis and Characterization of EBdAgNPs

4.1.1 Synthesis of Silver Nanoparticles by *Boerhavia diffusa* L.

Plate 2 shows the pale yellow to dark brown color shift visible due to effective silver nanoparticle synthesis. The color shift is a sign of *Boerhavia diffusa* L. extract-mediated reduction of silver ions in green synthesis.

PLATE 2

GREEN SYNTHESIS OF SILVER NANOPARTICLES OF EBdAgNPs

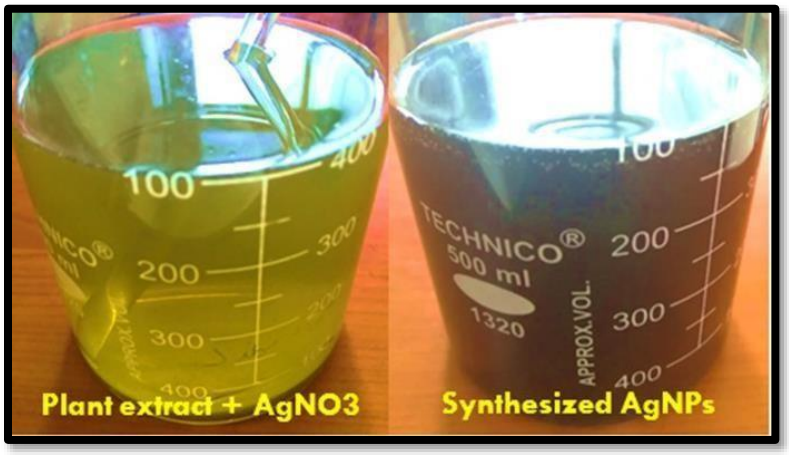

The reduction of AgNP by the ethanolic extract of *B. diffusa* was reflected by a visible color change of the reaction mixture from pale yellow to dark brown given in the Plate 2. This color change is a sign of silver ion (Ag^{+}) reduction to metallic silver nanoparticles (Ag^{0}), a bioactive compound catalyzed reaction by polyphenols and terpenoids in the plant extract. These compounds serve a dual purpose by acting as reducing agents to reduce silver ions and as stabilizing agents to prevent nanoparticle agglomeration (Sudhakar *et al*., 2025; James *et al*., 2025).

Use of *B. diffusa* extract to prepare nanoparticles is an environmentally friendly and sustainable method compared to chemical preparation. The green preparation method is free from toxic chemicals and harsh conditions, minimizing environmental risk and enhancing biocompatibility for biomedical applications (Radulescu *et al*., 2023). The naturally derived capping agents in the extract also provide homogeneity and stability in the prepared nanoparticles, which are critical for reproducible biological activity.

While other characterization techniques such as UV-Visible spectroscopy, FTIR, SEM and XRD are primarily required in describing such things as particle size, morphology and crystallinity, the primary colorimetric findings are evidence of the success of nanoparticle synthesis. This green synthesis process is entirely in accord with modern goals in nanotechnology that combine environmentally friendly production with enhanced biomedical applications.

4.1.2 Characterization of EBdAgNPs

Characterization of medicinal plants is an important process that encompasses the identification of their biochemical constituents, evaluation of pharmacological activity and analysis of their possible therapeutic value. This scientific investigation is multidisciplinary with the use of botanical evaluation, phytochemical screening and biological testing to enable the safe and effective creation of therapeutics of plant origin (Shah, 2024). In this research, EBdAgNPs producing the ethanolic extract of *Boerhavia diffusa* L. were suitably characterized with a variety of techniques. UV–Visible spectroscopy proved the presence of nanoparticles by showing the surface plasmon resonance (Gaur *et al*., 2021). X-ray diffraction (XRD) profiling demonstrated their crystalline nature and FTIR analysis identified the functional groups responsible for stabilizing the nanoparticles. Scanning Electron Microscopy (SEM) and Energy Dispersive X-ray Analysis (EDAX) were carried out for the study of morphology and elemental composition, respectively. In addition, zeta potential analyses were performed to determine the colloidal stability of EBdAgNPs. Detailed characterization provides valuable information on the structural, chemical and stability properties of EBdAgNPs, thereby validating their suitability for biomedical applications (Hosny *et al*., 2025).

4.1.2.1 UV-Visible Spectrum of EBdAgNPs

Figure 4.1 illustrates the UV–Visible spectrum of EBdAgNPs, showing a well-defined absorption peak that confirms the occurrence of surface plasmon resonance (SPR), thereby indicating successful nanoparticle formation.

FIGURE 4.1

UV–VISIBLE SPECTRUM OF EBdAgNPs

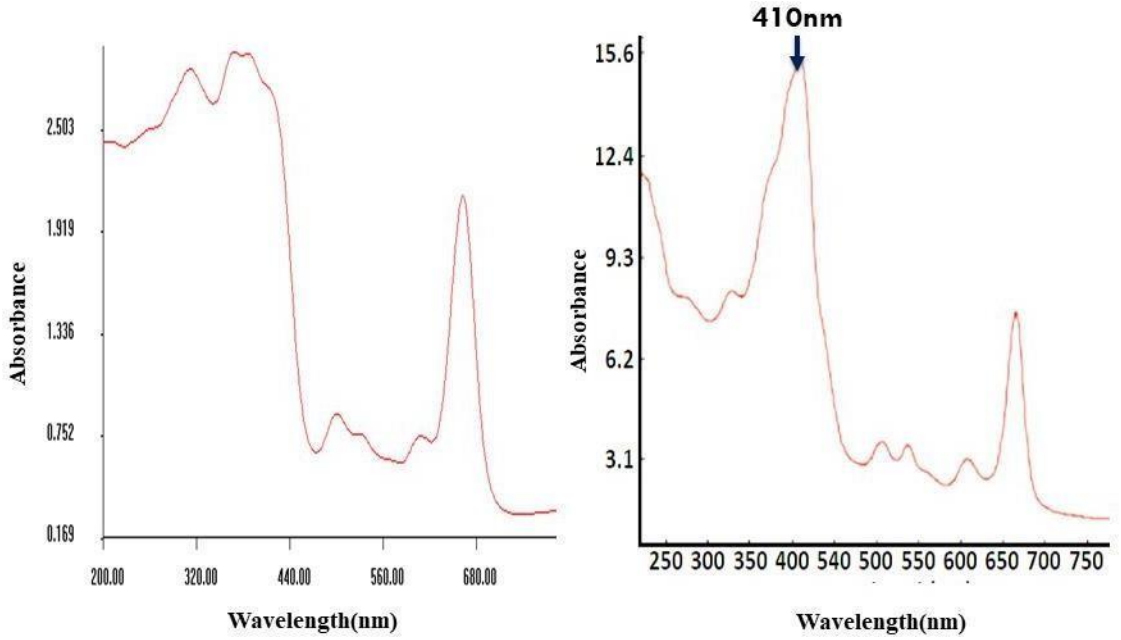

Crude extract of *B. diffusa* **Synthesized AgNPs of *B. diffusa***

Figure 4.1 shows the UV–Visible spectrum results, a simple technique used to ascertain the synthesis of metal nanoparticles through the detection of SPR. In the present study, EBdAgNPs exhibited a distinct SPR peak at approximately 410 nm, which is characteristic of spherical silver nanoparticles. This optical characteristic is due to the collective oscillation of the conduction electrons in the nanoparticles when exposed to light, which is a feature of nanoscale silver particles. The position and magnitude of this peak provide information on the size of the particles and dispersion in the colloidal solution. The identical SPR peaks, 390 to 430 nm, have been observed in silver nanoparticles prepared using synthesis from *Phagnalon niveum* and *Punica granatum*, characteristic of spherical shapes and nanoscale sizes (Ul Haq *et al*., 2022; Serdar, 2023). In addition, modifications in synthesis parameters such as pH, temperature and phytochemical content can modify the SPR band. The temporal stability of this absorption peak establishes the colloidal stability of the nanoparticles (Zuhrotun *et al*., 2023; Zaheer *et al*., 2023).

4.1.2.2 X-ray Diffraction (XRD) of EBdAgNPs

Figure 4.2 presents the XRD pattern of EBdAgNPs, displaying distinct diffraction peaks that confirm the face-centered cubic (FCC) crystalline structure of the synthesized silver nanoparticles.

FIGURE 4.2

XRD PATTERN OF EBdAgNPs

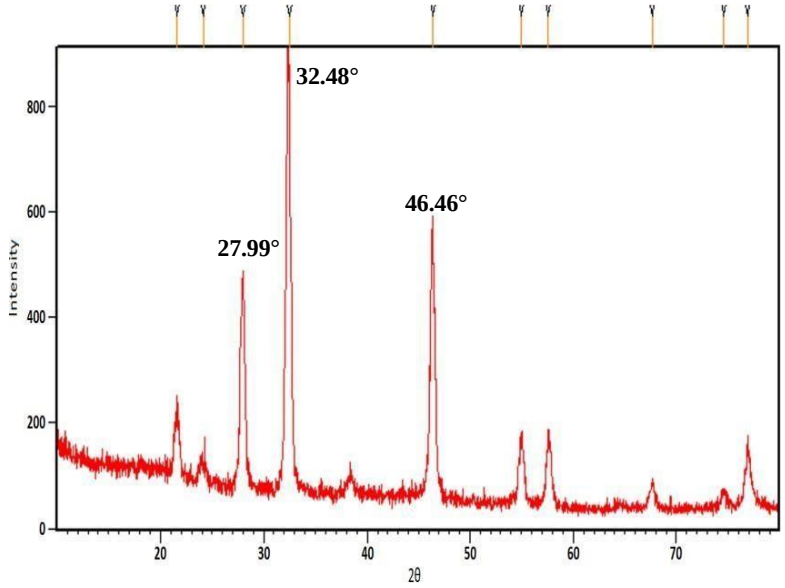

The X-ray diffraction (XRD) pattern obtained for the EBdAgNPs provides clear evidence of their crystalline nature. Distinct diffraction peaks were recorded at 2θ values of 27.99°, 32.48°, 46.46°, 55.00° and 57.60°, which correspond to the (111), (200), (220), (311) and (222) planes of a face-centered cubic (FCC) metallic silver lattice. The sharpness and intensity of these peaks indicate the formation of well-ordered crystalline domains. Using the Debye–Scherrer equation, the average crystallite size was estimated to be approximately 24 nm, confirming that the synthesized particles fall within the nanoscale range. Similar FCC diffraction patterns for AgNPs have been documented in biosyntheses using *Capparis zeylanica* and *Azadirachta indica*, suggesting consistency in crystal formation among plant-mediated nanoparticle systems (Suresh *et al*., 2024; Sharma *et al*., 2022). The formation of such crystalline arrangements was known to enhance particle stability and catalytic behaviour, characteristics that contribute significantly to their antimicrobial and antioxidant activities (Abuzeid *et al*., 2023).

The structural resemblance between EBdAgNPs and those synthesized from *C. zeylanica* and *A. indica* implies that the EBdAgNPs extract may contain phytochemicals functioning in a manner similar to those in the *C. zeylanica* and *A. indica* (Suresh *et al*., 2024; Sharma *et al*., 2022). In plant-mediated nanoparticle synthesis, biomolecules such as flavonoids, phenolic acids, alkaloids and terpenoids commonly act as reducing and stabilizing agents, influencing nanoparticle nucleation and growth (Adeyemi *et al*., 2022). The similarity in FCC structural motifs suggests that EBdAgNPs phytochemicals likely provide a comparable biochemical environment, enabling the formation of stable and uniformly structured silver nanoparticles. The EBdAgNPs may exhibit biological activities similar to those reported for AgNPs synthesized from these medicinal plants, underscoring the significant contribution of plant derived compounds to nanoparticle crystallinity and functional performance (Barathi *et al*., 2024).

The enhanced antioxidant behaviour of FCC-structured AgNPs can be linked to the high reactivity of their exposed crystallographic planes, especially the (111) facets (Princy *et al*., 2024). These surfaces promote efficient release of Ag^{+} ions and facilitate the generation of reactive oxygen species (ROS), both of which play a major role in microbial membrane damage, protein inactivation and oxidative stress (Vaishampayan and Gromhmann, 2021). Additionally, the catalytic surface properties of these crystalline planes support rapid electron transfer, contributing to effective scavenging of free radicals. Therefore, the crystalline pattern confirmed through XRD not only validates the structural integrity of EBdAgNPs but also explains their potential for improved biomedical applications.

4.1.2.3 Fourier Transform Infrared (FTIR) Spectrum of EBdAgNPs

The FTIR spectrum of EBdAgNPs, as depicted in the figure 4.3, indicates the presence of functional groups such as hydroxyl, carbonyl and amide, confirming the involvement of *Boerhavia diffusa* L. phytochemicals in the reduction and stabilization of silver nanoparticles.

FIGURE 4.3

FTIR PROFILE OF EBdAgNPs

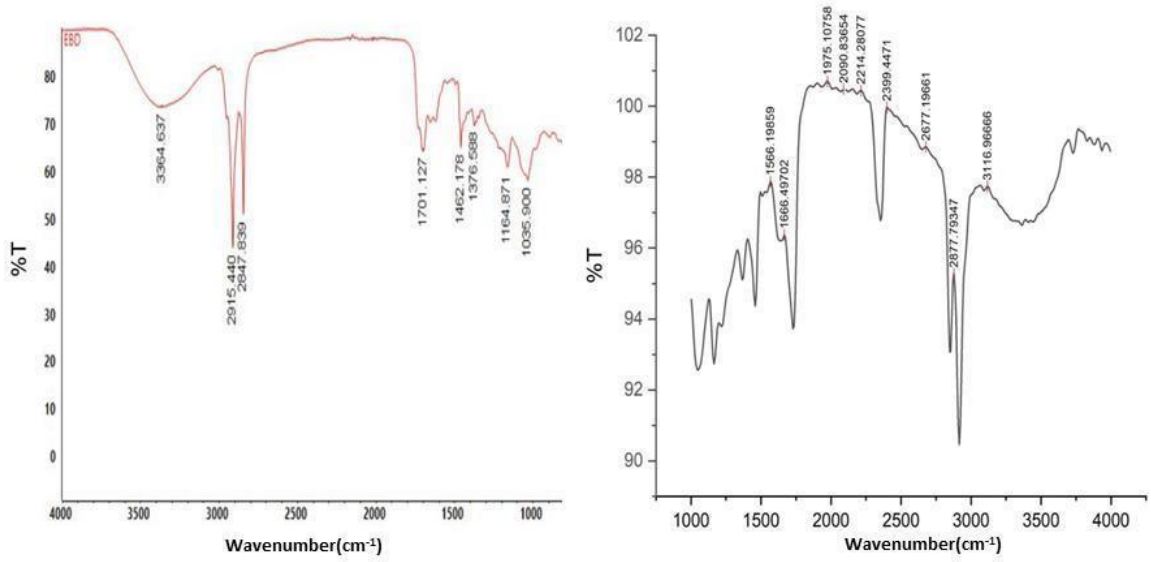

FTIR spectroscopy helps to identify the bioactive functional groups involved in the reduction and stabilization of silver ions during the synthesis of nanoparticles, as shown in figure 4.3. FTIR spectrum of EBdAgNPs revealed absorption peaks at 1566 cm^{-1} and 1666 cm^{-1} attributed to C=C stretching vibrations of alkenes. Absorption peaks at 1975 cm^{-1} and 2090 cm^{-1} were attributed to N=C=S stretching of isothiocyanates. A band at 2399 cm^{1} is likely due to O=C=O stretching due to the presence of CO_2. Bands at 2677 cm^{-1} and 2877 cm^{-1} correspond to aldehyde and alkane C–H stretching vibrations, respectively. Broad absorption at 3116 cm^{-1} was attributed to O–H stretching of hydroxyl groups present in carboxylic acids and thus it reflects that the hydroxyl group rich phytochemicals are responsible for the reduction of silver ions. This observation is consistent with earlier studies on silver nanoparticles synthesized from *Tabernaemontana ventricosa* and lemongrass extracts, where the formation and stabilization of AgNPs were primarily attributed to biomolecules such as flavonoids, phenolics and terpenoids (Naidoo *et al*., 2023). These compounds possess abundant hydroxyl and carbonyl groups that are capable of donating electrons to silver ions, thereby facilitating reduction, while their remaining functional groups adhere to the nanoparticle surface, providing steric and electrostatic stabilization.

The similarity between the FTIR signatures of EBdAgNPs and those reported for *T. ventricosa* and lemongrass suggests that the EBd extract likely contains phytoconstituents with comparable chemical functionalities. The presence of O–H, C=C, C–H and N=C=S stretching vibrations in EBdAgNPs implies that EBd phytochemicals may operate through mechanisms similar to those identified in these well-studied medicinal plants. This correspondence strengthens the inference that the EBd extract provides a suitable reducing and capping environment, enabling efficient nanoparticle formation through pathways driven by antioxidant rich metabolites. Therefore, the functional groups detected in the EBdAgNP FTIR spectrum not only confirm the participation of plant-derived biomolecules in nanoparticle synthesis but also support EBdAgNPs share similar stability, biocompatibility and biological performance characteristics with AgNPs produced from other bioactive plant systems (Kutner *et al*., 2021; Hakim *et al*., 2021).

4.1.2.4 Scanning Electron Microscopy (SEM) of EBdAgNPs

The following figure 4.4 presents SEM micrographs of EBdAgNPs, indicating the surface topography and confirming the presence of predominantly spherical nanoparticles with moderate agglomeration, characteristic of green synthesis.

FIGURE 4.4

SCANNING ELECTRON MICROSCOPY OF EBdAgNPs

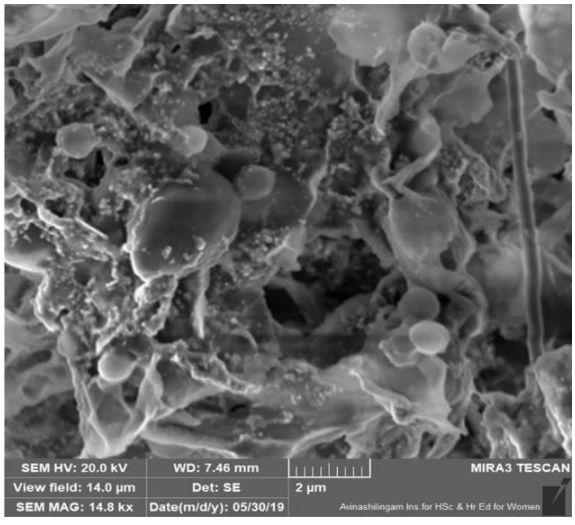

The SEM analysis produced detailed images that explain the morphology of EBdAgNPs. The figure 4.4 illustrates the predominantly spherical shape and moderate agglomeration of the nanoparticles. The nanoparticles were found to have a spherical shape with an average diameter of about 25 nm. Their surfaces were relatively smooth with negligible aggregation, indicating effective capping by phytochemicals. Uniformity in morphology is important to guarantee reproducibility in biomedical applications, e.g., antimicrobial coatings. The observations are in agreement with findings of AgNPs obtained from *Zingiber officinale* and *Curcuma amada*, which also presented spherical morphologies (Mohammed *et al*., 2022; Ramzan *et al*., 2024). The findings obtained from SEM complement the X-ray Diffraction (XRD) data by confirming the existence of uniform nano-sized particles (Netam *et al*., 2021).

Comparable morphological traits observed in ginger and mango ginger derived AgNPs offer a useful context for interpreting the structural behaviour of EBdAgNPs. In those plant systems, phytoconstituents such as phenolics, terpenoids and reducing sugars act as both electron donors and stabilizing molecules, guiding the formation of distinct spherical nanoparticles. *Boerhavia diffusa* L. contains a similar set of bioactive compounds particularly flavonoids, alkaloids and rotenoids which likely contributed to the controlled nucleation and growth seen in this study. The limited agglomeration and smooth surface features of EBdAgNPs indicate effective capping by these metabolites. Functional groups rich in electrons, especially hydroxyl and carbonyl groups, help reduce silver ions and subsequently bind to the nanoparticle surface, thereby preventing extensive clustering. This shared biochemical influence across the plant extracts explains the resemblance in nanoparticle stability and morphology, highlighting the capability of *Boerhavia diffusa* L. to generate uniform and stable AgNPs comparable to those synthesised from *Zingiber officinale* and *Curcuma amada* (Mohammed *et al*., 2022; Ramzan *et al*., 2024).

4.1.2.5 Energy-Dispersive X-ray (EDAX) Spectrum of EBdAgNPs

Figure 4.5 presents the EDAX spectrum of EBdAgNPs, confirming their elemental composition. EDAX analysis identifies the elements present in the sample based on their characteristic X-ray emission, there by validating the purity and composition of the synthesized nanoparticles.

FIGURE 4.5

EDAX SPECTRUM OF EBdAgNPs

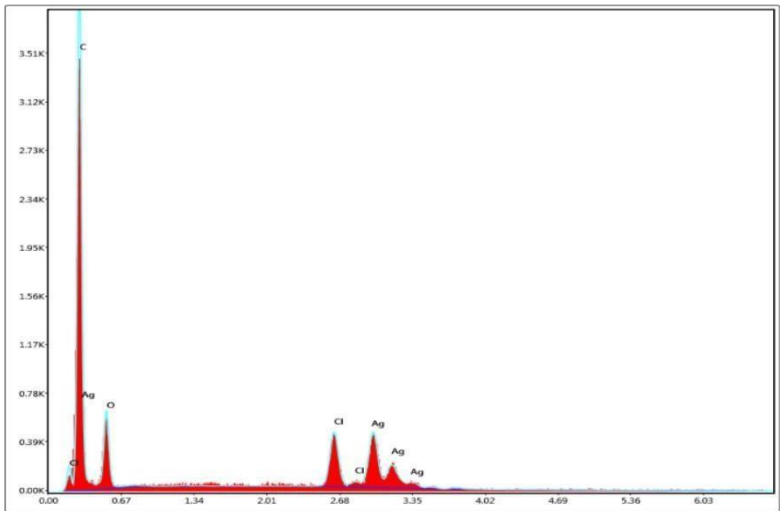

(keV)

Element	Weight %	Atomic %	Error %
C K	47.59	75.72	8.04
O K	10.87	12.98	13.01
Cl K	10.89	5.87	6.36
Ag L	30.65	5.43	7.61

EDAX spectroscopy validated the elemental constitution of EBdAgNPs. The spectrum revealed a prominent peak of silver corresponding to approximately 30.6 percent, confirming the presence of metallic silver, as shown in figure 4.5. Other elements that were detected include copper (47.6%), oxygen (10.9%) and chlorine (10.9%), which are likely to be of plant metabolites or residual substrates. The prominent peak of silver, with low oxygen signals, confirms efficient reduction and stabilization of silver ions by the phytoconstituents present in *Boerhavia diffusa* L. Moreover, the availability of oxygen containing biomolecules on the surface of the nanoparticles may also influence their biological activity (Wang *et al*., 2023a).

The elemental distribution observed in the EDAX profile also provides meaningful insight into the nature of phytochemical involvement during nanoparticle synthesis. The presence of oxygen and chlorine signals, although comparatively lower than silver,

reflects the adsorption of plant-derived compounds on the nanoparticle surface. Such biomolecules particularly phenolics, flavonoids and other polar constituents from *Boerhavia diffusa* L. are known to co-ordinate with metal surfaces, thereby enhancing particle stability and preventing uncontrolled growth (Patel *et al*., 2025). Their association with the nanosilver surface suggests a strong interaction between the plant extract and silver nuclei, which likely contributes to the controlled particle morphology seen in SEM analysis (Salayová *et al*., 2021). Additionally, the trace elemental peaks such as copper may originate from natural mineral traces within the plant matrix or analytical substrate and do not interfere with nanoparticle formation (Tombuloglu *et al*., 2020). Overall, the EDAX profile reinforces that the metabolites present in *Boerhavia diffusa* L. function effectively as both reducing agents and stabilizers, enabling efficient conversion of silver ions into metallic nanoparticles and imparting desirable physicochemical properties that support their potential use in various biological applications (Sati *et al*., 2025).

4.1.2.6 Zeta Potential Analysis of EBdAgNPs

Figure 4.6 from zeta potential analysis of EBdAgNPs reveals a negative surface charge, indicating good colloidal stability and effective capping by the bioactive molecules of *Boerhavia diffusa* L.

FIGURE 4.6

ZETA POTENTIAL ANALYSIS OF EBdAgNPs

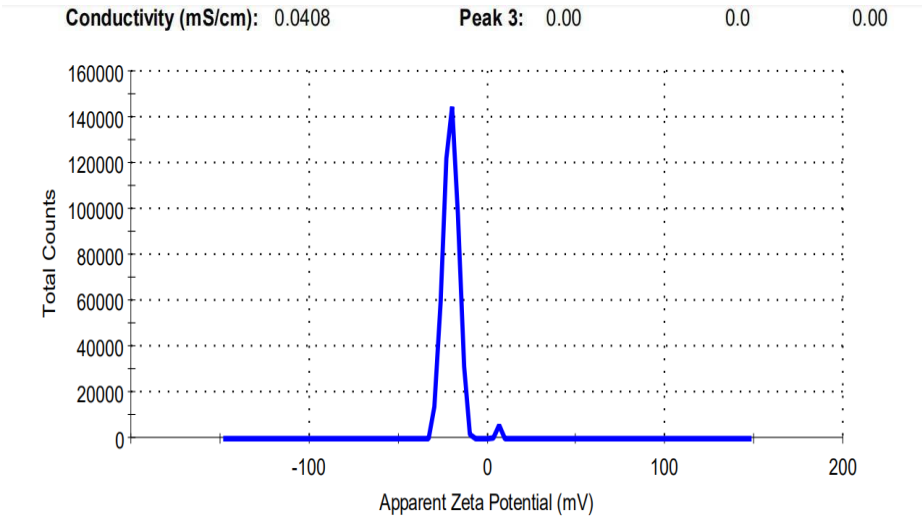

Zeta potential analysis determines the electrostatic interactions and surface charge of suspended nanoparticles, as shown in figure 4.6. EBdAgNPs maintained a zeta potential value of –20.2 mV, indicating good colloidal stability. Generally, zeta potential values between –20 mV and –30 mV indicate sufficient electrostatic repulsion and prevention of particle aggregation. Stable dispersion is essential for biomedical applications, as nanoparticle aggregation reduces efficacy and increases toxicity risks. Similar zeta potential values are reported for AgNPs synthesized from *Psidium guajava* (–18.2 mV) and *Ocimum sanctum* (–22.4 mV), which supports our findings (Sati *et al*., 2025; Baruah *et al*., 2021). Apart from physical stability, zeta potential influences nanoparticle interaction with biological membranes, affecting cellular uptake and toxicity profiles (Aibani *et al*., 2021).

The *Psidium guajava* and *Ocimum sanctum* are rich in polyphenols, flavonoids and other electron donating metabolites that contribute to the development of a negatively charged surface layer around nanoparticles (Sati *et al*., 2025; Baruah *et al*., 2021). A comparable pattern is likely in *Boerhavia diffusa* L. whose phytochemical constituents particularly flavonoids, alkaloids and phenolic acids are known to impart substantial surface functionalization. This biochemical coating enhances the negative charge, explaining the –20.2 mV value achieved in the present study. The similarity among these plant derived nanoparticles suggests that although the botanical sources differ, the underlying phytochemical mechanisms governing particle stabilization show a common trend. This supports the interpretation that *Boerhavia diffusa* L. possesses an effective reducing capping system capable of generating nanoparticles with stability characteristics equivalent to those produced by other medicinal plants (Sudhakar *et al*., 2025)

PHASE II

4.2 Antioxidant, Antidiabetic and Antiobesity Activities of EBdAgNPs

4.2.1 *in vitro* Antioxidant Activities of EBdAgNPs

Reactive oxygen species (ROS) are implicated in the etiology of a broad range of Chronic disorders, including diabetes, cardiovascular disease, cancer and neurodegenerative disorders. Antioxidants neutralize these ROS and are important in the prevention of cellular damage induced by oxidative stress (Engwa *et al*., 2022). In the present study, the antioxidant activity of silver nanoparticles synthesized from ethanolic extract of *B. diffusa* (EBdAgNPs) was examined in depth using *in vitro* assays. Particularly, three commonly used free radical scavenging assays 2,2-diphenyl-1-2-diphenyl-1 picrylhydrazyl (DPPH), 2,2'–azino–bis (3-ethylbenzothiazoline-6-sulfonic acid) (ABTS) and Ferric Reducing Antioxidant Power (FRAP) were employed. These assays provide valuable information on the electron donating capacity and radical quenching activity of the nanoparticles and are proof of their therapeutic utility as antioxidant agents under oxidative stress conditions. Additionally, they help evaluate the antioxidant activity of plant extracts and nanoparticles (Samrot *et al*., 2022).

4.2.1.1 DPPH Radical Scavenging Activity of EBdAgNPs

Figure 4.7 illustrates the DPPH radical scavenging activity of EBdAgNPs. It indicates the intense antioxidant activity of EBdAgNPs in scavenging free radicals.

FIGURE 4.7

DPPH RADICAL SCAVENGING ACTIVITY OF EBdAgNPs

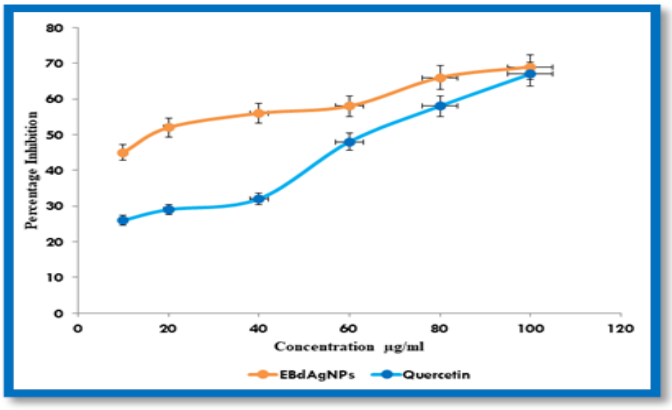

The results revealed that EBdAgNPs was found increased scavenging activity with increased concentration, with maximum inhibition of radicals in proportion from 10 to 100 µg/ml. At the highest concentration tested, EBdAgNPs had a significantly lower IC_{50} value of 20.8 µg/ml compared to the reference antioxidant quercetin (65.6 µg/ml), reflecting higher antioxidant activity.

The enhanced radical scavenging ability of EBdAgNPs may be attributed to the presence of phytoconstituents like flavonoids and phenolic compounds of *B. diffusa* that are effective in donating electrons or hydrogen atoms to neutralize free radicals (Jafri *et al*., 2023). The nanosize of the silver particles further provides increased surface area for interaction with DPPH radicals. This finding is in line with earlier research on AgNPs synthesized from *Thymus vulgaris*, which demonstrated potent DPPH scavenging due to thymol and carvacrol compounds known for their strong antioxidant behaviour (Aldosary *et al*., 2021). Similarly, silver nanoparticles derived from *Scoparia dulcis* also showed enhanced DPPH radical scavenging, highlighting the consistent antioxidant efficacy of plant based nanomaterials (Mini *et al*., 2023).

These observations are consistent with earlier reports on AgNPs derived from *Thymus vulgaris* and *Scoparia dulcis*, where bioactive molecules such as thymol, carvacrol and diverse phenolic constituents significantly enhanced radical scavenging activity. In those studies, the antioxidant strength was attributed to the ability of these compounds to donate electrons or hydrogen atoms rapidly, while their aromatic ring systems allowed stabilization of the resulting radical forms through resonance. When bound to the nanoparticle surface, these molecules displayed increased availability and reactivity, enabling more effective neutralization of DPPH radicals (Baschieri and Amorati, 2021). The similarity in behaviour suggests that the phytochemicals associated with EBdAgNPs operate through comparable interactions, which explains the strong antioxidant potential observed in the present study.

4.2.1.2 ABTS Radical Scavenging Activity of EBdAgNPs

Figure 4.8 demonstrates the ABTS radical scavenging activity of EBdAgNPs compared to Quercetin. It reflects the superior antioxidant activity of EBdAgNPs towards ABTS radical scavenging.

FIGURE 4.8

ABTS RADICAL SCAVENGING ACTIVITY OF EBdAgNPs

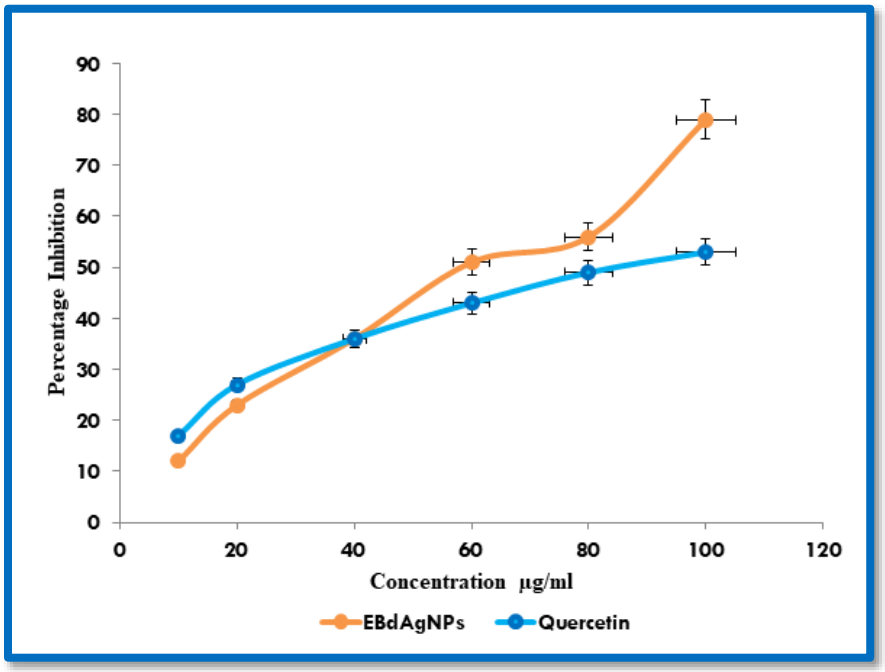

The ABTS (2, 2'-azino-bis (3-ethylbenzothiazoline-6-sulphonic acid)) radical cation decolorization assay was utilized to further evaluate the antioxidant activity of EBdAgNPs. The analysis demonstrated a dose dependent increase in ABTS radical scavenging, with maximum inhibition observed at 100 µg/ml. The IC_{50} value of EBdAgNPs (62.1 µg/ml) was lower than that of the standard antioxidant quercetin (84.4 µg/ml), indicating superior radical neutralizing capacity. This enhanced activity can be attributed to the bioactive phytochemicals present in *B. diffusa*, particularly flavonoids and phenolic acids enriched with hydroxyl groups that donate electrons and effectively quench free radicals (Nwozo *et al.*, 2023). Silver nanoparticles further act as stabilizing carriers, improving solubility, reactivity and bioavailability of these compounds. Similar results were reported for AgNPs synthesized from *Myrsine africana*, which also exhibited strong ABTS radical scavenging activity attributed to the synergistic interaction between silver and phytochemical antioxidants (Sarwer *et al.*, 2022). These findings collectively underscore the strong potential of EBdAgNPs as effective DPPH and ABTS radical scavengers.

Beyond the observed scavenging efficiency, the enhanced ABTS radical neutralization by EBdAgNPs can be explained by the mechanistic behavior of nanobiointerfaces. When phytochemicals are adsorbed onto a metallic nanoparticle surface, their electronic density becomes redistributed, often shifting reactive hydroxyl groups into more energetically favorable orientations for electron transfer. This reorganization reduces the activation energy required for radical quenching, making the antioxidant response faster and more effective. The nanoscale architecture of EBdAgNPs also creates a high curvature surface, which is known to increase surface energy and promote stronger interactions with charged radical species such as $ABTS^{+}$ (Fragou *et al*., 2023). Moreover, nanoparticles exhibit unique quantum effects that enable rapid redox cycling between Ag^{0} and Ag^{+} states, indirectly supporting continuous regeneration of bound antioxidant molecules (Dong *et al*., 2021). These nano specific characteristics, which do not occur in bulk plant extract, provide a logical explanation of EBdAgNPs for its outperformance against standard antioxidants like quercetin in terms of IC_{50} and overall scavenging kinetics.

4.2.1.3 Ferric Reducing Antioxidant Power Activity of EBdAgNPs

The 4.9 figure illustrates the Ferric Reducing Antioxidant Power (FRAP) activity of EBdAgNPs compared to Quercetin. This indicates the electron donating capacity of EBdAgNPs, confirming its high antioxidant activity.

FIGURE 4.9

FRAP RADICAL SCAVENGING ACTIVITY OF EBdAgNPs

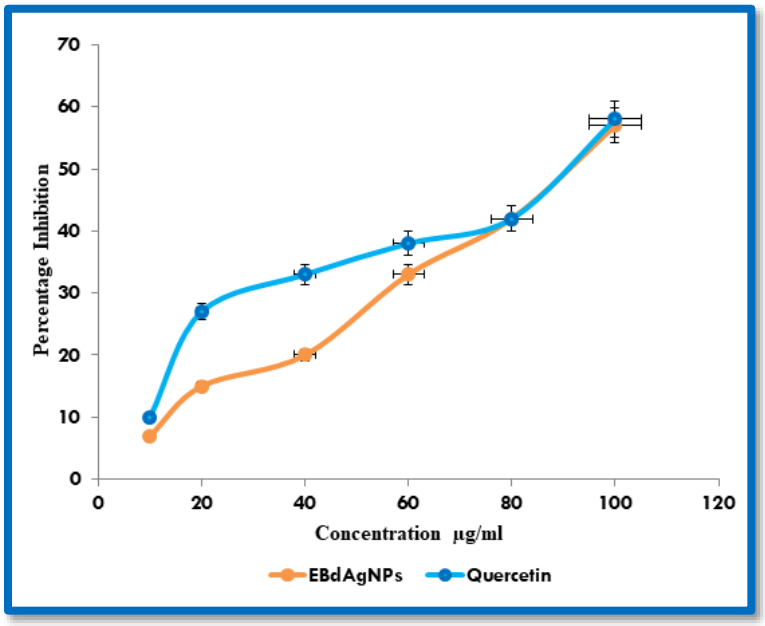

The capacity of EBdAgNPs was assayed using the FRAP (ferric reducing antioxidant power) assay to determine the reduction of ferric (Fe^{3+}) to ferrous (Fe^{2+}) ions in the presence of an antioxidant. EBdAgNPs had a high concentration dependent ferric reducing capacity from 10 to 100 µg/ml. The IC_{50} value of EBdAgNPs was 86.8 µg/ml, which was just below that of the quercetin standard (91.3 µg/ml), indicating similar or higher reducing power. The enhanced FRAP activity is a reflection of the electron donating ability of the nanoparticles, a significant process in the prevention of oxidative stress. This can be due to polyphenols and flavonoids in *B. diffusa* that are capable of chelating metal ions and possessing redox potential, enabling them to reduce ferric ions effectively (Mucha *et al*., 2021). The nanoscale synthesis also enhances the effect by increasing solubility and surface reactivity. These observations are consistent with findings from studies on *Clinacanthus nutans* derived silver nanoparticles, which also demonstrated significant FRAP activity due to the synergistic action of plant bioactives and nanoparticle enhanced surface chemistry (Islam *et al*., 2025). This reaffirms the efficacy of EBdAgNPs as potent antioxidants suitable for therapeutic applications.

The ferric-reducing performance exhibited by EBdAgNPs can be interpreted as a consequence of the distinct electron transfer dynamics occurring at the nanoparticle interface. At the nanoscale, silver nanoparticles possess a high density of reactive surface atoms, enabling rapid electron donation to ferric ions and accelerating the $Fe^{3+} \rightarrow Fe^{2+}$ conversion (Ullah *et al*., 2021b). When phytochemicals from *B. diffusa* bind to these surfaces, their redox active groups become more spatially accessible, facilitating more efficient participation in reduction reactions. Furthermore, nanoparticles create microenvironments that enhance electron mobility due to shortened diffusion pathways and increased charge carrier availability (Xu *et al*., 2021). These physicochemical conditions promote a sustained reducing effect that extends beyond the capability of plant extracts alone. The combined influence of nanoparticle surface energy, quantum level electron behavior and phytochemical assisted redox cycling therefore accounts for the pronounced FRAP response observed in EBdAgNPs, highlighting their mechanistic advantage in mitigating oxidative stress (Balkrishna *et al*., 2021).

4.2.2 Antidiabetic Activity of EBdAgNPs

To evaluate the antidiabetic potential of silver nanoparticles prepared from the ethanolic extract of *B. diffusa* (EBdAgNPs), a set of *in vitro* experiments was performed. These assays were specifically selected to examine various aspects of glucose metabolism and diabetic biochemical processes. In particular, the research included the inhibition of carbohydrate hydrolyzing enzymes, α-amylase and α-glucosidase directly responsible for postprandial hyperglycemia. Further, the activity was also evaluated for inhibiting non-enzymatic glycation of proteins, a critical process involved in long-term diabetic complications. Other tests examined the potential of EBdAgNPs to enhance glucose uptake in yeast cells, which represent a cellular system for assessing glucose utilization and to inhibit glucose diffusion, which reflects intestinal glucose absorption. Overall, these multi-dimensional assays provide a comprehensive understanding of the therapeutic potential of EBdAgNPs in diabetes management. The observed effects were also cross-checked with previous reports on bioactive plant-derived products and green-synthesized nanoparticles with similar antidiabetic activity (Santos *et al*., 2022; Schreck and Melzig, 2021).

4.2.2.1 α-Amylase Inhibitory Activity of EBdAgNPs

Figure 4.10 illustrates the inhibitory activity of EBdAgNPs against α-amylase, confirming their potential in retarding carbohydrate digestion by inhibiting this key enzyme

FIGURE 4.10

ALPHA AMYLASE INHIBITORY ACTIVITY BY EBdAgNPs

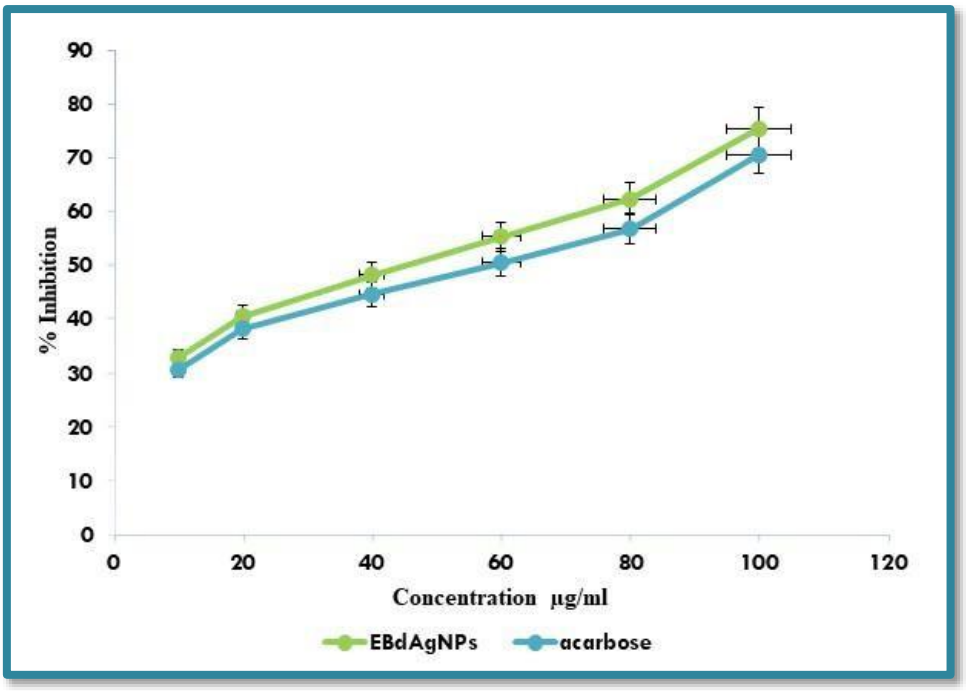

α-Amylase inhibitory activity of EBdAgNPs was tested in a dose-dependent manner (10–100 µg/ml), with the extract inhibiting up to 75.3 percent at the highest dose, which was superior to the standard drug acarbose 70.4 percent. The IC_{50} of EBdAgNPs was 46.2 µg/ml, which was lower than acarbose (55.4 µg/ml), indicating enhanced inhibitory activity. These results proves that EBdAgNPs have substantial inhibitory activity comparable to or even more effective than traditional antidiabetic drugs. α-amylase inhibition retards starch digestion and as a consequence, lowers postprandial blood glucose. Trends were similar in experiments using silver nanoparticles synthesized from *Cassia auriculata* and *Cynodon dactylon*, including substantial α-amylase inhibition *in vitro* (Thirumal and Sivakumar, 2021; Jyothish *et al*., 2025).

Moreover, the potent α-amylase inhibitory activity of EBdAgNPs can be attributed to the synergistic interaction between bioactive phytochemicals and the nanoscale properties of the silver nanoparticles. Phenolic compounds and flavonoids present in *B. diffusa* are known to bind to the active site of α-amylase via hydrogen bonding and hydrophobic interactions, thereby hindering substrate access and reducing enzyme catalytic efficiency (Viteri *et al*., 2024). When these phytoconstituents are conjugated or adsorbed onto the surface of silver nanoparticles, the high surface to volume ratio and enhanced electron density of the nanoscale matrix may facilitate stronger interactions with the enzyme, leading to more effective inhibition. Additionally, the nanoparticles can stabilize the bioactive compounds and improve their bioavailability, allowing for sustained interaction with α-amylase. This dual mechanism direct enzyme binding by phytochemicals combined with nanoscale mediated enhancement likely underpins the observed superior inhibitory effect of EBdAgNPs compared to both the plant extract alone and the standard drug acarbose. Therefore, the nanosystem not only acts as a carrier but also amplifies the enzyme inhibitory potential through enhanced molecular interactions at the enzyme's active site, resulting in delayed starch hydrolysis and reduced postprandial glucose levels (Lin *et al*., 2023).

4.2.2.2 α-Glucosidase Inhibitory Activity of EBdAgNPs

The following figure 4.11 indicates the inhibitory effect of EBdAgNPs on the α-glucosidase enzyme.

FIGURE 4.11

α-GLUCOSIDASE INHIBITORY ACTIVITY BY EBdAgNPs

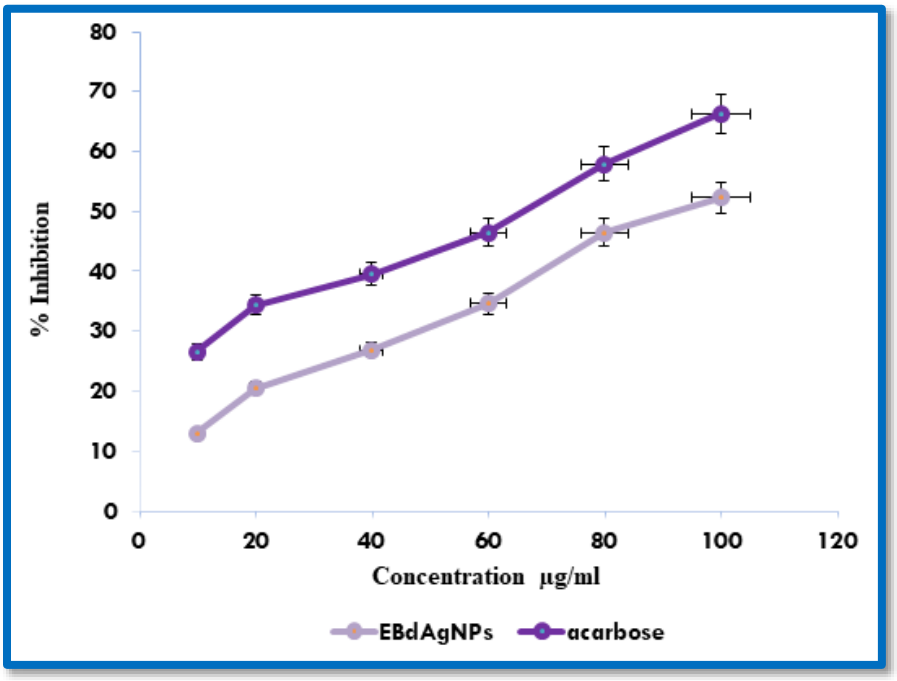

The assay indicates that they can be involved in lowering postprandial glucose levels through the delay of carbohydrate digestion. The α-glucosidase inhibition results for EBdAgNPs revealed a clear concentration dependent response, with the nanoparticles showing moderate yet meaningful inhibitory activity despite being less potent than acarbose. At 100 µg/ml, EBdAgNPs produced an IC_{50} of 93.0 µg/ml, while acarbose demonstrated a stronger IC_{50} of 63.4 µg/ml. This behaviour is consistent with observations from *Moringa oleifera* AgNPs, which also displayed medium-to-high affinity toward α-glucosidase inhibition (Olaoye *et al*., 2024).

The inhibitory effect of EBdAgNPs can be linked to the phytochemicals present on their surface, which interact with enzyme active sites and slow the breakdown of carbohydrates, helping regulate glucose release into the bloodstream. Additionally, flavonoid associated carbonyl and hydroxyl groups naturally known for inhibiting α-glucosidase may exhibit enhanced stability and bioavailability when incorporated into AgNP structures, thereby supporting the moderate inhibition pattern noted in this study (Proenca *et al*., 2022). Collectively, these findings indicate that EBdAgNPs may act as a

complementary antidiabetic agent and could reduce the drug related adverse effects when used alongside standard therapies.

A comparison with existing plant-based AgNP reports further strengthens the interpretation of the present results. The slightly higher IC_{50} observed for EBdAgNPs is in line with the inhibition efficiency reported for *Moringa oleifera* AgNPs (Olaoye *et al*., 2024), suggesting that the phytoconstituents of *Boerhavia diffusa* L. have a similar capacity to engage with catalytic regions of the α-glucosidase enzyme. Mechanistic insights from Proenca *et al*. (2022), highlighting the role of flavonoid carbonyl and hydroxyl groups in forming steric and functional barriers at the enzyme's active site, strongly support the inhibitory response noted in EBdAgNPs. The preservation of these functional groups after nanoparticle formation suggests that *Boerhavia diffusa* L. not only efficiently reduces and stabilizes silver ions but also retains its intrinsic bioactivity. Taken together, these points confirm that EBdAgNPs follow a phytochemical driven inhibition mechanism, validating their antidiabetic relevance and providing a solid basis for future molecular docking and structure activity investigations focusing on α-glucosidase interactions.

4.2.2.3 Inhibitory Effect of EBdAgNPs on Non-Enzymatic Glycosylation of Haemoglobin

Figure 4.12 demonstrates the effect of EBdAgNPs on hemoglobin non-enzymatic glycosylation inhibition. This indicates that they can prevent protein glycation with chronic hyperglycemia.

FIGURE 4.12

NON-ENZYMATIC GLYCOSYLATION BY EBdAgNPs

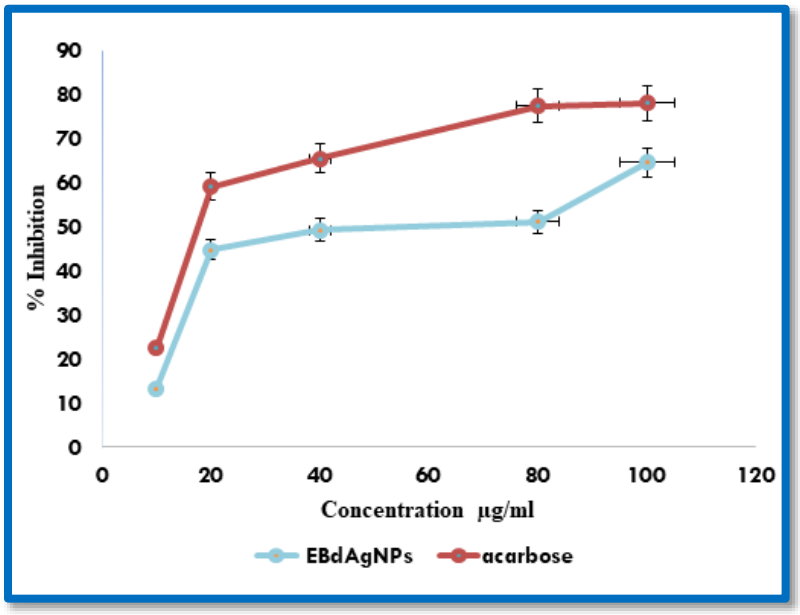

Hemoglobin non-enzymatic glycation, a sensitive indicator of chronic hyperglycemia, was effectively reduced by EBdAgNPs, which achieved 64.3 percent inhibition at 100 µg/ml, compared with metformin's 77.7 percent. The IC_{50} value of 63.9 µg/ml further confirms the strong antiglycation ability of the nanoparticles. This corresponds with the outcomes reported for *Ocimum gratissimum* and *Momordica charantia*, both of which substantially lowered glycation levels in earlier investigations (Ene, 2022; Kamiloglu *et al*., 2025). The action is presumed to involve the scavenging of reactive intermediates and interruption of the Amadori rearrangement, thereby reducing the progression toward advanced glycation end products. The nanosilver carrier may also improve the interaction with glucose and hemoglobin molecules, limiting their ability to undergo glycation.

When the present findings are viewed alongside observations from *Ocimum gratissimum* and *Momordica charantia*, it becomes clear that the phytochemical composition of *Boerhavia diffusa* L. contributes the antiglycation capacity of EBdAgNPs. The bioactive molecules of *B. diffusa* including flavonoids, rotenoids and alkaloids are known for their antioxidant and carbonyl quenching potential, allowing them to interfere

with glycation pathways comparable to the reported plant systems. Once these compounds are anchored onto the nanoparticle surface, their stability and reactivity are enhanced, enabling stronger interaction with early glycation intermediates. This synergy between the phytochemicals and the metallic core offers a plausible explanation for the notable inhibition observed, demonstrating that EBdAgNPs retain the functional advantages of the *B.diffusa* extract while benefiting from nanoscale delivery and enhanced molecular accessibility. (Ene, 2020; Kamiloglu *et al*., 2025).

4.2.2.4 Inhibition of Protein Glycation by EBdAgNPs

Figure 4.13 represents the protein glycation inhibitory activity of EBdAgNPs. This signifies that they possess the ability to inhibit diabetic complications related to advanced glycation end-products (AGEs).

FIGURE 4.13

PROTEIN GLYCATION INHIBITION BY EBdAgNPs

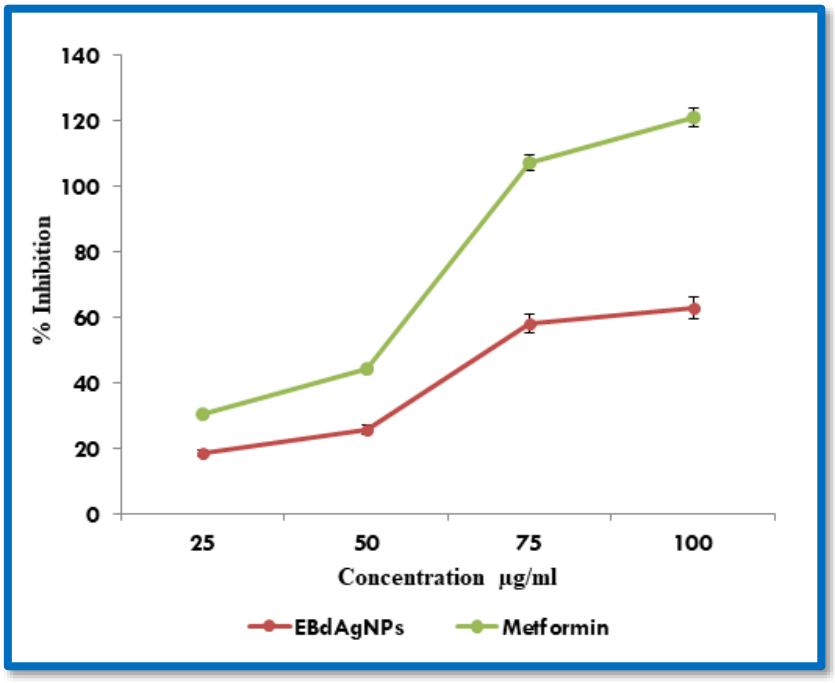

The inhibitory activity of EBdAgNPs on protein glycation was substantial, with 62.8 percent inhibition at 1000 µg/ml, slightly surpassing metformin 58.1 percent. The IC_{50} value of EBdAgNPs (756.3 µg/ml) was also lower than that of metformin (856.2 µg/ml), indicating stronger antiglycation potential. Protein glycation accelerates

the formation of AGEs, which play a critical role in the progression of diabetic vascular and neurological complications. Nanoparticle based systems are known to suppress glycation by trapping reactive carbonyl intermediates, thereby reducing AGE formation (Salau *et al*., 2024). The enhanced efficacy of EBdAgNPs at higher concentration highlights their potential in mitigating AGE accumulation and supporting long-term diabetes management.

Moreover, sustained *in vitro* exposure to reducing sugars simulates chronic hyperglycemic conditions, suggesting that EBdAgNPs may delay or prevent AGE mediated cellular damage. This protective capability is particularly relevant for tissues prone to glycation induced injury, such as the kidney and retina, offering further evidence of the therapeutic promise of EBdAgNPs.

4.2.2.5 Effect of EBdAgNPs on the Uptake of Glucose by Yeast Cells

Figure 4.14 illustrates the effect of EBdAgNPs on the uptake of glucose by yeast cells. This illustrates the capability of stimulating peripheral glucose usage, justifying their antidiabetic activity.

FIGURE 4.14

EFFECT OF EBdAgNPs ON THE UPTAKE OF GLUCOSE BY YEAST CELLS

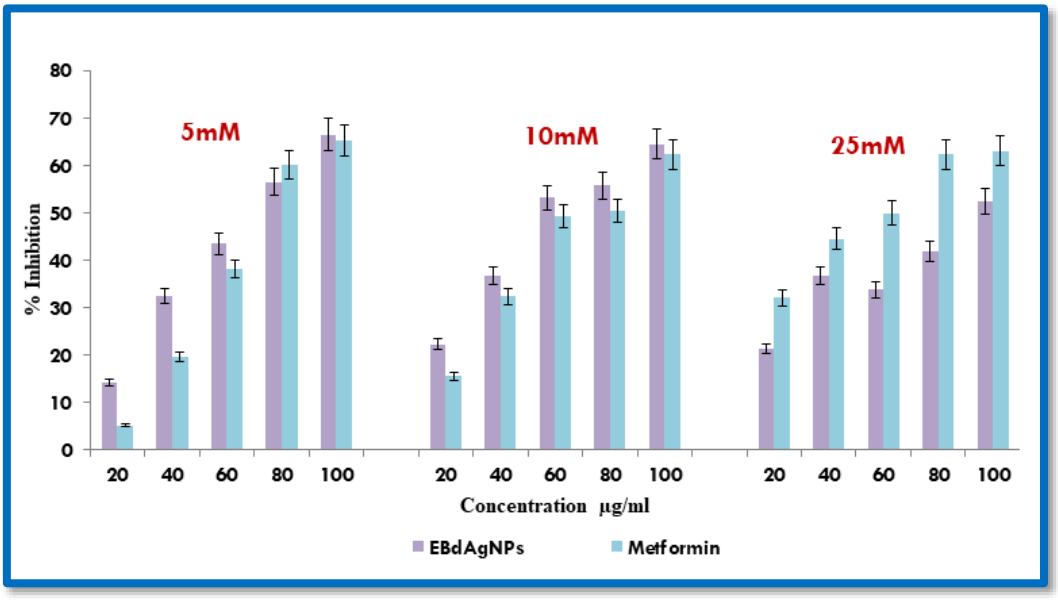

Glucose uptake assay in yeast cells is penetrant but it is a simple model for the assessment of antidiabetic activity by mimicking non-insulin-mediated glucose uptake. Yeast cells have glucose transporters comparable to mammalian systems and are therefore a low-cost, genetically accessible system to research glucose metabolism and screen antidiabetic agents (Bhoria *et al*., 2022). EBdAgNPs were assessed in the current study for their effect on glucose uptake at three glucose levels (5 mM, 10 mM and 25 mM) and five extract levels (20–100 µg/ml) and compared with metformin as given in figure 4.14.

At 5 mM glucose, EBdAgNPs exhibited significantly higher uptake compared to metformin at every concentration, with maximum uptake being 66.5 percent at 100 µg/ml, barely exceeding the control 65.2 percent. At 10 mM glucose, the nanoparticles again exhibited a higher glucose uptake was found to be 64.5 percent compared to metformin which is 62.3 percent at the maximum concentration tested. At 25 mM glucose and metformin was found to exhibit higher uptake at all concentrations except 100 µg/ml, was EBdAgNPs exhibited a significant increase as 52.4 percent. A dose-dependent stimulation of glucose uptake, particularly at low glucose levels, indicates the ability of EBdAgNPs was found to enhance cellular glucose uptake, which can be implicated in diabetic glycemic regulation. This agrees with findings by Chukwuma *et al*., (2022), where fractions of *Leptadenia hastata* leaves enhanced glucose uptake with the concentration-dependent trends. The efficacy of EBdAgNPs could be attributed due to the synergistic effect of *B. diffusa* phytoconstituents, especially flavonoids, which have been found to stimulate glucose transporter (GLUT) expression and augment glucose uptake (Mihailovic *et al*., 2021; Ansari *et al*., 2025).

Further, silver nanoparticles can also serve as carriers to enhance bioavailability and cell delivery of active compounds. The above action of EBdAgNPs, particularly at 5 mM and 10 mM glucose levels, can be due to increased transport activation or mimicry of insulin like activity. Similar effects were seen in *Centella asiatica* and *Moringa oleifera* nanoparticle based research where enhanced glucose uptake was noted in yeast and muscle cell models (Rachana and Sharma, 2024; Perumalsamy *et al*., 2024).

These findings demonstrated the potential of EBdAgNPs in the induction of glucose uptake and postprandial glucose regulation, especially at physiological glucose

levels. Additional mechanistic studies including gene expression studies of glucose transporters (such as GLUT4, GLUT2) and insulin signaling pathway in mammalian cell lines can validate the therapeutic application of these nanoparticles (Dini *et al*., 2021).

4.2.2.6 Inhibition of Glucose Diffusion by EBdAgNPs

Table 4.1 illustrates the ability of EBdAgNPs to inhibit glucose diffusion *in vitro* with time. This suggests their ability to regulate glucose uptake, which is comparable to that of the standard drug metformin.

TABLE 4.1

INHIBITION OF GLUCOSE DIFFUSION BY EBdAgNPs

Sample	Glucose Concentration in External Solution at Different Time Intervals (mM)				
	30mins	60mins	90mins	120mins	180mins
Control	51.9±0.6	61.5±0.6	61.6±0.5	107±0.8	135±0.9
EBdAgNPs	19±0.3	20.4±0.5	21.2±0.3	21.6±0.4	26.5±0.3
Metformin	18.6±0.3	19.3±0.5	19.8±0.8	19.3±0.2	20.7±0.3

Inhibition of glucose diffusion across the intestinal wall was one of the predominant mechanisms in regulating postprandial hyperglycemia, a serious issue in diabetic patients. Retardation of glucose absorption reduces the velocity of glucose entry into the circulatory system and hence permits glycemic control, reduces the need for insulin and inhibits the oxidative stress-mediated complications (Singh *et al*., 2024a). Suppression of glucose diffusion by silver nanoparticles synthesized from *Boerhavia diffusa* L. ethanolic extract (EBdAgNPs) was determined at time intervals of 30, 60, 90, 120 and 180 minutes table (4.1).

The results showed that EBdAgNPs inhibited glucose diffusion across the membrane in a time-dependent manner. Glucose concentration in the external solution at every time point was lower in the EBdAgNP treated sample than in the control untreated sample. For instance, at 180 minutes, the control group recorded a reading of 135±0.944 mM, while the EBdAgNP treated sample only recorded 26.5±0.343 mM. The results confirm the potency of EBdAgNPs in retarding glucose diffusion over metformin,

particularly at longer time points. Metformin, despite its antidiabetic activity, recorded less inhibitory activity at certain time points, with glucose concentrations recorded at 20.7±0.36 mM at 180 minutes.

The inhibition observed is may be due to the presence of polyphenols, flavonoids and alkaloids in *B. diffusa*, which are documented to interact with glucose and slow its transport across semi-permeable membranes (Baral *et al*., 2022). Further, the nanoparticulate nature of the drug increases the effect by enhancing the bioavailability and binding coefficient of active constituents, creating transient complexes that decrease glucose transport (Shahzad *et al*., 2024). The same trend of glucose retardation was seen in a study with *Anisochilus nilgiricum* extract, where the increasing glucose diffusion inhibition was noted over time, in favour of plant-derived agents to modulate carbohydrate absorption (Dedvisitsakul and Iad, 2022).

In addition, the progressive enhancement of glucose inhibition with time can be explained by the prolonged contact of phytoconstituents with glucose molecules in the diffusion chamber. Slowed-down glucose migration reflects a chemical or physical interaction either through hydrogen bonding or entrapment in the viscous colloidal character of the extract-nanoparticle matrix (Raghav *et al*., 2022). These mechanisms play a significant role in the development of natural-origin functional foods or supplements for diabetes treatment. Unlike synthetic enzyme inhibitors like acarbose that enzymatically slow down carbohydrate digestion, plant nanoparticle formulations offer a non-enzymatic pathway, which may potentially reduce gastrointestinal side effects (Thirugnanasambandan and Gopinath, 2024).

These findings demonstrated the antidiabetic activity of EBdAgNPs by inhibiting glucose diffusion, thereby control carbohydrate bioavailability and maintain postprandial glucose homeostasis. This test confirms the therapeutic potential of the application of nanoparticle-formulated plant extracts in the treatment of diabetes, particularly in retarding the absorption of glucose and increasing insulin sensitivity (Dimitriadis *et al*., 2021).

4.2.3 *in vitro* Antiobesity Activity of EBdAgNPs

Plant-derived nanoparticles and phytochemicals can inhibit pancreatic lipase activity an essential enzyme in dietary fat breakdown thus reducing lipid absorption and

supporting antiobesity effects. These green-synthesized agents offer enhanced bioavailability and targeted delivery in *in-vitro* models, providing a promising route for early stage screening (Khatik, 2022).

4.2.3.1 Inhibition of Pancreatic Lipase Activity by EBdAgNPs

Figure 4.15 presents the time dependent *in vitro* pancreatic lipase inhibitory activity of EBdAgNPs, highlighting their progressive ability to suppress enzyme function.

FIGURE 4.15

INHIBITION OF PANCREATIC LIPASE ACTIVITY BY EBdAgNPs

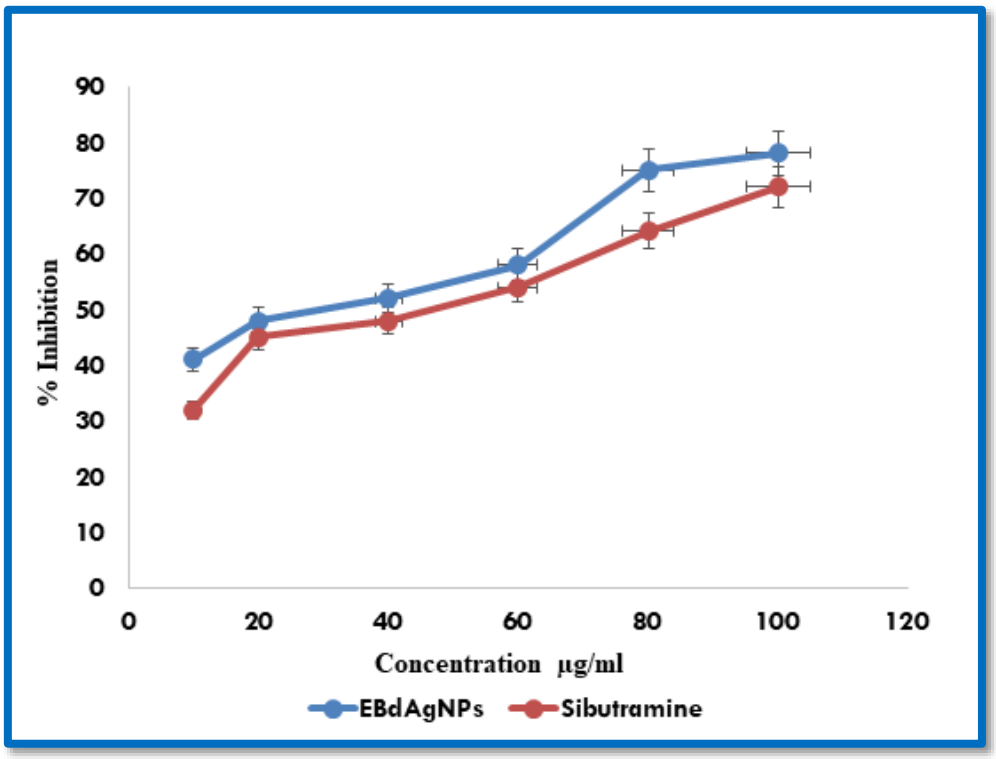

The ethanolic extract of *Boerhavia diffusa* L. mediated silver nanoparticles (EBdAgNPs) exhibited a clear concentration-dependent inhibition of pancreatic lipase, with an IC_{50} value of 56 µg/ml, outperforming the standard antiobesity drug sibutramine, which showed an IC_{50} of 69 µg/ml. The inhibition curve demonstrated that EBdAgNPs maintained comparable or slightly greater activity across all tested concentrations, suggesting strong potential for minimizing dietary fat absorption. These findings are in agreement with earlier reports that plant-derived silver nanoparticles exhibit significant

lipase suppression due to the combined influence of phytochemicals and improved bioavailability (Khormi *et al*., 2025). Such results indicate that EBdAgNPs may serve as an effective natural alternative or complementary therapeutic option to synthetic lipase inhibiting drugs, with the added advantage of potential multifunctional benefits.

The enhanced lipase inhibition observed in EBdAgNPs can be attributed to the intrinsic characteristics imparted by both the plant extract and the nanoparticle framework. The nanoscale structure provides a large interactive surface, allowing more consistent contact with the enzyme, while the phytochemical compounds from *B. diffusa* contribute additional inhibitory interfaces that strengthen the overall suppressive response. This synergy likely enhances the stability, reactivity and dispersion of the nanoparticles, enabling more efficient enzyme interaction throughout the assay. These collective properties explain the strong inhibitory pattern seen in EBdAgNPs and support their promise as a valuable candidate for fat modulation strategies in obesity management (Sayed *et al*., 2023).

PHASE III

4.3 *In vivo* Antidiabetic and Antiobesity of EBdAgNPs

The findings from both phase I and phase II investigations clearly demonstrates that the silver nanoparticles synthesized using ethanolic extract of *B. diffusa* (EBdAgNPs) exhibits significant antidiabetic and antioxidant properties, as validated through multiple *in vitro* assays. The study was extended to *in vivo* experimentation using rats to further explore the therapeutic efficacy and biological relevance of EBdAgNPs under physiological conditions.

Diabetes mellitus (DM) is a chronic metabolic disorder characterized by elevated blood glucose levels resulting from defects in insulin secretion, insulin action or both. The disease can lead to serious complications such as cardiovascular disease, kidney failure and neuropathy if not properly managed. Recent scientific advances have explored novel approaches for its management, including the use of nanotechnology based interventions such as silver nanoparticles due to their potential to enhance insulin sensitivity and reduce oxidative stress (Abo *et al*., 2025).

Obesity is strongly associated with the development of type 2 diabetes, primarily through its contribution to insulin resistance and systemic inflammation. Excess adipose tissue, especially visceral fat, disrupts normal metabolic signaling, leading to impaired glucose homeostasis and increased risk of diabetes. This bidirectional relationship has led researchers to consider diabetes and obesity as a part of a single pathological continuum often referred to as "diabesity" (Martemucci *et al*., 2023). As such, therapeutic strategies that can target both conditions simultaneously are gaining attention in current research.

Animal models, particularly rats, are widely utilized in preclinical research for evaluating novel therapeutic agents, including those synthesized with silver nanoparticles (AgNPs), due to their well-characterized physiology and metabolic similarity to humans. These models allow for detailed analysis of pharmacokinetics, biodistribution and potential toxicity of nanoparticle based drugs (Kutumova *et al*., 2022). Rats are especially suitable for biomedical experimentation because of their genetic, anatomical and physiological comparability to human systems, making them ideal for simulating human

disease conditions and responses to treatment. Their use enables researchers to monitor both short and long-term effects of AgNPs, which is crucial for validating their safety before advancing to clinical trials. Furthermore, rats respond to nanoparticle interactions in ways that mirror human biological pathways, reinforcing their translational significance in therapeutic development (Shoukani *et al*., 2025).

4.3.1 Body Weight of Experimental Rats

Figure 4.16 illustrates the differences in body weight, highlighting the metabolic outcomes of each intervention. Monitoring body weight changes is a key parameter in evaluating the metabolic impact of various treatments in experimental models of diabetes and obesity

FIGURE 4.16

EFFECT OF BODY WEIGHT IN EXPERIMENTAL RATS

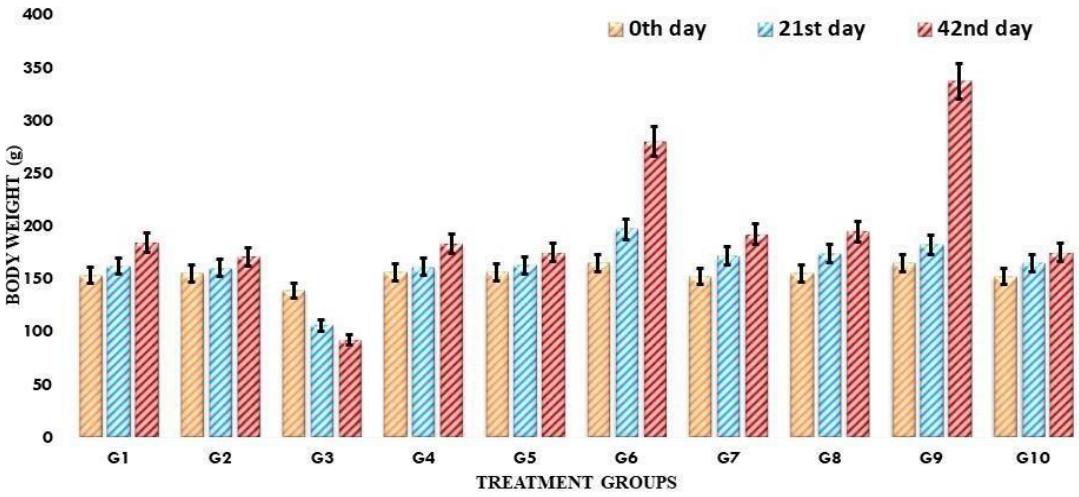

Values are expressed as mean ± S.E.M (n=6)

G1 Control	**G2 EBdAgNPs**	**G3 STZ-NI induced**
G4 STZ-NI + EBdAgNPs	**G5 STZ-NI + Glibenclamide**	**G6 HFD-induced**
G7 HFD + EBdAgNPs	**G8 HFD + Sibutramine**	**G9 STZ-NI + HFD**
G10 STZ-NI + HFD + EBdAgNPs		

G3 vs G1 and G2: ↓ body weight ($p < 0.001$)

G4 and G5 vs G3: ↑ body weight ($p < 0.001$)

G7, G8 and G10 vs G6 and G9: ↓ weight gain ($p < 0.01$)

(One Way ANOVO followed by Dunnett's Test)

The control group (G1) maintained a stable body weight of 184 ± 5.87 g, reflecting normal metabolic activity under balanced dietary conditions. Similarly, the EBdAgNPs-treated normal group (G2) showed a steady body weight of 171 ± 1.3 g, with no significant ($p < 0.001$) alteration from the control. This stability indicates that EBdAgNPs did not disrupt physiological processes such as nutrient absorption, basal metabolic rate or energy storage. The less significant ($p < 0.001$) increase observed in G2 suggests that the nanoparticles were biocompatible, causing no metabolic burden. As supported by earlier findings, plant-mediated silver nanoparticles possess antioxidant properties that help maintain oxidative balance without interfering with caloric metabolism, reinforcing the safety of EBdAgNPs in healthy animals (Madbouly *et al*., 2025). Together, these results confirm the normal physiological tolerance of EBdAgNPs.

The diabetic group (G3) showed a significantly decreased ($p < 0.001$) body weight of 92 ± 29.2 g when compared with both the control (G1) and the EBdAgNPs treated normal rats (G2). This marked reduction reflects classical STZ–NI induced β-cell damage, resulting in insufficient insulin secretion and impaired cellular glucose uptake. The energy deficit forces the body to rely on enhanced lipolysis and proteolysis, accelerating muscle wasting and adipose tissue depletion. Increased gluconeogenesis and dehydration further intensify the weight loss. These alterations are characteristic metabolic disturbances of uncontrolled diabetes, confirming successful induction of the diabetic state in G3 (Dilworth *et al*., 2021).

The EBdAgNPs treated diabetic group (G4) exhibited a significantly increased ($p < 0.001$) body weight of 183 ± 12.4 g relative to the diabetic group (G3). This substantial recovery suggests that EBdAgNPs enhanced insulin sensitivity, improved peripheral glucose uptake and reduced oxidative stress within pancreatic tissue. Phytochemicals from *B. diffusa* including punarnavine, boeravinones and flavonoids are known to stimulate endogenous antioxidant defenses, protect β-cells from oxidative injury and modulate hepatic carbohydrate-metabolizing enzymes. These combined actions promote restoration of energy homeostasis, explaining the near normalization of body weight in EBdAgNPs treated diabetic rats G4. Such recovery aligns with previous reports demonstrating that plant-derived nanoparticles promote glucose metabolism while reducing oxidative load in diabetic systems (Gupta *et al*., 2021).

The glibenclamide treated diabetic group (G5) also showed a significantly increased body weight (175 ± 3 g) in comparison with G3 ($p < 0.001$). This improvement reflects glibenclamide's action of stimulating pancreatic β-cells and enhancing insulin release, thereby promoting efficient nutrient utilization and tissue energy storage. However, the recovery was significantly decreased ($p < 0.001$) than that of EBdAgNP treated rats, indicating that EBdAgNPs may possess additional mechanisms including antioxidant, anti-inflammatory and lipid-modulating effects, offering a broader therapeutic range compared to the single pathway action of glibenclamide (Mishra *et al*., 2021).

The obese group (G6) demonstrated a significantly increased body weight ($p < 0.01$) of 280 ± 2.86 g compared with the control group (G1), confirming successful induction of obesity through a high-fat diet. Chronic HFD exposure leads to excessive adipose accumulation resulting from caloric surplus, hormonal dysregulation, impaired leptin and adiponectin signaling and reduced mitochondrial fatty acid oxidation. These changes promote adipocyte hypertrophy, oxidative stress and low-grade inflammation, collectively contributing to insulin resistance and metabolic imbalance. The weight increase observed in G6 closely parallels the physiological characteristics of human obesity and metabolic syndrome (Ion *et al*., 2023).

The EBdAgNPs-treated obese group (G7) exhibited a significantly decreased body weight of 192 ± 0.95 g relative to G6 ($p < 0.01$). This reduction indicates potent antiobesity activity, likely mediated through suppression of adipogenesis, enhancement of lipolysis and upregulation of mitochondrial fatty acid oxidation. Phytochemicals in EBdAgNPs have been reported to downregulate adipogenic transcription factors such as PPAR-γ and C/EBPα, while promoting pathways involved in lipid breakdown. Their antioxidant capacity also helps counteract inflammation associated adipocyte enlargement, supporting healthier lipid metabolism. Together, these mechanisms contribute to the strong weight reducing effect observed in G7 (Kazemi *et al*., 2025).

The sibutramine treated obese group (G8) showed a significantly decreased ($p < 0.01$) body weight of 195 ± 1.1 g compared with obese group (G6). Sibutramine promotes and increases thermogenesis through inhibition of serotonin and norepinephrine

reuptake, thereby elevating energy expenditure. The similarity in weight-reducing outcomes between G7 and G8 suggests that EBdAgNPs may possess comparable antiobesity efficacy but with the potential advantage of a better safety profile, as plant-based nanoparticles generally demonstrate superior biocompatibility (Gupta and Verma, 2024).

The obese diabetic group (G9) displayed the highest body weight among all groups (337 ± 14.5 g), reflecting severe metabolic dysfunction caused by the combined effects of obesity and diabetes. This dual metabolic burden intensifies insulin resistance, promotes impaired lipid utilization and triggers persistent oxidative stress and inflammatory signaling. In contrast, the EBdAgNPs treated obese diabetic group (G10) showed a significantly decreased body weight of 175 ± 37.1 g ($p < 0.01$), indicating a strong therapeutic response. The improvement may be attributed to activation of AMP-activated protein kinase (AMPK), enhanced fatty acid oxidation, improved glucose uptake and attenuation of oxidative and inflammatory stress. These multi-target effects demonstrate the ability of EBdAgNPs to correct complex metabolic disturbances across multiple organs, underscoring their potential as a comprehensive therapeutic strategy for managing combined obesity and diabetes (Colak and Pap, 2021; Li *et al*., 2025).

4.3.2 Fasting Blood Glucose in Experimental Rats

To investigate the hypoglycemic effects of EBdAgNPs, fasting blood glucose (FBG) levels were assessed on days 0, 21 and 42 across all ten experimental rat groups, as shown in the figure (4.17), reflecting early, mid and late responses to treatment efficacy.

FIGURE 4.17

EFFECT OF FASTING BLOOD GLUCOSE LEVELS ON EXPERIMENTAL RATS

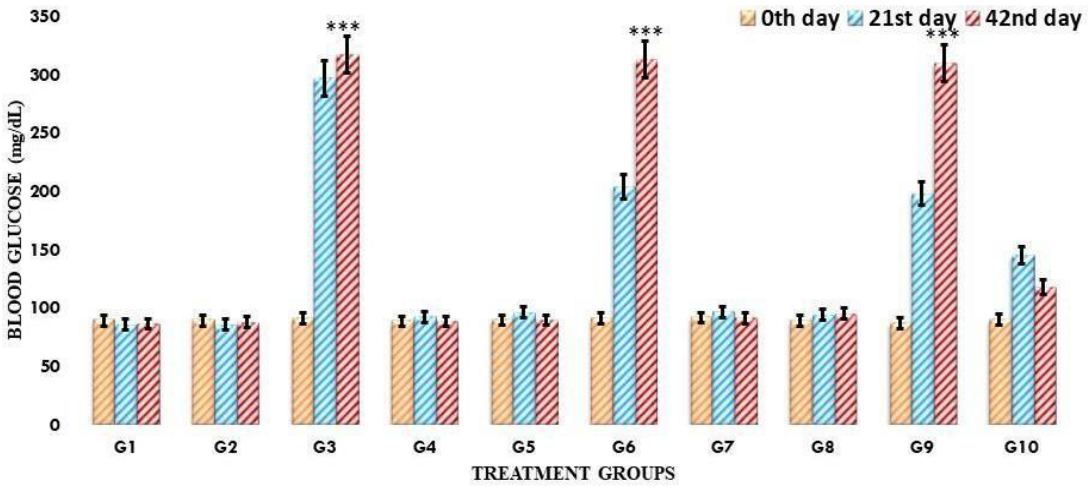

Values are expressed as mean ± S.E.M (n=6)

G1 Control	**G2 EBdAgNPs**	**G3 STZ-NI induced**
G4 STZ-NI + EBdAgNPs	**G5 STZ-NI + Glibenclamide**	**G6 HFD-induced**
G7 HFD + EBdAgNPs	**G8 HFD + Sibutramine**	**G9 STZ-NI + HFD**
G10 STZ-NI + HFD + EBdAgNPs		

G3 vs G1 and G2: ↑ blood glucose ($p < 0.001$)
G4 and G5 vs G3: ↓ blood glucose ($p < 0.001$)
G7, G8 and G10 vs G6 and G9: ↓ glucose levels ($p < 0.01$)
(One Way ANOVO followed by Dunnett's Test)

The normal control group (G1) and the healthy rats treated with EBdAgNPs (G2) maintained glucose values within physiological limits throughout the study period. The similarity between G1 and G2 indicates that EBdAgNPs did not disrupt endogenous glucose-regulating mechanisms such as insulin secretion, GLUT-4 translocation, hepatic gluconeogenesis, or glycogen turnover. This metabolic stability suggests that the nanoparticles are biologically safe in normoglycemic conditions and do not induce hypoglycemia or interfere with insulin sensitivity. The absence of adverse glycemic effects emphasizes their suitability for long-term therapeutic applications, especially since phytochemical stabilized nanoparticles often demonstrate improved biocompatibility, modulated oxidative stress and minimal interference with basal metabolic pathways (Karnwal *et al*., 2024).

The diabetic group (G3), produced using STZ-NI, exhibited a significant rise in blood glucose ($p < 0.001$) when compared with G1 and G2. Mean values increased from 297 ± 94 mg/dL on 21st day to 317 ± 104 mg/dL by 42nd day, confirming the establishment of a type-2 diabetic state characterized by inadequate insulin release and peripheral insulin resistance. STZ causes partial β-cell dysfunction while NI provides partial protection, resulting in a physiologically relevant type-2 diabetic phenotype. Hyperglycemia in G3 reflects impaired GLUT-4 activation, reduced hepatic insulin sensitivity, increased oxidative stress and inflammatory cytokines, all of which aggravate glucose intolerance. These mechanistic disturbances align with earlier reports describing compromised β-cell responsiveness and diminished insulin-mediated glucose uptake in STZ-NI-induced diabetes (Abarnadevika *et al*., 2024).

EBdAgNPs treated diabetic rats (G4) exhibited a significant decrease in glucose levels compared to G3 ($p < 0.001$), with values restored to near-normal levels 92.5 ± 3.1 mg/dL on 21st day and 88.3 ± 3.8 mg/dL on 42nd day. This improvement suggests that EBdAgNPs enhance insulin sensitivity, support residual β-cell function, reduce oxidative stress and promote peripheral glucose uptake through an increased GLUT-4 response. In addition, the phytochemicals capping the nanoparticles may inhibit α-amylase and α-glucosidase activity, reduce intestinal glucose absorption, modulate hepatic glucose production and alleviate inflammatory pathways involved in insulin resistance.

The glibenclamide-treated diabetic group (G5) also demonstrated a significant reduction in glucose compared to G3 ($p < 0.001$), with values (96.3 ± 1.76 mg/dL; 89.7 ± 3.43 mg/dL) closely resembling those of G4. Given that glibenclamide stimulates insulin secretion, the similarity in outcomes highlights the potential of EBdAgNPs to exert insulin-dependent and insulin-independent glucose regulatory actions. These may include decreased oxidative load, suppression of inflammatory markers and improved post-receptor insulin signaling efficiency (Rampin *et al*., 2022).

The high-fat-diet-induced obese group (G6) displayed a progressive increase in fasting glucose, rising from 204 ± 30.2 mg/dL to 313 ± 12.8 mg/dL. This increase relative to G1 reflects a significant impairment in insulin sensitivity driven by chronic

lipid excess. High-fat feeding increases circulating free fatty acids, promotes ectopic lipid deposition in muscle and liver, induces low-grade inflammation, disrupts insulin receptor substrate phosphorylation and impairs downstream Akt activation required for glucose transport. This mechanistic cascade reduces GLUT-4 mobilization and results in hyperglycemia characteristic of obesity associated insulin resistance (Gallo *et al*., 2025).

EBdAgNPs-treated obese rats (G7) showed a significant reduction in glucose levels compared to G6 ($p < 0.01$), reaching 96.7 ± 0.76 mg/dL on 21st day and 91.3 ± 0.91 mg/dL on 42nd day. This improvement indicates that EBdAgNPs counteract obesity-related metabolic disturbances by enhancing insulin receptor activity, improving lipid handling, lowering inflammation in adipose tissue, inhibiting oxidative stress and facilitating better glucose disposal.

Similarly, sibutramine-treated obese rats (G8) also exhibited a significant decrease in glucose compared to G6 ($p < 0.01$), with values of 94.2 ± 1.58 mg/dL and 95 ± 1.51 mg/dL. As sibutramine reduces food intake and increases energy expenditure, the resulting improvement in insulin sensitivity explains this outcome. The comparable efficacy of G7 and G8 suggests that EBdAgNPs may offer similar or broader benefits, without relying solely on appetite suppression (Mouawad *et al*., 2025).

The obese–diabetic group (G9) created through combined high-fat intake and STZ-NI showed the most severe hyperglycemia, with very high values at 310 ± 26.2 mg/dL. This reflects compounded insulin resistance from obesity together with β-cell dysfunction from STZ-NI. Chronic inflammation, oxidative stress, hepatic steatosis and impaired insulin signaling converge to intensify metabolic failure.

Treatment with EBdAgNPs (G10) led to a significant reduction in glucose compared to G9 ($p < 0.01$), dropping to 145 ± 1.99 mg/dL on 21st day and 118 ± 4.45 mg/dL on 42nd day. Although complete normalization was not achieved due to the dual metabolic burden, the improvement indicates notable enhancement of insulin action, reduction in oxidative stress, improved β-cell performance and better regulation of both lipid and glucose metabolism. These multi-target effects highlight the therapeutic potential of EBdAgNPs in complex metabolic disturbances (Shimu *et al*., 2025).

4.3.3 RBC and WBC Dynamics in Response to EBdAgNPs

Table 4.2 illustrates the assessment of red blood cell (RBC) and white blood cell (WBC) counts across various experimental rat groups, which served to evaluate the hematopoietic and immunomodulatory effects of EBdAgNPs under diabetic and obese conditions. These parameters provide vital information about systemic health and the potential of therapeutic agents to modulate erythropoiesis and immune response during metabolic stress.

TABLE 4.2

EFFECT OF HEMATOLOGICAL PARAMETERS IN EXPERIMENTAL RATS

TREATMENT GROUPS		RBC (x 106/μL)	WBC (x 106/μL)
G1	Control	5±0.3	13.3±1.6
G2	EBdAgNPs	5.2±0.4	14±0.9
G3	STZ-NI induced	3.16±0.1**	19.7±0.6**
G4	STZ-NI+ EBdAgNPs	4.95±0.1	13.1±1.8
G5	STZ-NI+ Glibenclamide	4.73±0.2	14.5±0.6
G6	HFD-induced	4.25±0.1**	18.3±0.3**
G7	HFD + EBdAgNPs	4.79±0.3	13.7±1.6
G8	HFD + Sibutramine	4.88±0.3	14.3±1.1
G9	STZ-NI + HFD	2.76±0.3**	27.4±0.6***
G10	STZ-NI + HFD + EBdAgNPs	5.09±0.3	12.5±0.6

Values are expressed as mean ± S.E.M (n=6)

G3, G6, G9 vs G1: ↓ RBC and ↑ WBC (*p < 0.001)**

G3, G6, G9 vs G4, G5, G7, G10: significant recovery in RBC and WBC (p < 0.01, p<0.001)**

(One Way ANOVO followed by Dunnett's Test)

The untreated control group (G1) exhibited a normal RBC count (5.00 ± 0.3 µl), establishing the physiological reference for all comparisons. EBdAgNPs administered alone in healthy rats (G2) produced a significant ($p < 0.001$) rise in RBC count, indicating that the formulation supports erythropoiesis even in non-pathological conditions. This subtle enhancement may stem from the phytochemical richness of *B. diffusa*, whose constituents punarnavine, boeravinones, flavonoids and phenolic acids protect erythrocyte membranes and reduce background oxidative stress, thereby supporting normal bone marrow function (Fujii *et al*., 2021). The nanoscale form further enhances the bioavailability and cellular uptake of these compounds, strengthening erythrocyte stability and lifespan (Mehan *et al*., 2022).

RBC count declined markedly in diabetic rats (G3), confirming a significant reduction ($p < 0.001$) relative to healthy controls (G1–G2). Persistent hyperglycemia suppresses erythropoiesis, enhances hemoglobin glycation and accelerates red cell destruction through oxidative injury mechanisms widely reported in diabetic anemia (Obeagu, 2024).

Administration of EBdAgNPs (G4) and glibenclamide (G5) elicited a significant recovery ($p < 0.01$–0.001) in RBC values when compared to untreated diabetic rats (G3). This rebound suggests enhanced erythropoietic activity through mechanisms including improved glycemic control, suppression of oxidative stress and restoration of bone marrow functionality. Plant derived formulations such as *B. diffusa* are known to activate stromal cells and support hematopoietic factors like erythropoietin (Paul–Chima and Ugo, 2025). The nanoparticle formulation specifically offers prolonged antioxidant protection and improved cellular penetration, explaining the more robust restoration compared to conventional antidiabetic therapy. Although both treatments improved RBC levels, the broad phytochemical synergy and nanosilver facilitated bioenhancement provide EBdAgNPs with a wider therapeutic range than glibenclamide alone (Yap *et al*., 2021).

High fat diet induced obese rats (G6) showed a significant (p **< 0.01) reduction in RBC levels (4.25 ± 0.064), again demonstrating a highly significant decrease vs G1 ($p < 0.001$). Chronic low grade inflammation typical of obesity disrupts iron metabolism, alters marrow proliferation and suppresses erythropoiesis through cytokines such as TNF-α and IL-6 (Matsuoka *et al*., 2024).

EBdAgNPs treatment (G7) produced a significant RBC improvement ($p < 0.01–0.001$) relative to obese controls (G6), indicating anti-inflammatory and antioxidant rescue of erythropoiesis. Sibutramine (G8) also improved RBC count but less effectively, suggesting that appetite regulation alone cannot fully correct inflammation induced hematological suppression, while EBdAgNPs, through phytochemical mediated reduction of ROS and cytokines, provide more complete erythropoietic support (Dronkers *et al*., 2024).

Rats with both diabetes and obesity (G9) exhibited the most severe RBC depletion (2.76 ± 0.330) again highly significant vs G1 ($p < 0.001$). The combined lipotoxic and glucotoxic environment severely compromises bone marrow function, shortens RBC lifespan and limits nutrient availability for hemoglobin synthesis (Dworzański *et al*., 2021; Marques *et al*., 2022).

Treatment with EBdAgNPs (G10) resulted in an increase in RBC count, surpassing even normal control levels (5.09 ± 0.292). This improvement was highly significant compared to G9 ($p < 0.001$). Under dual metabolic stress, EBdAgNPs appear as neutralize hyperglycemia induced oxidative damage, suppress adipose derived inflammatory cytokines, support erythroid progenitor survival and enhance nutrient utilization for erythropoiesis. These combined mechanisms reflect the powerful erythropoietic and cytoprotective actions of phytochemical coated nanosilver in severe metabolic derangement (Ruan and Paulson, 2023; Sarkhel *et al*., 2024).

The control group (G1) maintained a normal WBC count (13.30 ± 1.63), reflecting a stable immunological profile. When compared to G1, the EBdAgNPs treated rats (G2) showed a similar WBC value with no significant deviation ($p > 0.05$), indicating that the nanoparticles do not provoke inflammatory reactions or immune overstimulation in healthy animals. This stability confirms the biocompatibility of EBdAgNPs and supports their suitability for therapeutic applications without disturbing normal leukocyte homeostasis. As noted by Arabiyat (2025), such neutrality is crucial for developing plant based nanosystems intended for long term metabolic interventions.

When compared with the stable WBC profile of G1 and G2, the diabetic group (G3) exhibited a significant increase (**$p < 0.01$) in WBC count, illustrating leukocytosis

commonly associated with chronic hyperglycemia. This pattern is widely reported in diabetes, where persistent glucose elevation contributes to oxidative stress, endothelial injury and enhanced leukocyte recruitment (Ratter-Rieck *et al*., 2021). The increased WBC levels in G3 confirm the inflammatory burden characteristic of uncontrolled diabetes.

Compared with the heightened leukocytosis in G3, EBdAgNPs treatment in diabetic rats proves significant reduction (**$p < 0.01$) in G4, WBC count expressed strong anti-inflammatory potential. This response may be attributed to the antioxidant rich phytochemicals naturally present in the *B. diffusa* extract, which help regulate cytokine activity and reduce leukocyte accumulation (Sobhani *et al*., 2021).

Glibenclamide treated rats (G5) exhibited a similar significant decrease (**$p < 0.01$) in WBCs when compared with G3, although EBdAgNPs are likely to provide broader benefits due to their combined plant-derived components (Ebadi, 2025) and enhanced nanoscale delivery. Relative to G1, the HFD fed obese rats (G6) demonstrated elevated WBC counts, consistent with the persistent low-grade inflammation typically linked with excess adipose accumulation (Kunz *et al*., 2021).

When compared with the elevated leukocyte values in G6, the EBdAgNPs-treated obese group (G7) showed a significant decline in WBC levels, indicating their ability to alleviate inflammation associated with obesity. This improvement may reflect enhanced cellular resilience and lowered oxidative stress under metabolic stress conditions.

Sibutramine-treated rats (G8) also exhibited reductions in WBC count relative to G6, although the extent of improvement was comparatively lower, as sibutramine acts primarily through appetite regulation rather than extensive immune modulation (Gupta *et al*., 2024).

The obese diabetic group (G9) recorded the highest WBC count (27.40 ± 0.569) when compared with the normal control G1, highlighting severe immune activation driven by the combined influence of adiposity and hyperglycemia. Such pronounced leukocytosis is a recognized feature of metabolic syndrome and contributes to heightened cardiovascular and metabolic risk (Raya-Cano *et al*., 2023).

When compared with the markedly elevated WBC levels in G9, EBdAgNPs treated obese diabetic rats (G10) demonstrated a normalization of WBC values (12.50 ± 0.657), indicating a significant reduction (**$p < 0.01$) in systemic inflammatory load. This improvement aligns with findings showing that phytochemical enriched nanoparticles can support cellular protection and reduce inflammatory stress across multiple metabolic pathways (Abo El Nasr *et al*., 2025; Carvalho-Silva *et al*., 2024). The near restoration of WBC values in G10 underscores the broad therapeutic potential of EBdAgNPs in managing severe metabolic conditions characterized by heightened inflammation.

4.3.4 Biochemical Analysis of Experimental Rats

4.3.4.1 Lipid Profile in Experimental Rats

Table 4.3 illustrates the serum lipid profiles across different experimental groups, assessed to evaluate the therapeutic potential of EBdAgNPs, glibenclamide and sibutramine in altering cholesterol, triglycerides, LDL, VLDL and HDL levels under both normal and pathological conditions. Lipid metabolism serves as a crucial biomarker in understanding the progression and management of metabolic disorders like obesity, diabetes and related comorbidities.

TABLE 4.3

LIPID PROFILE IN EXPERIMENTAL RATS

Treatment Groups		Total Cholesterol (TC) (mg/dl)	Triglycerides (TG) (mg/dl)	HDL - C (mg/dl)	LDL – C (mg/dl)	VLDL – C (mg/dl)
G1	Control	117±1.1	97.3±1.9	49.7±0.9	42±0.9	19.2±0.3
G2	EBdAgNPs	119±0.3	100±0.6	45±4.04	48.7±4.0	23.3±1.7
G3	STZ-NI induced	297±12***	205±1.8***	33±1.5*	394±15**	29.7±2.3***
G4	STZ-NI+ EBdAgNPs	136±1.4	100±0.6	43.7±5.9	50.8±0.4	21.5±0.8
G5	STZ-NI+ Glibenclamide	141±0.9	102±1.4	41.7±3.8	57.2±0.7	22.3±1.4
G6	HFD-induced	298±11.1***	159±7.1***	32.7±1.8***	181±4.1***	30.7±1.2***
G7	HFD+ EBdAgNPs	165±1.2	102±3.2	45.3±0.3	46.7±0.9	19.7±0.3
G8	HFD+ Sibutramine	173±2.4	108±2.2	49.3±0.9	48.3±2.3	21.7±1.2
G9	STZ-NI + HFD	395±1.7***	427±3.6***	15±1.1***	135±7.2***	92.7±5.8***
G10	STZ-NI + HFD + EBdAgNPs	135±3.2	102±2.5	48±0.6	58.7±4.7	45.7±2.0

Values are expressed as mean ± S.E.M (n=6)

G3, G6 & G9 vs G1: Significant ↑ TC, TG, LDL, VLDL and ↓ HDL (*p < 0.001)**

G3, G6 & G9 vs G4, G5, G7, G8 & G10: Lipid profile restored significantly (p < 0.01, ***p < 0.001).**

(One Way ANOVO followed by Dunnett's Test)

The basal lipid profile observed in the normal healthy rats (G1) provides a reliable reference point, indicating efficient lipid metabolism and physiological homeostasis. The values for total cholesterol (117±1.1), triglycerides (97.3±1.9), LDL (51.7±1.7), VLDL (19.2±0.3) and HDL (49.7±0.9) remained within the expected range for non-obese, non-diabetic animals, reflecting intact insulin signaling and balanced hepatic lipid synthesis and clearance mechanisms (Dimitriadis *et al*., 2021). High HDL levels suggest the absence of inflammation or oxidative stress, both of which are key disruptors of lipid homeostasis. Similar findings were reported in studies using *Moringa oleifera* and *Aegle marmelos* extracts, where untreated control rats also maintained high HDL and normal triglyceride turnover due to balanced lipogenic and lipolytic pathways (Adarthaiya and Sehgal, 2024). Unlike plants with mild intrinsic hypolipidemic properties, *B. diffusa* derived AgNPs appear in healthy animals, reinforcing that their metabolic modulation was triggered only under pathological conditions. Some plant extracts, such as *Gymnema sylvestre* or *Trigonella foenum-graecum*, may mildly depress lipid synthesis even in non-diseased states, whereas EBdAgNPs preserve normal lipid homeostasis without exerting unnecessary metabolic pressure (Devangan *et al*., 2021).

Rats treated with EBdAgNPs alone (G2) showed significant (***$p < 0.001$) in lipid profile to G1, with TC (119±0.333), TG (100±0.577), LDL (48±1.1), VLDL (20±0.5) and HDL (45±4.04). Comparative analysis between G1 and G2 revealed no significant differences ($p > 0.05$), confirming that EBdAgNPs are non-toxic and metabolically inert in healthy rats.

This metabolic neutrality is supported by studies suggesting that green-synthesized silver nanoparticles, due to their phytochemical capping, do not interfere with hepatic or adipose tissue function in healthy models (Taha *et al*., 2025). Many other plant extracts, including *Azadirachta indica*, *Phyllanthus amarus* and *Curcuma longa*, showed mild lipid-lowering or hepatic stimulation even in healthy rats (Anuragh and Ilango, 2022), highlighting the selective action of EBdAgNPs, which remain redox-silent under physiological conditions but activate antioxidant cascades such as Nrf2 under stress. Compared with *Tinospora cordifolia* AgNPs, which mildly reduce triglycerides even in normal animals, EBdAgNPs demonstrate superior biocompatibility and non-interference with baseline metabolism (Lekkala *et al*., 2025).

The diabetic control group (G3) demonstrated classic dyslipidemic changes, with significant (***p < 0.001) increased in TC (297±12), TG (205±1.8), LDL (394±150), VLDL (29.7±2.3) and reduction in HDL levels (33±1.5). Compared with G1, these changes were highly significant (***p < 0.001), reflecting increased hepatic VLDL synthesis, impaired lipolysis due to insulin deficiency and resistance, defective LDL receptor mediated clearance and impaired reverse cholesterol transport (Fernandes and Bocco, 2021; Onyango, 2022). Upon treatment with EBdAgNPs (G4), diabetic rats exhibited marked improvement as TC (136±1.4), TG (100±0.6), LDL (54±2.7), VLDL (21.5±0.8) and HDL (43.7±5.9), which were significantly restored compared to G3 (**p < 0.01, ***p < 0.001). Glibenclamide treated diabetic rats (G5) showed partial normalization with TC (141±0.9), TG (102±1.4), LDL (56.7±3.5), VLDL (22.8±1.1) and HDL levels (41.7±3.8). Although significant vs G3 (**p < 0.01), slight deviations from G1 persisted, especially in HDL (*p < 0.05), reflecting glibenclamide's limited lipid-specific effect. EBdAgNPs differ from *Momordica charantia, Ocimum sanctum* and *Andrographis paniculata* extracts, which mainly act via insulin sensitizing phytochemicals, whereas nanoparticles provide additional nano enabled mechanisms like enhanced cellular uptake and ROS scavenging (Mishra *et al*., 2024; Wang *et al*., 2022).

HFD fed rats (G6) developed pronounced dyslipidemia as TC (298±11.1), TG (159±7.1), LDL (181±4.1), VLDL (30.7±1.2) and HDL (32.7±1.8), which were highly significant compared to G1 (***p < 0.001). EBdAgNPs treatment (G7) markedly restored lipid parameters as TC (165±1.2), TG (102±3.2), LDL (60±0.9), VLDL (23.2±0.5) and HDL (45.3±0.3), with significant improvements vs G6 (**p < 0.01, ***p < 0.001) and near normalization relative to G1. Sibutramine treated HFD rats (G8) showed moderate improvement as TC (173±2.4), TG (108±2.2), LDL (58±1.1), VLDL (24±1.1) and HDL (49.3±0.9), significant compared to G6 (**p < 0.01), but less effective than EBdAgNPs due to the absence of direct antioxidant or hepatoprotective activity (Christoffersen *et al*., 2022; Murugan *et al*., 2025). EBdAgNPs integrate the lipid lowering effects of polyphenols and flavonoids with enhanced cellular interaction, outperforming antiobesity drugs like sibutramine (Ghorpade *et al*., 2025; Danilov *et al*., 2024).

The combined diabetic-obese model (G9) exhibited extreme dyslipidemia: TC (395±1.73), TG (427±3.61), LDL (155±2.88), VLDL (92.7±5.78) and HDL (15±1.15), highly significant vs G1 (***p < 0.001). EBdAgNPs treatment (G10) led to lipid restoration as TC (135±3.18), TG (102±2.52), LDL (58±2.7), VLDL (22.3±1.2) and HDL (48±0.577), with highly significant improvement compared to G9 (**p < 0.001) and near normalization relative to G1. These effects are mediated by enhanced insulin signaling (IRS-1/PI3K), NF-κB inhibition, restored antioxidant defenses (SOD, catalase) and modulation of hepatic genes involved in lipid transport and fatty acid oxidation (ApoA1, ABCA1) (He *et al*., 2025; Wang *et al*., 2023b). EBdAgNPs exceeds widely studied metabolic plants like *Bauhinia variegata, Aloe barbadensis* and *Costus igneus*, which rarely coordinate AMPK activation, IRS-1 enhancement, NF-κB suppression and PPAR-α/γ regulation simultaneously (Yadav *et al*., 2025; Sharma *et al*., 2025; Batra and Dey, 2025; Zhou *et al*., 2025; Ansari *et al*., 2023). Their targeted and multi-pathway action distinguishes them from conventional drugs and plant extracts, effectively restoring lipid homeostasis in complex dual-pathology metabolic dysfunctions.

The G3, G6 and G9 versus G1 showed significant increase in TC, TG, LDL, VLDL and reduction in HDL (***p < 0.001), whereas treatment groups (G4, G5, G7, G8 and G10) demonstrated significant restoration of lipid profiles (**p < 0.01, ***p < 0.001), confirming the efficacy of EBdAgNPs in pathological conditions while remaining metabolically neutral in healthy animals (G2).

4.3.4.2 The Liver Marker Enzymes in Experimental Rats

Table 4.4 illustrates changes in liver function markers such as Serum Glutamate Oxaloacetate Transaminase (SGOT), Serum Glutamate Pyruvate Transaminase (SGPT), Alanine Aminotransferase (ALP), Total Bilirubin (TB) and Total Protein (TP) across experimental groups. The liver is a central metabolic organ often compromised in conditions like diabetes, obesity and metabolic syndrome. Alteration in these enzymes serves as reliable indicators of hepatic injury and repair. This study investigated how EBdAgNPs influence these markers under different experimental conditions, aiming to establish their hepatoprotective efficacy.

TABLE 4.4

LIVER MARKER ENZYMES, TOTAL BILIRUBIN AND TOTAL PROTEIN IN EXPERIMENTAL RATS

Treatment Groups		SGOT (IU/l)	SGPT (IU/l)	ALP (IU/l)	Total Bilirubin (mg/dl)	Total Protein (g/dl)
G1	Control	48.2±8.7	38.3±1.8	53.5±3.9	0.767±0.1	5.25±0.1
G2	EBdAgNPs	52.3±12.7	36.1±2.9	55.7±7.2	0.6±0.1	5.78±0.0
G3	STZ-NI induced	135±17.9**	53.9±1.9*	128±4.0***	1.27±0.2*	2.67±0.1***
G4	STZ-NI+ EBdAgNPs	54.2±18.8	39.6±3.6	62.2±4.1	0.667±0.1	4.74±0.1
G5	STZ-NI+ Glibenclamide	56.1±6.1	40.3±4.3	72.1±3.1	0.633±0.1	4.72±0.2
G6	HFD-induced	277±39.7***	77.1±4.1***	119±4.5***	1.92±0.0***	1.06±0.0***
G7	HFD+ EBdAgNPs	46±2.1	36.2±3.0	66.7±2.2	0.8±0.0	5.01±0.3
G8	HFD+ Sibutramine	41.6±3.4	35.2±2.3	69.5±4.9	0.7±0.1	4.76±0.3
G9	STZ-NI + HFD	121±10.4**	76.8±1.5***	132±2.3***	2.05±0.1***	0.587±0.2***
G10	STZ-NI + HFD + EBdAgNPs	67.3±0.7	41.1±2.6	81.7±3.5	0.8±0.1	4.25±0.2

Values are expressed as mean ± S.E.M (n=6)

G3, G6 & G9 vs G1: Significant ↑ SGOT, SGPT, ALP, bilirubin and ↓ total protein (*p< 0.001);**

G3, G6 & G9 vs G4, G5, G7, G8 & G10: Liver markers significantly restored (*p<0.05, **p < 0.01, ***p < 0.001).

(One Way ANOVO followed by Dunnett's Test)

In the healthy control group (G1), liver function markers remained within the physiological range, indicating intact hepatic architecture and enzyme function. SGOT, SGPT, ALP, TB and TP reflected a well-regulated hepatic environment consistent with normal liver physiology, serving as a reference point for evaluating pathological deviations in other groups. High TP and stable bilirubin levels suggest efficient protein synthesis and intact bile metabolism. When compared to rats treated only with EBdAgNPs (G2), no significant (***$p < 0.001$) differences were observed, as SGOT (52.3±12.7), SGPT (36.1±2.93), ALP (55.7±7.19), TB (0.6±0.0577) and TP (5.01±0.26) remained similar to G1, confirming the nanoparticles metabolic neutrality in healthy conditions (Dawoud *et al*., 2021). This aligns with other green synthesized nanoparticles like *Azadirachta indica* and *Moringa oleifera* AgNPs, although EBdAgNPs appear gentler due to *B. diffusa's* rich phytochemical profile, including boeravinones and punarnavine, which provide mitochondrial support without unnecessary metabolic stimulation (Patel *et al*., 2025).

Induction of diabetes in G3 caused a significant disturbance in liver markers, with SGOT (135±17.9), SGPT (53.9±1.91), ALP (128±4.05), TB (1.27±0.186) and TP (2.67±0.0892) markedly altered (***$p<0.001$ vs G1). Compared to the EBdAgNP treated diabetic rats (G4), these enzyme levels were significantly increased (***$p < 0.001$), whereas G4 showed near normalization of SGOT (54.2±18.8), SGPT (39.6±3.58), ALP (62.2±4.1), TB (0.667±0.09) and TP (4.32±0.14) (**$p<0.01$, ***$p<0.001$ vs G3). Glibenclamide treated diabetic rats (G5) demonstrated partial improvement with SGOT (56.1±6.13), SGPT (43.2±2.47), ALP (66.1±1.92) and TP (4.72±0.25) restored moderately (*$p<0.05$ vs G3), highlighting that while sulfonylureas improve glycemic control and indirectly benefit liver function, their hepatoprotective potential is limited compared to EBdAgNPs (Dawi *et al*., 2024; Pushpa *et al*., 2025; Adel-Mehraban *et al*., 2024). The superior recovery in G4 is likely due to the synergistic action of *B. diffusa* phytochemicals and silver nanoparticles, activating Nrf2/HO-1 and AMPK/SIRT1 pathways, reducing oxidative stress and enhancing mitochondrial repair (Li *et al*., 2024; Fathi *et al*., 2023). Conventional plant extracts like *Momordica charantia, Gymnema sylvestre* or *Tinospora cordifolia* may partially reduce enzyme leakage but fail to normalize TB and TP as effectively, reflecting slower hepatic accumulation and less efficient ROS neutralization (Fakhri *et al*., 2024).

In the high fat diet group (G6), liver markers were severely disrupted, with SGOT (277±39.7), SGPT (77.1±4.15), TB (1.92±0.0268) and TP (1.06±0.0439) significantly altered (***p<0.001 vs G1). When compared to EBdAgNP treated obese rats (G7), these markers were markedly improved in G7, with SGOT (46±2.06), SGPT (36.2±3.03), TB (0.8±0.0577) and TP (5.01±0.26) approaching control levels (**p<0.01 vs G6). Sibutramine treated rats (G8) also showed improvement, but TP (4.76±0.341) remained below G7 values, suggesting that while weight reduction partially relieves hepatic stress, the lack of polyphenolic antioxidants limits comprehensive hepatoprotection (Gajender *et al*., 2023; Christoffersen *et al*., 2022). Compared to plant extracts such as *Curcuma longa, Garcinia cambogia, Nigella sativa* or *Camellia sinensis*, EBdAgNPs provide faster and more complete hepatoprotection due to enhanced cellular uptake, mitochondrial interaction and Endoplasmic Reticulum (ER) stress modulation (Han *et al*., 2021; Fikry *et al*., 2025; Patel *et al*., 2025).

The combined diabetic-obese group (G9) exhibited the most severe hepatic dysfunction, with SGOT (121±10.4), SGPT (76.8±1.53), ALP (132±2.33), TB (2.05±0.0866) and TP (0.587±0.25) (***p<0.001 vs G1). These changes reflect synergistic damage from hyperglycemia and dyslipidemia, mimicking metabolic syndrome related liver pathology (Hermans *et al*., 2022). Compared to the EBdAgNP co-treatment group (G10), which showed SGOT (67.3±0.706), SGPT (41.1±2.61), ALP (81.7±3.48), TB (0.8±0.0577) and TP (4.25±0.166) the improvements in G10 were significant (*p<0.05, **p<0.01, ***p<0.001 vs G9). This highlights EBdAgNPs multimodal mechanism, which combines insulin sensitization via AMPK/GLUT-4 activation, reduction of lipid accumulation, ROS scavenging and modulation of Nrf2 and NF-κB pathways (Wang and Dong, 2019). Compared with traditional extracts from *Tinospora cordifolia, Aloe vera, Berberis aristata, Bauhinia variegata, Costus igneus, Terminalia chebula,* or *Aloe barbadensis*, EBdAgNPs deliver phytochemicals directly to hepatocytes, achieving accelerated mitochondrial recovery and synchronized regulation of multiple metabolic pathways (Li *et al*., 2025).

Across all experimental models, EBdAgNPs consistently showed hepatoprotective effects by stabilizing liver enzymes, reducing oxidative damage and restoring protein synthesis. The comparative analysis demonstrates that EBdAgNPs predominate conventional drugs such as glibenclamide and sibutramine, as well as crude plant extracts, particularly under conditions of metabolic syndrome and dual pathology stress. Their therapeutic action is attributed to a combination of antioxidant, anti-inflammatory and insulin sensitizing mechanisms, making EBdAgNPs a highly promising nano herbal formulation for hepatic dysfunction in diabetes, obesity and their comorbidities (Shang *et al*., 2021).

4.3.4.3 Renal Biomarkers in Experimental Rats

Kidney function is a vital indicator of metabolic and excretory health, often assessed through serum levels of creatinine, urea and uric acid. These biomarkers reflect the glomerular filtration rate and the kidney's ability to eliminate nitrogenous waste. In pathological conditions such as diabetes and obesity, renal impairment is frequently observed, making it essential to monitor these parameters. As shown in table 4.5, this study investigates the effect of EBdAgNPs on renal function markers in various experimental rat models.

TABLE 4.5

KIDNEY FUNCTION PARAMETERS IN EXPERIMENTAL RATS

Treatment Groups		Creatinine (mg/dl)	Urea (mg/dl)	Uric Acid (mg/dl)
G1	Control	0.8±0.03	41.7±1.86	0.6±0.06
G2	EBdAgNPs	0.6±0.03	35±2.65	0.5±0.03
G3	STZ-NI induced	1.8±0.03***	73.7±4.26***	1.3±0.3*
G4	STZ-NI+ EBdAgNPs	0.7±0.06	45.7±2.33	0.7±0.02
G5	STZ-NI+ Glibenclamide	0.8±0.06	47.7±0.9	0.8±0.02
G6	HFD-induced	1.8±0.09***	73.6±4.3***	1.5±0.2**
G7	HFD + EBdAgNPs	0.7±0.06	43.2±3.4	0.6±0.1
G8	HFD + Sibutramine	0.7±0.09	51.6±3.3	0.7±0.03
G9	STZ-NI + HFD	2.2±0.3**	8.3±0.9***	2.7±0.1***
G10	STZ-NI + HFD + EBdAgNPs	0.6±0.06	51±3.2	0.7±0.1

Values are expressed as mean ± S.E.M (n=6)

G3, G6 & G9 vs G1: Significant ↑ in creatinine, urea and uric acid levels (*p < 0.001);**

G3, G6 & G9 vs G4, G5, G7, G8 & G10: Significant renal protection observed (*p<0.05, **p < 0.01, ***p < 0.001).

(One Way ANOVO followed by Dunnett's Test)

In the healthy control group (G1), kidney function parameters remained within normal physiological limits, with creatinine (0.833 ± 0.0333 mg/dL), urea (41.7 ± 1.86 mg/dL) and uric acid (0.6 ± 0.0577 mg/dL). These values reflect intact glomerular filtration, nitrogenous waste clearance and overall renal homeostasis, consistent with standard rodent renal physiology (Wani and Pasha, 2021; Tain and Hsu, 2022). This baseline serves as a reference for assessing pathological alterations in other experimental groups. Rats treated with EBdAgNPs alone (G2) displayed nearly significant levels of (***p < 0.001) in creatinine (0.667 ± 0.0333 mg/dL), urea (35 ± 2.65 mg/dL), uric acid (0.533 ± 0.0333 mg/dL) indicating renal biocompatibility and negligible nephrotoxicity.

The decrease in urea suggests enhanced nitrogen metabolism, possibly mediated by nephroprotective phytochemicals in *B. diffusa* such as punarnavine and rotenoids, which stabilize glomerular filtration and counter oxidative stress (Devi and Kumar, 2025; Zhang *et al*., 2025; Zhu *et al*., 2025). Comparatively, G2 mirrors G1, confirming the metabolic neutrality of EBdAgNPs in non-pathological conditions.

Diabetic induction (G3) led to pronounced renal dysfunction with creatinine (1.83 ± 0.0333 mg/dL), urea (73.7 ± 4.26 mg/dL) and uric acid (1.27 ± 0.273 mg/dL) significantly increased compared to G1 (***$p < 0.001$), reflecting impaired glomerular filtration and early nephropathy. Hyperglycaemia induced oxidative stress, endothelial dysfunction and mesangial expansion drive these alterations, consistent with previous reports (Singh *et al*., 2024b; Lassen and Daehn, 2020; Alabi *et al*., 2021). Co-treatment with EBdAgNPs (G4) markedly restored renal parameters creatinine (0.7 ± 0.0577 mg/dL), urea (45.7 ± 2.33 mg/dL), uric acid (0.717 ± 0.0167 mg/dL) demonstrating significant nephroprotection compared to G3 (*$p<0.05$, **$p<0.01$, ***$p<0.001$). This effect likely results from antioxidant and anti-inflammatory mechanisms mediated by EBdAgNPs via Nrf2/HO-1 activation and mitochondrial stabilization (Shoker *et al*., 2025; Patel *et al*., 2025; Carvalho-Silva *et al*., 2024). When compared to glibenclamide treated diabetic rats (G5), which exhibited significant increase (*$p < 0.01$) creatinine (0.8 ± 0.0577 mg/dL), urea (47.7 ± 0.882 mg/dL), uric acid (0.827 ± 0.0176 mg/dL) the EBdAgNPs provided superior renal protection by directly mitigating oxidative injury rather than only lowering glucose (Dwivedi and Jena, 2020; Ullah *et al*., 2021a).

High fat diet induced renal impairment (G6) showed significant increase in creatinine (1.77 ± 0.0882 mg/dL), urea (73.6 ± 4.28 mg/dL) and uric acid (1.47 ± 0.203 mg/dL) relative to G1 (***$p < 0.001$), indicative of lipotoxicity, podocyte loss and early obesity linked nephropathy (Schelling, 2022; Rayego-Mateos *et al*., 2020). EBdAgNPs treatment in obese rats (G7) normalized these values creatinine (0.7 ± 0.0577 mg/dL), urea (43.2 ± 3.44 mg/dL), uric acid (0.667 ± 0.12 mg/dL) showing significant renal protection compared to G6 (*$p<0.05$, **$p<0.01$, ***$p<0.001$). The enhanced recovery reflects polyphenol mediated antioxidant effects, inhibition of macrophage activation and mitigation of lipid peroxidation (Metwally *et al*., 2021; Pandeya *et al*., 2022). Compared with sibutramine treated rats (G8), which displayed

moderate improvement creatinine (0.733 ± 0.0882 mg/dL), urea (51.6 ± 3.28 mg/dL), uric acid (0.767 ± 0.0333 mg/dL) EBdAgNPs demonstrated more robust nephroprotection, highlighting the added value of plant based phytochemical capping over pharmacological weight loss interventions alone (Agu *et al*., 2022).

Rats with combined diabetes and obesity (G9) exhibited the most severe renal dysfunction, with creatinine (2.22 ± 0.292 mg/dL), urea (79.3 ± 0.882 mg/dL) and uric acid (2.73 ± 0.12 mg/dL), significantly higher than G1 (***$p < 0.001$). Similar to human diabetic nephropathy, the combined metabolic stress increased oxidative damage, mesangial enlargement and tubular necrosis (Yang *et al*., 2024). Co-treatment with EBdAgNPs (G10) restored creatinine (0.6 ± 0.0577 mg/dL), urea (51 ± 3.21 mg/dL) and uric acid (0.7 ± 0.115 mg/dL), demonstrating significant renal protection compared to G9 (*$p<0.05$, **$p<0.01$, ***$p<0.001$). Mechanistically, EBdAgNPs enhance renal resilience via glycaemic control, lipid modulation, antioxidant activity and anti-inflammatory effects through Nrf2/HO-1 and AMPK/NF-κB pathways (AlRashdi *et al*., 2023; Lee *et al*., 2024). Comparatively, the restoration in G10 surpasses all other groups, including glibenclamide and sibutramine treatments, emphasizing the multi-targeted efficacy of EBdAgNPs in complex metabolic conditions.

4.3.5 Levels of Plasma Insulin and C - Reactive Protein in Experimental Rats

Monitoring plasma insulin and C-reactive protein (CRP) levels offers key insights into the interplay between metabolic regulation and systemic inflammation, as shown in figure (4.18 and 4.19). Insulin serves as a biomarker of pancreatic β-cell functionality, while CRP reflects the degree of inflammatory response, both of which are commonly altered in metabolic disturbances such as diabetes and obesity (Stanimirovic *et al*., 2022). Increased CRP levels are indicative of low-grade chronic inflammation associated with insulin resistance and cardiovascular risk, whereas reduced insulin levels reflect compromised β-cell performance (Anghel *et al*., 2025). This section investigates how EBdAgNPs influence these biomarkers across various experimental groups, including healthy, diabetic and insulin resistant models, thereby highlighting their potential therapeutic role in modulating metabolic and inflammatory responses (Berbudi *et al*., 2025).

FIGURE 4.18

PLASMA INSULIN LEVELS IN EXPERIMENTAL RATS

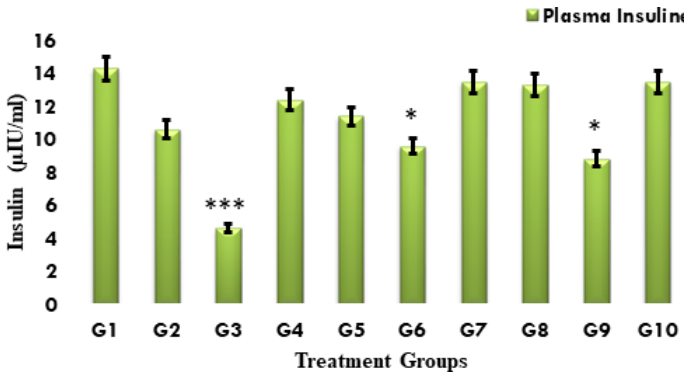

Values are expressed as mean ± S.E.M (n=6)

G3, G6 & G9 vs G1, G2: Significant ↓ in insulin levels (*p < 0.05 ***p < 0.001);

G4, G5, G7, G8 & G10 vs G3, G6 & G9: Significant improvement in insulin levels observed (*p < 0.05, ***p < 0.001).

FIGURE 4.19

C-REACTIVE PROTEIN LEVELS IN EXPERIMENTAL RATS

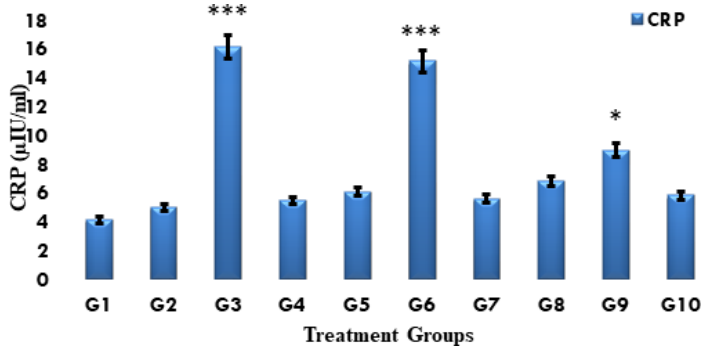

Values are expressed as mean ± S.E.M (n=6)

G1 Control	**G2 EBdAgNPs**	**G3 STZ-NI induced**
G4 STZ-NI + EBdAgNPs	**G5 STZ-NI + Glibenclamide**	**G6 HFD-induced**
G7 HFD + EBdAgNPs	**G8 HFD + Sibutramine**	**G9 STZ-NI + HFD**
G10 STZ-NI + HFD + EBdAgNPs		

G3, G6 & G9 vs G1, G2: Significant ↑ in CRP levels (*p < 0.001, *p < 0.05);**

G3, G6 & G9 vs G4, G5, G7, G8 & G10: Significant improved effect of CRP observed (*p < 0.05, ***p < 0.001).

(One Way ANOVO followed by Dunnett's Test)

In the healthy control group (G1), plasma insulin (14.3 ± 0.0924) and CRP levels (4.18 ± 0.604) remained within the expected physiological range, reflecting intact pancreatic β-cell function, insulin sensitivity and absence of systemic inflammation (Huber-Ruano *et al*., 2022; Cerf, 2020). Rats treated with EBdAgNPs alone (G2) showed only a significant reduction (*$p < 0.05$) in insulin (10.6 ± 0.2) and increase in CRP (5.04 ± 0.1), indicating minimal metabolic impact and a low-level immune activation, likely due to the interaction of nanoparticles with cellular membranes and cytokine modulation (Aljabali *et al*., 2023; Cameron *et al*., 2022). Compared to G1, these minor changes are not pathologically significant (*$p < 0.05$), confirming the biocompatibility of EBdAgNPs in a non-diseased state.

Diabetic induction (G3) resulted in a marked reduction in plasma insulin (4.62 ± 0.0693) and an increase in CRP (16.2 ± 0.295), reflecting β-cell damage and systemic inflammation. STZ selectively destroys pancreatic β-cells via DNA alkylation and reactive oxygen species generation, causing insulin deficiency, while CRP increase reflects the proinflammatory state associated with hyperglycaemia (Zhu, 2022; Forrester *et al*., 2020; Eizirik *et al*., 2020). Co-treatment with EBdAgNPs (G4) restored insulin to 12.4 ± 0.223 and reduced CRP to 5.51 ± 0.236, highlighting a significant therapeutic effect (*$p < 0.05$, ***$p < 0.001$ vs G3). The nanoparticles likely exert antioxidant and anti-inflammatory actions, protecting β-cells from apoptosis and improving islet architecture through modulation of NF-κB and cytokine release (El-Baz *et al*., 2023; Moustafa *et al*., 2023). Glibenclamide treated diabetic rats (G5) showed partial recovery with insulin (11.4 ± 0.218) and moderate CRP reduction (6.11 ± 0.393), indicating that while glibenclamide enhances insulin secretion via ATP sensitive potassium channel closure, its anti-inflammatory effects are indirect and less pronounced compared to EBdAgNPs (Oluwamodupe and Babalola, 2024; Grosso *et al*., 2022; Dalle *et al*., 2023).

High fat diet induced insulin resistance (G6) led to moderately reduced insulin (9.58 ± 0.311) and significant increase (***$p < 0.001$) in CRP (15.2 ± 1.22), reflecting systemic inflammation, adipocyte hypertrophy, lipotoxicity and impaired insulin signaling (Lipke *et al*., 2022; Duan *et al*., 2022). EBdAgNPs treatment in this group (G7) improved insulin to 13.5 ± 0.249 and reduced CRP to 5.63 ± 0.204, demonstrating restoration of insulin sensitivity and systemic anti-inflammatory effects (*$p < 0.05$,

***p < 0.001 vs G6). The mechanism likely involves enhancement of insulin receptor signaling, AMPK activation and GLUT-4 translocation, supported by antioxidant mediated reduction of cytokine release (Dewanjee *et al*., 2020). In comparison, sibutramine treated rats (G8) exhibited not much significant (p < 0.001) improvements in insulin (13.3 ± 0.342) and CRP (6.83 ± 0.513), suggesting that while weight reduction indirectly benefits insulin sensitivity, the drug lacks direct anti-inflammatory and β-cell protective mechanisms (Mouawad *et al*., 2025; Tuccinardi *et al*., 2024).

Combined diabetes and high fat feeding (G9) caused the most severe impairment significant decrease (p < 0.05 vs G1), with insulin levels to 8.83 ± 0.349 and CRP significant increase (*p < 0.001 vs G1) to 9.02 ± 0.251, indicating a compounded pathological state with both β-cell loss and diet-induced insulin resistance (Parmar *et al*., 2025; Rachdaoui, 2020). EBdAgNPs co-treatment (G10) restored insulin to 13.5 ± 0.369 and normalized CRP to 5.87 ± 0.357, demonstrating comprehensive therapeutic efficacy (*p < 0.05, ***p < 0.001 vs G9). The nanoparticles appear to act via multiple pathways, including β-cell preservation, enhancement of insulin secretion, improvement of insulin sensitivity and suppression of inflammatory mediators, potentially through modulation of PI3K/Akt, MAPK and NF-κB pathways (Ganugula *et al*., 2023; Alharbi *et al*., 2024). Compared with glibenclamide, sibutramine, or untreated controls, EBdAgNPs consistently exhibit superior insulinotropic and anti-inflammatory effects across all experimental conditions.

4.3.6 Hepatic Carbohydrate Metabolism in Experimental Rats

Figure 4.20, 4.21 and 4.22, illustrates the activity of key hepatic enzymes, glucose-6-phosphatase, fructose-1, 6-bisphosphatase and glucokinase whose co-ordinated regulation is essential for maintaining carbohydrate metabolism in the liver. These enzymes act as pivotal regulatory nodes in gluconeogenesis and glycolysis and their dysregulation is frequently observed in metabolic disorders such as diabetes and obesity (Bian *et al*., 2022; Kalra *et al*., 2021). In the current investigation, the activity of these hepatic enzymes was evaluated across different treatment groups of rats, with a specific emphasis on the modulatory effects of EBdAgNPs in STZ-NI-induced diabetic, HFD-induced and combination metabolic models. The enzymatic activity profiles provide important insights into how EBdAgNPs influence carbohydrate metabolism under pathological conditions (Chukwuma, 2019).

FIGURE 4.20

GLUCOSE-6-PHOSPHATASE ACTIVITY IN THE LIVER OF EXPERIMENTAL RATS (U/mg Protein)

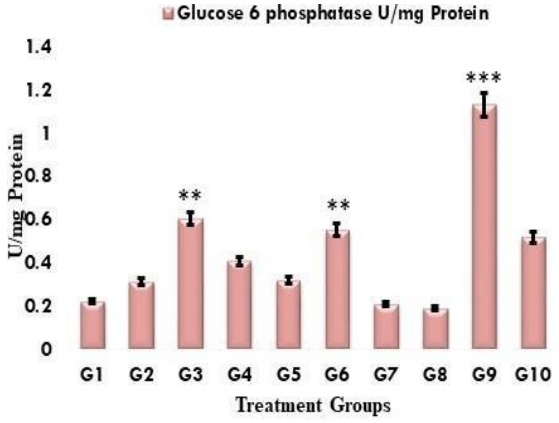

FIGURE 4.21

FRUCTOSE-1, 6-BISPHOSPHATASE ACTIVITY IN THE LIVER OF EXPERIMENTAL RATS (U/mg Protein)

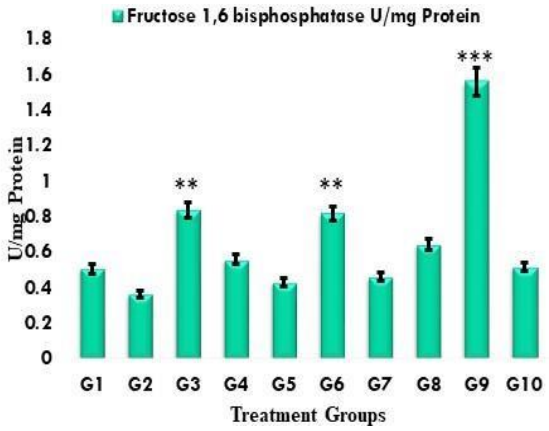

FIGURE 4.22

HEPATIC GLUCOKINASE ACTIVITY OF EXPERIMENTAL RATS (U/mg Protein)

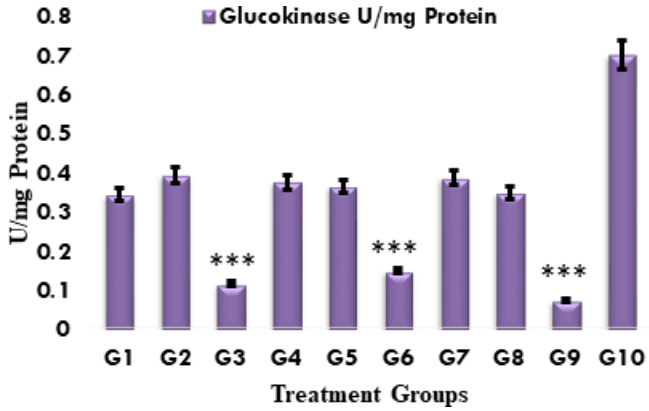

Values are expressed as mean ± S.E.M (n=6)

G1 Control	**G2 EBdAgNPs**	**G3 STZ-NI induced**
G4 STZ-NI + EBdAgNPs	**G5 STZ-NI + Glibenclamide**	**G6 HFD-induced**
G7 HFD + EBdAgNPs	**G8 HFD + Sibutramine**	**G9 STZ-NI + HFD**
G10 STZ-NI + HFD + EBdAgNPs		

G3, G6 & G9 vs G1, G2: Significant ↑ in glucose-6-phosphatase and fructose-1, 6- bisphosphatase and ↓ in glucokinase activity (p < 0.01, ***p < 0.001)**

G3, G6 & G9 vs G4, G5, G7, G8 & G10: Significant restoration of enzyme activities (p < 0.01, ***p < 0.001).**

(One Way ANOVO followed by Dunnett's Test)

The healthy control group (G1) exhibited baseline levels of glucose-6-phosphatase (0.219 U/mg protein), fructose-1,6-bisphosphatase (0.503 U/mg protein) and glucokinase (0.342 U/mg protein), reflecting normal hepatic glucose homeostasis. Low gluconeogenesis enzyme activity alongside moderate glucokinase activity indicates physiological balance between glucose production and utilization (Wang *et al*., 2019). Rats treated with EBdAgNPs alone (G2) showed glucose-6-phosphatase (0.3 U/mg protein), fructose-1, 6-bisphosphatase (0.3 U/mg protein) and glucokinase (0.4 U/mg protein), suggesting mild modulation of gluconeogenesis with enhanced glucose utilization, consistent with previous studies on nanoparticle-mediated hepatic enzyme regulation (Shehata *et al*., 2022).

Diabetic rats (G3) demonstrated elevated glucose-6-phosphatase (0.605 U/mg protein) and fructose-1,6-bisphosphatase (0.8 U/mg protein) with suppressed glucokinase (0.1 U/mg protein), indicative of excessive gluconeogenesis and impaired glycolysis, typical of insulin deficient states (Sargsyan and Herman, 2019; Lee *et al*., 2022). EBdAgNPs treatment in G4 restored glucose-6-phosphatase (0.4 U/mg protein), fructose-1,6-bisphosphatase (0.5 U/mg protein) and glucokinase (0.4 U/mg protein), highlighting insulin-mimetic and insulin-sensitizing actions via GLUT-2 upregulation and PPARγ activation (Blazquez *et al*., 2022; Singh *et al*., 2020). Comparatively, glibenclamide (G5) partially corrected the imbalance (G6Pase 0.3 U/mg, FBPase 0.4 U/mg, glucokinase 0.4 U/mg protein), emphasizing the enhanced efficacy of EBdAgNPs.

High fat diet-induced dysregulation (G6) resulted in glucose-6-phosphatase (0.5 U/mg protein), fructose-1, 6-bisphosphatase (0.8 U/mg protein) and glucokinase (0.1 U/mg protein), reflecting insulin resistance (Fuchs *et al*., 2021; Ekta *et al*., 2020). EBdAgNPs administration (G7) normalized enzyme activities (G6Pase 0.206 U/mg protein, FBPase 0.4 U/mg protein, glucokinase 0.4 U/mg protein), indicating improved insulin sensitivity and reduced hepatic oxidative stress. Sibutramine treatment (G8) showed modest modulation (G6Pase 0.2 U/mg, FBPase 0.6 U/mg, glucokinase 0.347 U/mg protein), reflecting indirect effects on hepatic metabolism via appetite suppression (Christaki *et al*., 2025).

Dual-pathology rats (G9) had the most severe perturbations as glucose-6-phosphatase (1.1 U/mg protein), fructose-1,6-bisphosphatase (1.6 U/mg protein) and glucokinase (0.1 U/mg protein), demonstrating synergistic effects of insulin deficiency and resistance (Zhao *et al*., 2023). EBdAgNPs co-treatment (G10) restored G6Pase (0.5 U/mg protein), FBPase (0.5 U/mg protein) and glucokinase (0.7 U/mg protein), reflecting potent hepatoprotective, insulin sensitizing and antioxidant effects, likely mediated through suppression of gluconeogenesis transcription factors and enhanced hepatic insulin signaling (Gu *et al*., 2019).

Overall, EBdAgNPs effectively restored hepatic carbohydrate metabolism across all groups, with G4, G7 and G10 showing the most pronounced improvements, outperforming standard therapies like glibenclamide and sibutramine. These findings underscore the nanoparticles potential for managing complex metabolic disorders involving both insulin deficiency and insulin resistance.

4.3.7 Atherogenic Index as a Predictive Marker of Cardiometabolic Risk in Experimental Rats

The atherogenic index (AI), calculated as the log ratio of triglycerides to HDL mcholesterol, serves as a reliable marker for evaluating the risk of developing atherosclerosis and cardiovascular complications. An elevated AI indicates higher cardiovascular risk due to lipoprotein imbalance and lipid accumulation in arterial walls (Celik *et al*., 2021). This study investigates the atherogenic index across various experimental rat groups, each subjected to different treatments involving diabetic induction, high fat diet exposure and administration of therapeutic agents such as EBdAgNPs, Glibenclamide and Sibutramine. The following table 4.6 offer a comparative interpretation of the AI values, underlying mechanisms and relevance with supporting literature.

TABLE 4.6

ATHEROGENIC INDEX IN EXPERIMENTAL RATS

TREATMENT GROUPS		AI
G1	Control	2.78±0.1
G2	EBdAgNPs	2.13±0.1
G3	STZ-NI induced	8.2±0.5***
G4	STZ-NI + EBdAgNPs	3.37±0.2
G5	STZ-NI + Glibenclamide	4.02±0.2
G6	HFD-induced	12.5±0.1***
G7	HFD + EBdAgNPs	3.14±0.1
G8	HFD + Sibutramine	3.38±0.3
G9	STZ-NI + HFD	13.6±0.3***
G10	STZ-NI + HFD + EBdAgNPs	3.84±0.4

Values are expressed as mean ± S.E.M (n=6)

G3, G6 & G9 vs G1: Significant ↑ in AI values (*p < 0.001)**

G3, G6 & G9 vs G4, G5, G7, G8 & G10: Significant cardioprotective effect observed (*p < 0.001).**

(One Way ANOVO followed by Dunnett's Test)

In the healthy control group (G1), the AI was measured at 2.78 ± 0.0696, reflecting a normal lipid homeostasis and low cardiovascular risk. Rats treated with EBdAgNPs alone (G2) exhibited a significant decrease (***p < 0.001) AI of 2.13 ± 0.0722, indicating that the nanoparticles are largely biocompatible and may exert mild lipid modulating effects even under normal physiological conditions. This reduction, while modest, could be attributed to the antioxidative and hypolipidemic potential of silver nanoparticles, which may enhance reverse cholesterol transport, improve hepatic lipid metabolism and stabilize lipoprotein profiles (Ayeni *et al*., 2024; Lata *et al*., 2025). Furthermore, phytochemicals present in *Boerhavia diffusa* L. including flavonoids, rotenoids and punarnavine, are known to modulate hepatic lipid metabolism and

scavenge reactive oxygen species, potentially contributing to the observed mild cardioprotective effect (Devi and Kumar, 2025). The AI comparison between G1 and G2 highlights the baseline effect of EBdAgNPs in preserving lipid homeostasis without introducing systemic stress.

In the diabetic group induced by STZ-NI (G3), a significant increase (***$p < 0.001$) in AI to 8.2 ± 0.5 was observed, indicative of hypertriglyceridemia, reduced HDL and heightened cardiovascular risk. Treatment with EBdAgNPs (G4) reduced AI markedly to 3.37 ± 0.2, whereas glibenclamide (G5) produced a slightly higher AI of 4.02 ± 0.2. The superior efficacy of EBdAgNPs over glibenclamide may be due to its dual action as insulin-mimetic activity that reduces gluconeogenesis flux and enhanced antioxidant capacity mitigating lipid peroxidation (Kaushik and Kaushik, 2022; Babic *et al*., 2019). Mechanistically, the nanoparticles may decrease oxidative stress by neutralizing ROS in hepatocytes, suppress NF-κB-mediated inflammatory signaling and restore HDL synthesis, collectively improving lipid profiles. Glibenclamide, although effective in enhancing insulin secretion, primarily exerts indirect lipid lowering effects and lacks robust antioxidative action (Muller and Muller, 2023). The comparison of G3 with G4 and G5 clearly demonstrates the added advantage of EBdAgNPs in modulating both metabolic and inflammatory pathways to restore AI toward normal values.

The high-fat diet (HFD) group (G6) exhibited a rise in AI to 12.5 ± 0.08, reflecting profound dyslipidemia caused by chronic lipid overload, insulin resistance and hepatic steatosis (Wali *et al*., 2020). EBdAgNPs co-treatment (G7) reduced AI substantially to 3.14 ± 0.06, while sibutramine treatment (G8) lowered it to 3.38 ± 0.3. The nanoparticle mediated improvements may involve multiple mechanisms, including enhanced reverse cholesterol transport, inhibition of hepatic lipogenesis, reduction of inflammatory cytokines such as TNF-α, IL-6 and scavenging of ROS to prevent oxidative damage to lipids (Durrington *et al*., 2025; Caiati *et al*., 2023). Moreover, bioactive phytochemicals in *B. diffusa* may synergistically stabilize hepatic lipid metabolism, attenuate adipose tissue inflammation and enhance antioxidant enzyme activity, collectively contributing to AI normalization (Metwally *et al*., 2021). Compared to sibutramine, EBdAgNPs offer a more integrated cardiometabolic benefit, addressing both lipid transport and oxidative inflammatory pathways rather than merely reducing caloric intake or appetite.

The comorbid diabetic + HFD group (G9) recorded the highest AI at 13.6 ± 0.3, showing a significantly increased value (***$p < 0.001$), underscoring the synergistic impact of hyperglycemia and lipid overload on cardiovascular risk. Treatment with EBdAgNPs (G10) markedly reduced AI to 3.84 ± 0.4, demonstrating potent cardioprotective and lipid normalizing effects even under severe metabolic stress. The observed improvement likely arises from the combined effects of glycemic control, lipid modulation and antioxidative action: nanoparticles enhance insulin sensitivity, restore hepatic lipoprotein synthesis and suppress NF-κB and other proinflammatory pathways. Phytochemicals in *Boerhavia diffusa* L. further contribute to reducing lipid peroxidation, protecting endothelial function and facilitating reverse cholesterol transport (Ziolkowska *et al*., 2021). The comparison between G9 and G10 highlights the comprehensive therapeutic potential of EBdAgNPs in counteracting both diet and diabetes induced atherogenic risk, surpassing interventions that target only a single metabolic aspect.

Overall, the comparative evaluation across all groups demonstrates that EBdAgNPs consistently modulate AI through synergistic mechanisms involving oxidative stress reduction, anti-inflammatory effects and improvement of lipid metabolism. This effect is amplified by the presence of *B. diffusa* phytoconstituents, which enhance both hepatoprotective and cardioprotective outcomes. The integration of these findings with related studies supports the rationale for EBdAgNPs as a promising nanotherapeutic agent for managing complex metabolic disorders with increased cardiovascular risk (Ayeni *et al*., 2024; Lata *et al*., 2025; Kaushik and Kaushik, 2022).

4.3.8 Enzymatic and Non-Enzymatic Antioxidants in the Liver of Experimental Rats

4.3.8.1 Hepatic Antioxidant Enzyme Activities in Experimental Rats

Oxidative stress plays a critical role in the pathogenesis of diabetes and obesity, leading to tissue damage through excessive reactive oxygen species (ROS). Enzymic antioxidants such as catalase (CAT), superoxide dismutase (SOD) and glutathione peroxidase (GPX) serve as primary defense mechanisms against oxidative insult. Evaluating these enzyme activities, as shown in table 4.7, provides insight into the protective or damaging nature of various interventions, including EBdAgNPs, glibenclamide and sibutramine, in STZ-NI and HFD-induced metabolic disorders.

TABLE 4.7

ENZYMATIC ANTIOXIDANT ACTIVITIES IN THE LIVER OF EXPERIMENTAL RATS

Treatment Groups		Catalase (U/mg protein)	Superoxide Dismutase (U/mg protein)	Glutathione Peroxidase (U/mg protein)
G1	Control	41.6±1.9	3.28±0.01	7.86±0.05
G2	EBdAgNPs	36.9±1.8	2.9±0.3	7.62±0.3
G3	STZ-NI induced	20.8±0.7***	1.82±0.3***	3.25±0.04***
G4	STZ-NI+ EBdAgNPs	39.9±1.4	2.95±0.3	7.53±0.3
G5	STZ-NI+ Glibenclamide	37.3±1.5	2.6±0.3	7.28±0.3
G6	HFD-induced	24.8±0.8***	0.096±0.01***	3.79±0.2***
G7	HFD + EBdAgNPs	39.9±0.3	2.38±0.01	7.55±0.02
G8	HFD + Sibutramine	36±2.8	2.11±0.1	6.73±0.3
G9	STZ-NI + HFD	13.3±1.5***	0.225±0.02***	3.8±0.03***
G10	STZ-NI+HFD+ EBdAgNPs	37.9±0.9	2.28±0.01	6.41±0.3

Values are expressed as mean ± S.E.M (n=6)

G3, G6 & G9 vs G1: Significant ↓ in antioxidant enzyme levels (*p < 0.001)**

G3, G6 & G9 vs G4, G5, G7, G8 & G10: Significant antioxidant restoration observed (*p < 0.001).**

(One Way ANOVO followed by Dunnett's Test)

Control rats (G1) displayed robust antioxidant defense, with CAT activity of 41.6 ± 1.9 U/mg protein, SOD of 3.28 ± 0.01 U/mg protein and GPX of 7.86 ± 0.05 U/mg protein, reflecting intact hepatic redox homeostasis. These baseline values indicate strong enzymatic protection against endogenous reactive oxygen species (ROS) and provide a reference for therapeutic evaluation (Salehi *et al*., 2020). Rats treated with EBdAgNPs alone (G2) maintained comparable enzymatic activity CAT as 36.9 ± 1.8, SOD as 2.9 ± 0.3 and GPX as 7.62 ± 0.3, suggesting that the nanoparticles do not provoke oxidative stress under normal physiological conditions.

The slight decrease in CAT and SOD may reflect mild adaptive modulation rather than toxicity. *Boerhavia diffusa* L. phytochemicals, including flavonoids and rotenoids, likely contribute to sustaining antioxidant balance through free radical scavenging and metal chelating effects (Iancu *et al*., 2023). This comparison confirms the biocompatibility of EBdAgNPs and hints at their potential in supporting basal antioxidant defenses.

Diabetic rats (G3), induced with STZ-NI, showed a marked decline in antioxidant defenses CAT as 20.8 ± 0.7, SOD as 1.82 ± 0.3 and GPX as 3.25 ± 0.04, reflecting pronounced oxidative stress caused by β-cell destruction and hyperglycemia induced ROS overproduction (Eguchi *et al*., 2021). The concomitant rise in lipid peroxidation and depletion of endogenous antioxidants mirrors earlier observations in STZ-induced diabetic models (Sharma *et al*., 2023). Co-treatment with EBdAgNPs (G4) restored CAT to 39.9 ± 1.4, SOD to 2.95 ± 0.3 and GPX to 7.53 ± 0.3, demonstrating potent antioxidant recovery. This improvement can be attributed to the dual action of silver nanoparticles and *B. diffusa* phytochemicals, which enhance ROS scavenging, stabilize mitochondrial function and suppress NF-κB-mediated oxidative signaling (Rajkumar *et al*., 2025). Glibenclamide treatment (G5) also improved antioxidant activity CAT as 37.3 ± 1.5, SOD as 2.6 ± 0.3 and GPX as 7.28 ± 0.3 but was slightly less effective than EBdAgNPs. While glibenclamide primarily lowers hyperglycemia, it indirectly reduces ROS production, highlighting that the nanoparticle mediated approach provides more direct hepatoprotective and antioxidative benefits (Jia *et al*., 2024). The comparative restoration underscores the enhanced therapeutic potential of EBdAgNPs in diabetic oxidative stress.

High-fat diet (HFD) rats (G6) exhibited severe depletion of antioxidant enzymes CAT as 24.8 ± 0.9, SOD as 0.096 ± 0.01 and GPX as 3.79 ± 0.2, reflecting increased lipid peroxidation and chronic low-grade inflammation (Feillet-Coudray *et al*., 2019). The dramatic fall in SOD highlights impaired superoxide radical neutralization, contributing to hepatic oxidative injury, in line with prior HFD studies (Anwar *et al*., 2025). EBdAgNPs treatment (G7) restored enzymatic activities close to normal levels CAT as 39.9 ± 0.3, SOD as 2.38 ± 0.01 and GPX as 7.55 ± 0.01, suggesting that the nanoparticles mitigate oxidative damage induced by lipid overload through free radical scavenging, inhibition of lipid peroxidation and modulation of hepatic antioxidant gene expression. *B. diffusa* compounds, particularly punarnavine and

rotenoids, likely synergize with the nanoparticles to stabilize ROS levels and reduce proinflammatory cytokine production (Kaur *et al*., 2025). Sibutramine-treated HFD rats (G8) also showed improvement CAT as 36 ± 2.8, SOD as 2.11 ± 0.1 and GPX as 6.73 ± 0.3, but the antioxidant restoration was slightly inferior to EBdAgNPs. This suggests that while pharmacological appetite suppressants reduce lipid driven ROS generation indirectly, EBdAgNPs provide a more robust direct antioxidative effect through phytochemical assisted nanotherapeutic action.

Rats subjected to combined diabetic and HFD stress (G9) displayed the most compromised antioxidant profile CAT as 13.3 ± 1.5, SOD as 0.225 ± 0.02 and GPX as 3.8 ± 0.03, reflecting compounded oxidative burden from hyperglycemia and lipotoxicity. This severe enzymatic depletion correlates with elevated ROS, mitochondrial dysfunction and chronic inflammation, validating the dual-induced metabolic stress model (Shang *et al*., 2025). EBdAgNPs co-treatment (G10) effectively restored CAT to 37.9 ± 0.9, SOD to 2.28 ± 0.01 and GPX to 6.41 ± 0.3. The recovery emphasizes the potent hepatoprotective and systemic antioxidative capacity of EBdAgNPs, which likely act through multiple mechanisms: scavenging ROS, enhancing endogenous antioxidant enzyme transcription, stabilizing mitochondrial redox homeostasis and reducing proinflammatory cytokine levels. The synergistic effects of *B. diffusa* phytochemicals, including flavonoids and rotenoids, amplify these protective effects, promoting normalization of oxidative stress markers even under severe metabolic stress (Ghiniwa *et al*., 2025). This comparative analysis confirms that EBdAgNPs provide superior antioxidant restoration compared to pharmacological interventions or diet modification alone.

4.3.8.2 Non-Enzymic Antioxidants Hepatic Tissue of Experimental Rats

Non-enzymic antioxidants such as vitamin C, vitamin E and reduced glutathione (GSH) play a crucial role in maintaining hepatic redox homeostasis by scavenging free radicals and preventing oxidative stress induced cellular damage. Disruptions in these molecules often reflect underlying pathologies such as diabetes, obesity and their complications. As shown in table 4.8, the current dataset explores the alterations in hepatic levels of these antioxidants across various experimental groups, especially highlighting the restorative effects of EBdAgNPs.

TABLE 4.8

NON-ENZYMATIC ANTIOXIDANT ACTIVITIES IN THE LIVER OF EXPERIMENTAL RATS

Treatment Groups		Vitamin C (µg/g tissue)	Vitamin E (µg/g tissue)	Reduced Glutathione (µmoles/g tissue)
G1	Control	1.26±0.01	1.2±0.31	13.3±0.02
G2	EBdAgNPs	1.19±0.03	0.9±0.04	12.9±0.7
G3	STZ-NI induced	0.8±0.03***	0.3±0.01**	8.1±0.3***
G4	STZ-NI+ EBdAgNPs	1.2±0.01	1.04±0.01	13±0.4
G5	STZ-NI+ Glibenclamide	1.2±0.0	0.9±0.02	11.9±0.9
G6	HFD-induced	0.02±0.0***	0.09±0.0**	6.8±0.3***
G7	HFD + EBdAgNPs	1.2±0.1	0.9±0.0	12.5±0.3
G8	HFD + Sibutramine	1.1±0.00	0.8±0.0	12.7±0.4
G9	STZ-NI + HFD	0.02±0.01***	0.08±0.01**	7.9±0.3***
G10	STZ-NI+ HFD+ EBdAgNPs	0.2±0.01	1.01±0.05	12.2±0.01

Values are expressed as mean ± S.E.M (n=6)

G3, G6 & G9 vs G1: Significant ↓ in non-enzymatic antioxidant levels (*p < 0.001) G3, G6 & G9 vs G4, G5, G7, G8 & G10: Significant improvement in antioxidant status observed (**p < 0.01, ****p < 0.001).**

(One Way ANOVO followed by Dunnett's Test)

Control rats (G1) displayed optimal non-enzymatic antioxidant levels, with vitamin C at 1.26 ± 0.01 mg/g, vitamin E at 1.20 ± 0.3 mg/g and GSH at 13.3 ± 0.01 µmol/g, representing a stable hepatic redox environment. These baseline values reflect sufficient free radical scavenging and detoxification capacity under normal physiological conditions (Sravani *et al*., 2024). EBdAgNPs-treated normal rats (G2) showed a slight, non-significant reduction in these antioxidants, suggesting that the nanoparticle formulation is biocompatible and does not perturb endogenous antioxidant homeostasis. The phytoconstituents of *B. diffusa*, such as rotenoids, flavonoids and polyphenols, likely contribute to maintaining redox balance, supporting cellular defense systems even in the presence of exogenous nanoparticles.

Diabetic rats (G3), induced with STZ-NI, exhibited marked depletion in non-enzymatic antioxidants vitamin C as 0.812 ± 0.02 mg/g, vitamin E as 0.325 ± 0.01 mg/g and GSH as 8.14 ± 0.3 µmol/g, highlighting extensive oxidative damage due to hyperglycemia and β-cell dysfunction (Serbis *et al*., 2023). Increased ROS levels in the liver promote glutathione depletion and lipid peroxidation, exacerbating hepatocellular injury. Treatment with EBdAgNPs (G4) restored antioxidant levels close to control values in vitamin C as 1.21 ± 0.003 mg/g, vitamin E as 1.04 ± 0.01 mg/g and GSH as 13.0 ± 0.4 µmol/g, indicating strong hepatoprotective and free radical scavenging capacity. In comparison, glibenclamide (G5) achieved moderate recovery GSH showed 11.9 ± 0.89 µmol/g, reflecting its indirect antioxidative effect through glycemic control. The superior efficacy of EBdAgNPs may stem from dual action the silver nanoparticles enhance cellular antioxidant defenses, while *B. diffusa* phytochemicals directly neutralize ROS and stabilize mitochondrial function (Roohi *et al*., 2023).

High-fat diet-fed rats (G6) showed pronounced depletion of non-enzymatic antioxidants vitamin C as 0.0177 ± 0.002 mg/g, vitamin E as 0.0187 ± 0.004 mg/g and GSH as 6.85 ± 0.3 µmol/g), indicative of severe hepatic oxidative stress due to chronic lipid overload and mitochondrial ROS generation (Prasun *et al*., 2021). EBdAgNPs treatment in HFD-fed rats (G7) restored antioxidant levels in vitamin C as 1.22 ± 0.07 mg/g, vitamin E as 0.933 ± 0.005 mg/g and GSH as 12.5 ± 0.3 µmol/g, highlighting their efficacy in counteracting lipid-induced oxidative insults. The potent ROS scavenging action is likely facilitated by the synergistic effect of silver nanoparticles and *B. diffusa* phytochemicals, which enhance glutathione recycling and reduce peroxidative damage (Mondal and Rahman, 2020). Sibutramine (G8) showed moderate improvement, reflecting partial mitigation of oxidative stress through appetite suppression and indirect reduction in lipid peroxidation, but its effect remained less pronounced compared to EBdAgNPs.

Rats exposed to combined diabetic and HFD stress (G9) exhibited the most severe non-enzymatic antioxidant depletion in vitamin C as 0.0163 ± 0.007 mg/g, vitamin E as 0.079 ± 0.01 mg/g and GSH as 7.87 ± 0.3 µmol/g, reflecting synergistic oxidative injury from hyperglycemia and lipotoxicity. This model replicates complex metabolic syndrome, where chronic ROS accumulation impairs hepatic detoxification and antioxidant enzyme regeneration (Matyas *et al*., 2021). Remarkably, EBdAgNPs co-treatment (G10) restored

non-enzymatic antioxidants in vitamin C as 0.201 ± 0.01 mg/g, vitamin E as 1.01 ± 0.055 mg/g and GSH as 12.2 ± 0.01 µmol/g, showing significant increase in ($p < 0.01$, $p < 0.001$ vs G9), suggesting that the therapy mitigates oxidative damage from both diabetic and dietary insults. Mechanistically, EBdAgNPs may enhance hepatic glutathione synthesis, scavenge free radicals, inhibit lipid peroxidation and modulate inflammatory signaling pathways (Omeye, 2025). The phenolic and flavonoid content of *B. diffusa* further contributes to ROS neutralization and stabilization of hepatic antioxidant status, underscoring its therapeutic synergy with nanoparticles in metabolic disorders.

4.3.9 Histopathological Studies of Experimental Rats

The histopathological findings of the pancreas, liver, kidney and adipose tissue are illustrated in plates 3–6 and a detailed summary of these observations is provided in table 4.9.

TABLE 4.9

HISTOPATHOLOGY OF PANCREAS, LIVER, KIDNEY AND ADIPOSE TISSUE OF EXPERIMENTAL RATS

Groups	Treatment	Pancreas	Liver	Kidney	Adipose tissue
G1	Control	Normal acini, intact islets	Normal lobular structure,	Normal histology	Normal histology
G2	EBdAgNPs	Normal histology, slight vacuolation	Preserved architecture, mild sinusoidal dilatation	Normal histology	Normal histology
G3	STZ–NI	Reduced islet number/size, vacuolation, vascular congestion	Necrosis, inflammation, dilated sinusoids, severe disruption	Mesangial expansion, focal tubular loss, mild inflammation	Mild stromal inflammation, early diabetic adipose pathology
G4	STZ-NI + EBdAgNPs	Regenerating islets, minimal vacuolation	Marked improvement, reduced necrosis/ inflammation	Restored glomeruli and tubules, minimal inflammation	Normal adipocytes, inflammation absent
G5	STZ-NI + Glibenclamide	Preserved islets, minimal changes	Moderate recovery, slight periportal inflammation	mild residual inflammation	Improved morphology, glycemic-control mediated recovery
G6	HFD	Disrupted islets, vacuolation, lipotoxic stress	Cytoplasmic vacuolation, congestion, early steatohepatitis	Mesangial expansion, hypercellularity	Mild inflammation; adipocyte enlargement
G7	HFD + EBdAgNPs	Restored acini, minimal vacuolation	Preserved architecture, reduced inflammation	Near-normal morphology	Normal adipocytes, inflammation prevented
G8	HFD + Sibutramine	Partial recovery, mild inflammation	Improved morphology, minor vacuolation persists	Improved histology, slight interstitial changes	Preserved adipocytes, mild improvements
G9	STZ–NI + HFD	Reduced islets, vacuolation, inflammation	Severe vacuolation, necrosis, inflammation, disrupted architecture	Pronounced mesangial expansion, inflammation	Marked inflammation, vascular congestion
G10	STZ-NI + HFD + EBdAgNPs	Regenerating islets, minimal vacuolation	Structural restoration, reduced necrosis and vacuolation	Architecture restored, intact glomeruli and tubules	Normal adipocytes, inflammation completely prevented

4.3.9.1 Histopathological Observations of Pancreas in the Experimental Rats

The pancreas is a vital organ in regulating glucose metabolism through insulin secretion by islet β-cells. Diabetes and obesity-related interventions significantly impact pancreatic architecture.

PLATE 3

HISTOPATHOLOGICAL OBSERVATIONS OF PANCREAS IN THE EXPERIMENTAL RATS

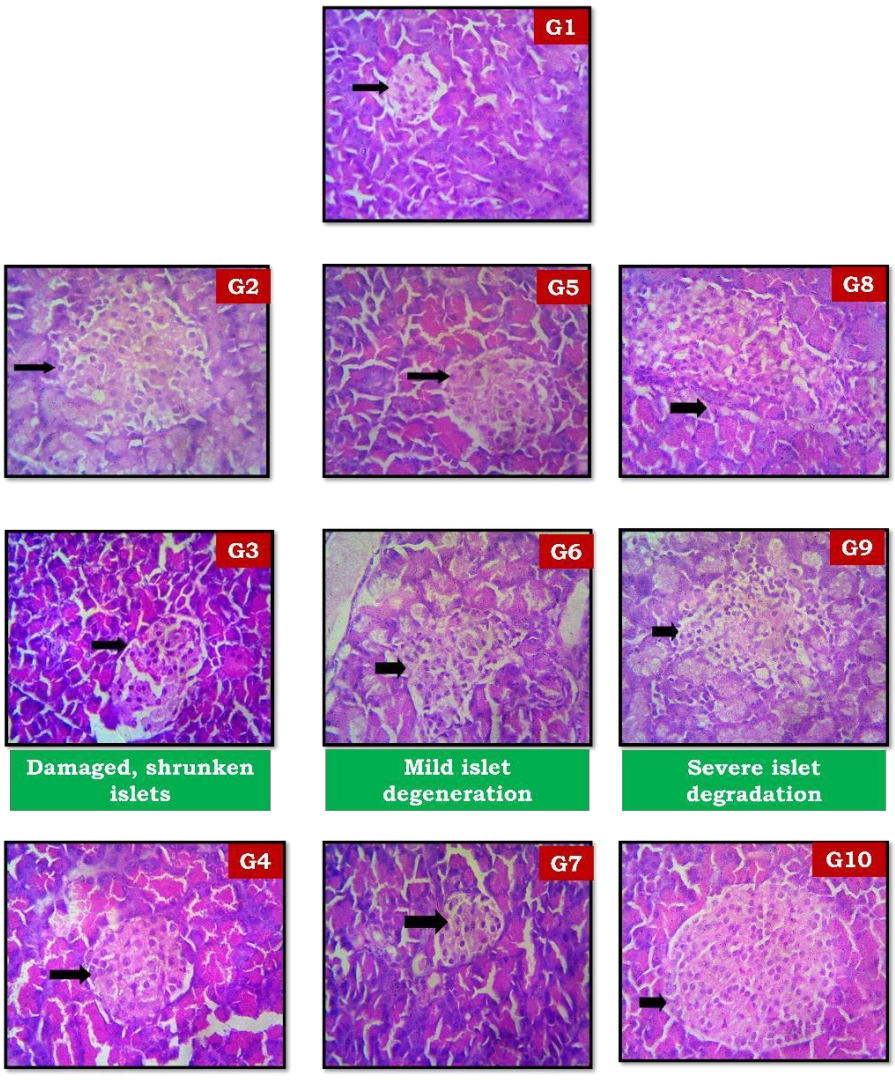

G1 Control	**G2 EBdAgNPs**	**G3 STZ-NI induced**
G4 STZ-NI + EBdAgNPs	**G5 STZ-NI + Glibenclamide**	**G6 HFD-induced**
G7 HFD + EBdAgNPs	**G8 HFD + Sibutramine**	**G9 STZ-NI + HFD**
G10 STZ-NI + HFD + EBdAgNPs		

In this context, the histopathological study of pancreatic tissue, as shown in Plate 3, across various experimental rat groups elucidates the protective and regenerative potential of EBdAgNPs. The following sections discuss group-wise morphological alterations and their alignment with existing scientific evidence. In the control group (G1), pancreatic tissues displayed normal acinar structures and well-defined islets, representing standard physiological morphology. When compared to the EBdAgNPs treated normal rats (G2), the pancreas largely maintained its structural integrity, with only a slight reduction in islet number and minimal cytoplasmic vacuolation. This comparison demonstrates that EBdAgNPs do not induce cytotoxicity under normal conditions, while the minor vacuolation may reflect a subtle cellular adaptation to the nanoparticle presence rather than pathological damage. The marginal differences between G1 and G2 support the biosafety profile of *B. diffusa* mediated silver nanoparticles and suggest that even under normal physiological conditions, EBdAgNPs may subtly interact with pancreatic tissue without compromising function (Roy *et al*., 2022).

STZ-NI-induced diabetic rats (G3) exhibited severe pathological alterations, including significant reduction in islet number and size, cytoplasmic vacuolation and vascular congestion, indicative of β-cell destruction and early inflammatory changes (Adepoju *et al*., 2024). When comparing G3 with the EBdAgNPs-treated diabetic group (G4), there was a noticeable regeneration of islets with minimal vacuolation, reflecting the therapeutic effect of EBdAgNPs through antioxidant and anti-inflammatory pathways. Glibenclamide treated diabetic rats (G5) also demonstrated preserved islet morphology, with little to no vacuolation, attributable to its insulinotropic action via sulfonylurea receptor modulation (Kuo *et al*., 2020). Direct comparison of G4 and G5 reveals that EBdAgNPs may provide additional cytoprotective benefits beyond the insulin secreting effects of glibenclamide, likely due to the combined phytochemical and nanometal activity facilitating tissue recovery (Saleh *et al*., 2021).

Rats fed a high-fat diet (G6) displayed disrupted islet architecture and cytoplasmic vacuolation, reflecting early lipotoxic stress and insulin resistance (Vilas-Boas, 2021). EBdAgNPs supplementation in HFD-fed rats (G7) markedly restored acinar structures with minimal vacuolation, demonstrating their ability to counteract HFD-induced oxidative and metabolic stress. Sibutramine-treated HFD rats (G8) showed partial

recovery, with preserved islet numbers but presence of inflammatory infiltrates, indicating that while pharmacological intervention can improve morphology, it may not fully address underlying oxidative or inflammatory stress (Danilov *et al*., 2024). Comparison among G6, G7 and G8 highlights the superior efficacy of EBdAgNPs in restoring pancreatic architecture under dietary stress, likely mediated by *B. diffusa* phytochemicals antioxidant and anti-inflammatory activities (Saad , 2023).

Obese diabetic rats (G9), subjected to both STZ-NI and high-fat diet, exhibited the most severe pancreatic damage, including extensive reduction in islet number, cytoplasmic vacuolation and inflammatory infiltrates, reflecting compounded diabetic and dietary insults (Tramonti *et al*., 2022). In contrast, EBdAgNPs treated obese diabetic rats (G10) showed near-normal pancreatic morphology with regenerating islets, minimal vacuolation and absence of vascular damage. Direct comparison between G9 and G10 illustrates the therapeutic potential of EBdAgNPs even under dual metabolic stress, effectively reversing structural compromise likely through combined antioxidant, anti-inflammatory and cytoprotective actions of *B. diffusa* phytochemicals (Fatima *et al*., 2021). These findings confirm that EBdAgNPs can mitigate severe pancreatic damage in obese diabetic conditions, supporting their integration into multifactorial metabolic therapy strategies.

4.3.9.2 Histopathological Observations of Liver in the Experimental Rats

Histopathological examination of the liver offers essential clues into the extent of hepatocellular injury, inflammation and regenerative responses. In this study, liver sections from ten experimental rat groups, as shown in Plate 4, were analyzed to assess the protective role of EBdAgNPs against damage induced by HFD and STZ-NI models.

PLATE 4

HISTOPATHOLOGICAL OBSERVATIONS OF LIVER IN THE EXPERIMENTAL RATS

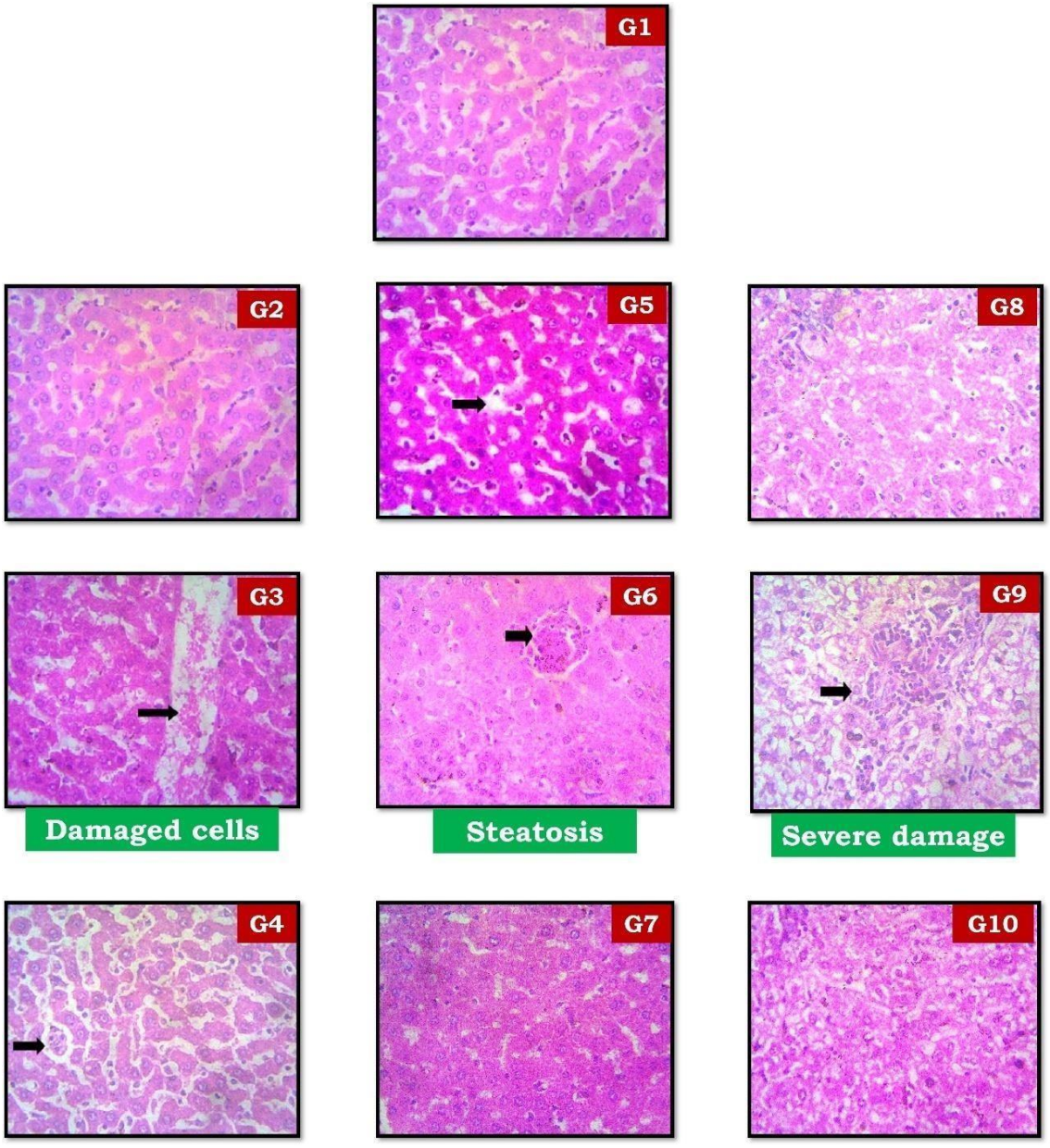

G1 Control	**G2 EBdAgNPs**	**G3 STZ-NI induced**
G4 STZ-NI + EBdAgNPs	**G5 STZ-NI + Glibenclamide**	**G6 HFD-induced**
G7 HFD + EBdAgNPs	**G8 HFD + Sibutramine**	**G9 STZ-NI + HFD**
G10 STZ-NI + HFD + EBdAgNPs		

In the control group (G1), liver tissues exhibited typical lobular architecture with well-preserved hepatocytes, central veins and mild sinusoidal dilatation (Carotti *et al*., 2020a). This baseline morphology indicates a normal hepatic environment with minimal stress. EBdAgNPs treatment alone (G2) maintained this structural integrity, with only minor sinusoidal dilatation and no evidence of hepatocellular degeneration or portal inflammation. The negligible differences between G1 and G2 suggest that EBdAgNPs are biocompatible in healthy livers and may even subtly support hepatic homeostasis through mild antioxidant activity inherent to the phytochemicals in *B. diffusa* (Anand *et al*., 2019).

STZ-NI induced diabetic rats (G3) displayed severe hepatic disruption characterized by parenchymal necrosis, binucleated hepatocytes, interface hepatitis and periportal inflammation, accompanied by sinusoidal and central vein dilatation. These changes reflect pronounced oxidative stress and inflammatory injury due to hyperglycemia and insulin deficiency, consistent with literature reports (Mohammed *et al*., 2021; Mossenta *et al*., 2020). In contrast, EBdAgNPs treatment in diabetic rats (G4) resulted in marked improvement as necrosis and inflammation were substantially reduced, lobular architecture was largely preserved and hepatocytes displayed signs of recovery. Similarly, glibenclamide-treated rats (G5) showed moderate restoration of liver structure, although some periportal inflammation persisted. The comparative analysis indicates that EBdAgNPs may provide superior hepatoprotective effects by mitigating oxidative damage and enhancing endogenous antioxidant defenses, while glibenclamide primarily acts through glycemic control to indirectly reduce hepatic injury (Maranta *et al*., 2021; Li *et al*., 2023).

High-fat diet-fed rats (G6) demonstrated notable cytoplasmic vacuolation, sinusoidal congestion and interface hepatitis, indicative of early steatohepatitis and lipid accumulation (Abo El-Khair *et al*., 2020; Carotti *et al*., 2020b). EBdAgNPs administration in HFD rats (G7) preserved hepatic architecture with minimal vacuolation and reduced inflammatory signs, suggesting effective antioxidant and anti-lipotoxic actions. Sibutramine treatment (G8) similarly improved liver morphology, though minor cytoplasmic vacuolation and periportal inflammation remained. When comparing G6 to G7 and G8, EBdAgNPs appear to exert stronger protective effects, potentially through enhanced hepatic lipid metabolism, modulation of oxidative stress and suppression of inflammatory cascades inherent to *B. diffusa* phytochemicals (Ashqar *et al*., 2025).

The dual-obese-diabetic model (G9) exhibited the most severe hepatic damage, with extensive vacuolation, necrosis, disrupted lobular organization and marked periportal inflammation. The synergistic effect of STZ-NI and HFD amplifies oxidative stress, lipotoxicity and inflammatory signaling, leading to compounded hepatocyte degeneration (Rajsekhar *et al*., 2024). Remarkably, EBdAgNPs treatment in this group (G10) resulted in substantial structural restoration as necrosis and vacuolation were reduced, hepatocytes showed regenerative binucleation and portal areas displayed minimal inflammation. This comparative analysis underscores the ability of EBdAgNPs to counteract complex metabolic insults by combining antioxidant, anti-inflammatory and lipid-modulating actions, effectively preserving hepatic architecture even under severe dual stress (Hussain *et al*., 2021).

Overall, these histopathological observations provide strong evidence that EBdAgNPs confer hepatoprotection across normal, diabetic, high-fat diet and combined obese diabetic conditions, with effects often surpassing standard pharmacological treatment. The comparative flow from G1–G10 highlights how EBdAgNPs mitigate oxidative stress, reduce inflammatory damage and promote hepatic regeneration in a dose and context dependent manner.

4.3.9.3 Histopathological Observations of Kidney in the Experimental rats

The kidney plays a vital role in metabolic homeostasis and its histological integrity is often compromised in metabolic disorders such as diabetes and obesity. In this study, the histopathological evaluation of renal tissues across ten experimental groups (G1–G10), as shown in Plate 5, was conducted to assess the impact of STZ-NI induced diabetes, HFD and therapeutic interventions using EBdAgNPs, glibenclamide and sibutramine. The structural changes in glomeruli, tubules, interstitium and vasculature provide valuable insights into the nephroprotective or nephrotoxic effects under different physiological and pathological conditions.

PLATE 5

HISTOPATHOLOGICAL OBSERVATIONS OF KIDNEY IN THE EXPERIMENTAL RATS

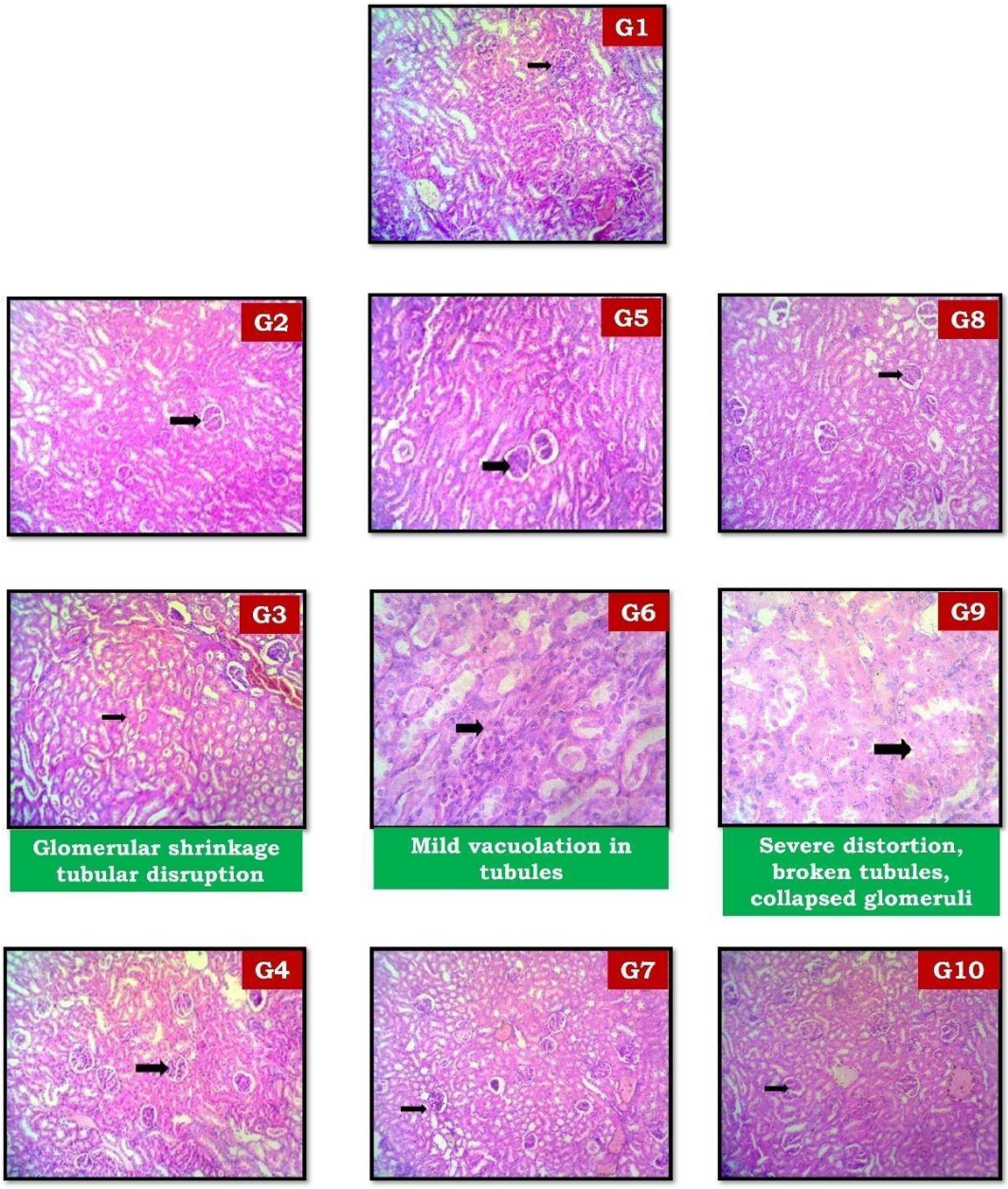

G1 Control	**G2 EBdAgNPs**	**G3 STZ-NI induced**
G4 STZ-NI + EBdAgNPs	**G5 STZ-NI + Glibenclamide**	**G6 HFD-induced**
G7 HFD + EBdAgNPs	**G8 HFD + Sibutramine**	**G9 STZ-NI + HFD**
G10 STZ-NI + HFD + EBdAgNPs		

Histological examination of kidney sections in the control group (G1) revealed well-preserved cortical and medullary structures, with intact glomeruli and renal tubules and only mild vascular congestion, indicating normal physiological architecture (Boorsma *et al*., 2020). The EBdAgNPs alone group (G2) displayed similar renal morphology, with no additional pathological changes, confirming the biocompatibility and safety of *B. diffusa* derived silver nanoparticles. The slight vascular congestion observed in both groups is likely a normal physiological variation rather than a sign of toxicity and the maintained glomerular and tubular integrity underscores that EBdAgNPs do not disturb baseline renal homeostasis (Karunakar *et al*., 2025). Comparative analysis between G1 and G2 demonstrates that EBdAgNPs are well tolerated in healthy renal tissue, serving as a reference for evaluating therapeutic efficacy under metabolic stress.

In STZ-NI-induced diabetic rats (G3), mild pathological changes were observed, including mesangial matrix expansion, focal tubular epithelial loss and scattered interstitial inflammation, reflecting early hyperglycemia-mediated renal stress (Akhtar *et al*., 2020; Yan, 2022). Co-treatment with EBdAgNPs (G4) restored glomerular and tubular architecture, with minimal interstitial changes, whereas glibenclamide-treated rats (G5) showed comparable improvement but with slightly more residual inflammation. The comparison clearly demonstrates that EBdAgNPs (G4) confer renoprotective effects by combining antioxidant and anti-inflammatory mechanisms, whereas glibenclamide primarily acts through insulin-mediated glycemic regulation (Salama *et al*., 2023).

Rats fed a high-fat diet (G6) exhibited mild mesangial expansion, glomerular hypercellularity and interstitial inflammation, consistent with obesity-associated renal stress (Guan *et al*., 2024). Treatment with EBdAgNPs (G7) effectively normalized glomerular and tubular morphology with minimal inflammatory changes, whereas sibutramine-treated rats (G8) showed improvement with slight residual interstitial alterations. Comparative analysis indicates that EBdAgNPs (G7) provide direct renoprotective effects through antioxidant and anti-inflammatory mechanisms, whereas sibutramine offers indirect benefits via metabolic modulation (Sayed *et al*., 2023; Buys-Goncalves *et al*., 2019).

In the obesediabetic group (G9), combining STZ-NI and HFD resulted in pronounced mesangial expansion, glomerular hypercellularity and interstitial inflammation, confirming severe renal compromise due to compounded metabolic stress (Podkowinska and Formanowicz, 2020). Treatment with EBdAgNPs (G10) markedly restored renal architecture, with intact glomeruli, tubules and minimal interstitial involvement. The comparative evaluation between G9 and G10 highlights the potent renoprotective effect of EBdAgNPs (G10) in mitigating oxidative and inflammatory damage induced by both hyperglycemia and lipid overload. These benefits likely arise from the combined antioxidant, anti-inflammatory and cytoprotective properties of *B. diffusa*, underscoring the therapeutic potential of EBdAgNPs in complex metabolic conditions (Dhir *et al*., 2024).

4.3.9.4 Histopathological Observation of Adipose Tissue in the Experimental Rats

In pathological states like diabetes and obesity, adipose tissue undergoes structural and functional remodeling, which is often marked by adipocyte hypertrophy, inflammatory infiltration and altered stromal composition (Kawai *et al*., 2021). As shown in Plate 6, histological analysis across experimental groups provides insights into the protective or aggravating effects of various interventions, including EBdAgNPs.

PLATE 6

HISTOPATHOLOGICAL OBSERVATIONS OF ADIPOSE TISSUE IN THE EXPERIMENTAL RATS

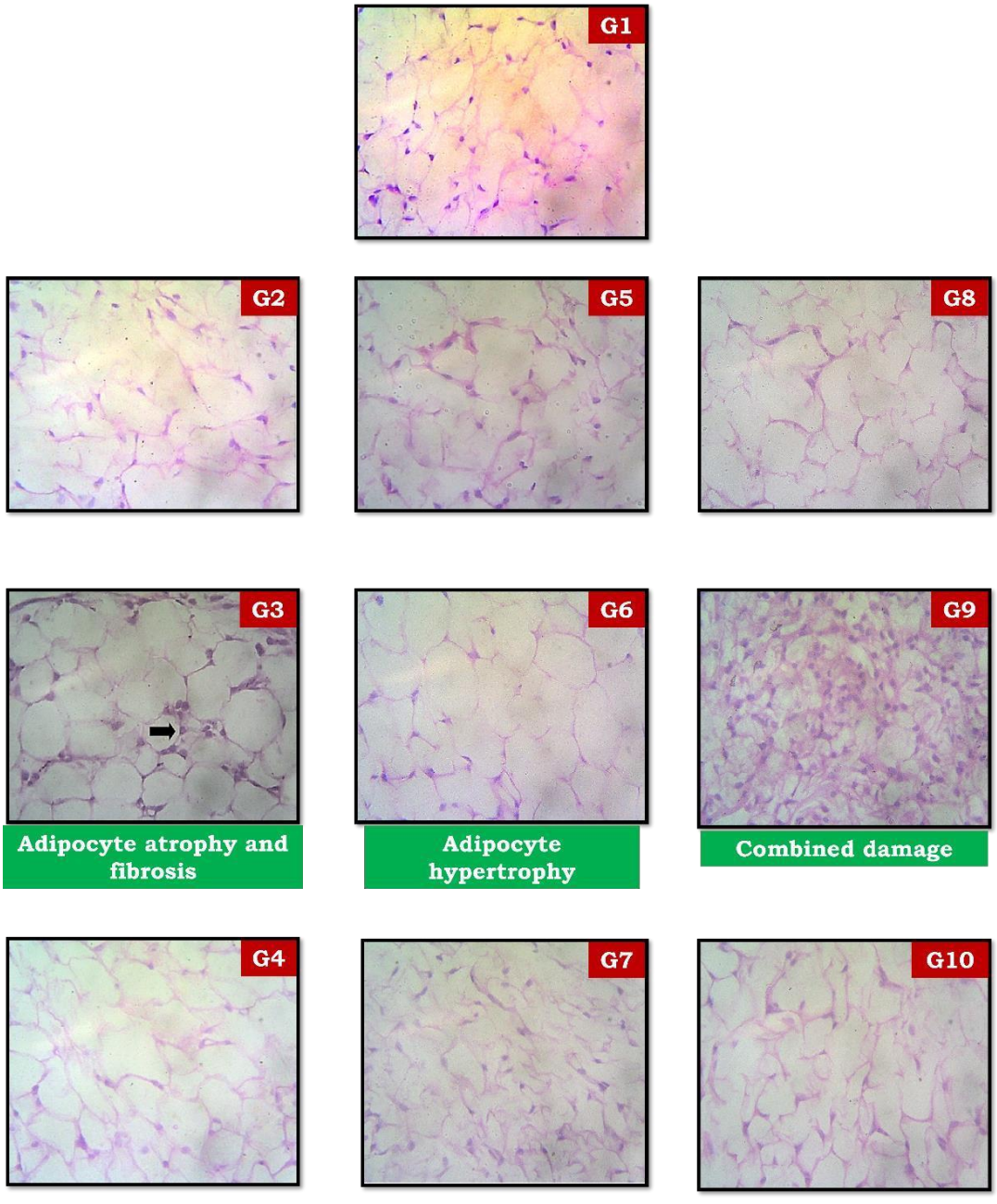

G1 Control	**G2 EBdAgNPs**	**G3 STZ-NI induced**
G4 STZ-NI + EBdAgNPs	**G5 STZ-NI + Glibenclamide**	**G6 HFD-induced**
G7 HFD + EBdAgNPs	**G8 HFD + Sibutramine**	**G9 STZ-NI + HFD**
G10 STZ-NI + HFD + EBdAgNPs		

In both the control group (G1) and the EBdAgNPs-alone group (G2), adipose tissue exhibited intact histological architecture. The adipocytes were polygonal with clear cytoplasm and peripherally displaced nuclei and there were no signs of inflammation, stromal edema or vascular congestion. The similarity between G1 and G2 indicates that EBdAgNPs do not induce cytotoxic effects in healthy adipose tissue and maintain tissue homeostasis. This observation supports the biocompatibility of *B. diffusa* derived silver nanoparticles and aligns with prior studies highlighting the safe use of phyto mediated nanoparticles in normal tissues. (Shang *et al*., 2021). The comparative analysis of G1 and G2 confirms that EBdAgNPs alone do not alter baseline adipose morphology.

STZ-NI-induced diabetic rats (G3) displayed mild focal inflammation within the stromal matrix of adipose tissue, reflecting early diabetic adipose pathology. STZ-mediated β-cell destruction triggers hyperglycemia, which promotes macrophage infiltration and cytokine upregulation in adipose tissue, leading to low-grade inflammation (Harrell *et al*., 2022). In contrast, diabetic rats treated with EBdAgNPs (G4) exhibited normal adipose histology with well-preserved adipocytes and no inflammatory infiltrates, indicating a reversal of STZ-induced adipose damage. Similarly, glibenclamide treated rats (G5) showed comparable improvements, though the effect is primarily mediated through insulin enhancing action and glycemic control. Comparative evaluation between G3, G4 and G5 demonstrates that EBdAgNPs (G4) not only normalize adipocyte morphology but may also directly suppress inflammation via antioxidative and anti-inflammatory mechanisms intrinsic to *B. diffusa* constituents (Teodoro *et al*., 2019).

High fat diet fed rats (G6) showed mild stromal inflammation and slightly enlarged adipocytes, characteristic of HFD-induced adipose tissue stress. Chronic lipid overload leads to adipocyte hypertrophy, increased reactive oxygen species and infiltration of pro-inflammatory macrophages, setting the stage for insulin resistance (Puschel *et al*., 2022). Administration of EBdAgNPs in HFD-fed rats (G7) preserved normal adipocyte morphology and completely prevented inflammatory infiltration, indicating robust protective effects of EBdAgNPs against lipid-induced oxidative and inflammatory stress. Sibutramine-treated rats (G8) also showed preserved adipose architecture, but EBdAgNPs appear to confer additional molecular protection through

ROS scavenging and modulation of adipose inflammation (Lazzaroni *et al*., 2021). The comparison among G6, G7 and G8 underscores that EBdAgNPs can be as effective, to standard pharmacological interventions in mitigating HFD-induced adipose damage.

In the obesediabetic group (G9), combining STZ-NI and HFD resulted in marked adipose tissue pathology, including significant stromal inflammatory infiltrates and mild vascular congestion. The dual metabolic insult synergistically exacerbates oxidative stress and lipotoxicity, promoting systemic insulin resistance and heightened inflammatory signaling (Cavaliere *et al*., 2023). Remarkably, EBdAgNP treatment in the corresponding group (G10) preserved adipocyte morphology and completely prevented inflammation. This indicates that EBdAgNPs are highly effective in protecting adipose tissue even under compounded metabolic stress, likely through a combination of antioxidative effects, inhibition of NF-κB mediated inflammatory pathways and restoration of cellular homeostasis. Comparative evaluation between G9 and G10 highlights the therapeutic potential of EBdAgNPs in managing adipose tissue injury in obesediabetic conditions, reinforcing the role of *B. diffusa* phytochemicals in mediating tissue resilience (Chen *et al*., 2022).

PHASE IV

4.4 Gene Expression of PPAR-alpha, PPAR-gamma and RBP4 in Experimental Rats

The study was expanded to examine molecular reactions using gene expression profiling after the *in vivo* evaluation of EBdAgNPs in diabetic and obese mice was completed. The first phase showed significant enhancements in metabolic markers like plasma insulin, CRP, antioxidant enzyme activity and tissue structure after administration of EBdAgNPs. These observations led to further exploration of the genetic pathways that might be influenced by the treatment. Consistent with this, tissue samples were collected for molecular studies of pancreatic tissue from diabetic models to assess genes involved in insulin secretion and β-cell function and adipose tissue from obese models to analyze genes involved in lipid metabolism and inflammatory status (Zatterale *et al*., 2020). This shift to cellular rather than systemic level study is meant to set up the genetic foundation for the therapeutic effects seen in the *in vivo* phase.

Gene expression analysis provides a robust tool to explain the modes of action by which EBdAgNPs achieve their metabolic advantages. In diabetic pathologies, the pancreas is the chief location of insulin biosynthesis and secretion and, therefore, is important in evaluating the expression of genes like PPAR-α, PPAR-γ and RBP4, which have imperative roles to play in controlling insulin sensitivity, glucose homeostasis and lipid metabolism (Malodobra-Mazur *et al*., 2024). Similarly, adipose tissue acts not only as an energy reservoir but also as an active endocrine organ involved in inflammatory signaling and metabolic regulation. Therefore, analyzing gene expression in adipose tissue can help uncover how EBdAgNPs impact adipocyte functionality and systemic insulin response (Aruwa and Sabiu, 2024). All together, these molecular studies reinforce the biochemical and histological observations to provide a more harmonized picture of EBdAgNPs mechanism of action in polygenic metabolic disorders.

4.4.1 Target Gene Expression in the Pancreas of EBdAgNPs Treated Rats

Gene expression profiling offers insightful information regarding the molecular mechanisms of pancreatic dysfunction in diabetes. In the present work, we investigated the mRNA level of three important genes PPAR-α, PPAR-γ and RBP4 in the pancreatic tissues of STZ-NI-induced rats under different experimental conditions, such as the induction by STZ-NI and treatment with either a conventional antidiabetic medication or EBdAgNPs. These genes were chosen because of their established roles in lipid metabolism, insulin sensitivity and glucose homeostasis. The relative expression patterns provide mechanistic explanations of how the treatments can improve diabetes-associated pancreatic defects.

4.4.1.1 PPAR-α, PPAR-γ and RBP4 Expression in Experimental Rats

FIGURE 4.23

GENE EXPRESSION OF PPAR-α PPAR-γ AND RBP4 IN STZ-NI INDUCED RATS

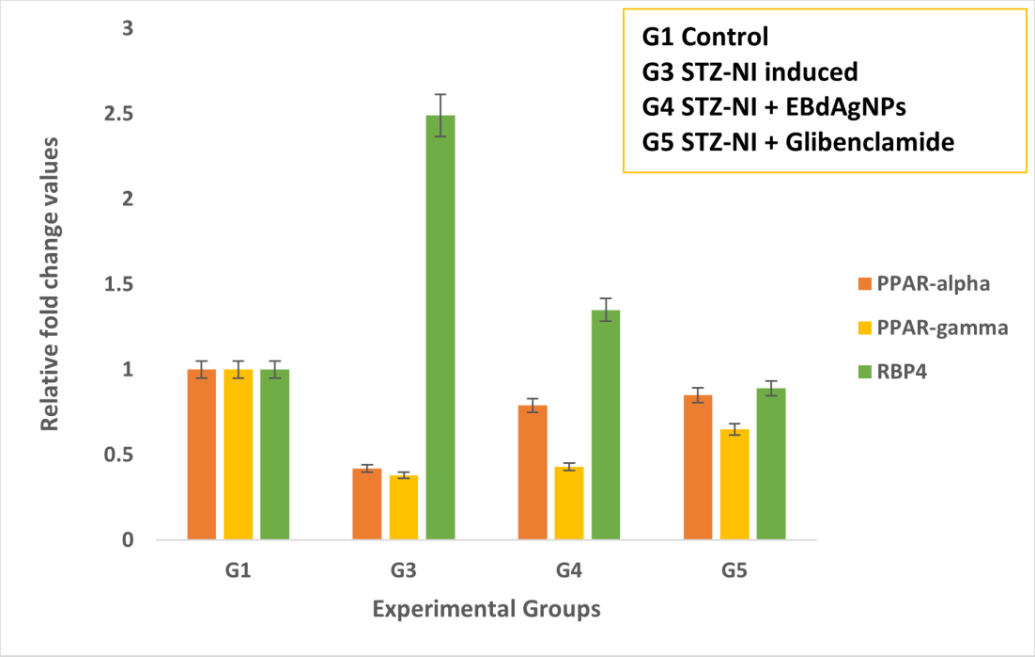

TABLE 4.10

OVERLAID FOLD CHANGE VALUES OF TARGET GENES IN PANCRETIC TISSUES OF STZ-NI INDUCED RATS

Target Gene	PPAR-alpha	PPAR-gamma	RBP4
G1 (Control)	1.0 ± 0.17	1.0 ± 0.22	1.0 ± 0.41
G3 (STZ-NI)	0.42 ± 0.23	0.38 ± 0.16	2.49 ± 0.43
G4 (STZ-NI + EBdAgNPs)	0.79 ± 0.23	0.43 ± 0.23	1.35 ± 0.41
G5 (STZ-NI + Glibenclamide)	0.85 ± 0.19	0.65 ± 0.18	0.89 ± 0.40

Relative fold change values of PPAR-α, PPAR-γ and RBP4 genes in control, STZ-NI, STZ-NI+extract-treated and STZ-NI+standard groups in pancreatic tissues of rats. Values represent the mean ± SD from three independent experiments (N = 3).

Figure 4.23 and table 4.10 present the relative fold change values of PPAR-α, PPAR-γ and RBP4 genes in control, STZ-NI alone, STZ-NI with standard treatment and STZ-NI with extract treatment groups, measured in pancreas tissues of rats using the RT-qPCR method. The data show that PPAR-α gene expression in pancreatic tissues was significantly reduced in the STZ-NI alone treated group G3 as 0.42 ± 0.23 compared to the control group G1 as 1.0 ± 0.17. This comparison clearly shows that diabetic induction in G3 results in more than a 50 percent reduction in PPAR-α levels relative to the normal metabolic profile seen in G1, indicating marked impairment in lipid oxidation pathways. In contrast, both the EBdAgNPs extract treatment (G4 (0.79 ± 0.23) and standard antidiabetic treatment G5 (0.85 ± 0.19) restored PPAR-α expression close to control levels and when comparing these treatment groups with G3, both G4 and G5 demonstrate substantial recovery of PPAR-α transcription, indicating reversal of the STZ-NI induced suppression. This suggests a potential role in alleviating STZ-NI-induced pancreatic dysfunction.

PPAR-α plays a critical role in fatty acid oxidation, lipoprotein metabolism and energy homeostasis (Tahri-Joutey *et al*., 2021). Within pancreatic β-cells, PPAR-α stimulation regulates intracellular lipid content, thereby protecting against lipotoxicity that worsens insulin resistance. The suppression of PPAR-α in G3 could be attributed to oxidative stress and impaired mitochondrial β-oxidation caused by hyperglycemia, whereas the upregulation observed in G4 and G5 indicates activation of lipid catabolism and improved β-cell function. This effect is more pronounced in the plant silver nanoparticle conjugate

group, which may enhance nuclear receptor binding affinity and transcriptional regulation. Similar findings have been reported in studies showing that natural antioxidants and nanoparticle preparations enhance nuclear receptor activity of PPARs (Sengani *et al*., 2022). In G4, the increased expression may be linked to *B. diffusa* phytoconstituents stimulating AMP-activated protein kinase (AMPK) signaling, which in turn boosts PPAR-α transcription (Enayati *et al*., 2022).

For PPAR-γ, the STZ-NI treated diabetic group (G3) showed significant downregulation (0.38 ± 0.16) relative to the control (1.0 ± 0.22). A direct comparison between G1 and G3 clearly demonstrates that STZ-NI administration leads to an approximately 60 percent reduction in PPAR-γ expression, reflecting severe disruption of adipogenesis and glucose uptake pathways compared to the normal control state in G1. Meanwhile, the EBdAgNPs treatment (G4) and standard drug (G5) demonstrated partial recovery of expression (0.43 ± 0.23 and 0.65 ± 0.18, respectively). When compared with G3, both G4 and G5 show marked improvement, with G5 demonstrating stronger recovery than G4, indicating differential efficacy of the two treatments in reversing the STZ-induced reduction. This downregulation in G3 reflects disrupted adipogenesis and glucose uptake pathways, a known consequence of STZ-induced insulin resistance (Sun *et al*., 2019).

PPAR-γ, an intracellular receptor, governs adipocyte differentiation and insulin function by promoting GLUT4 translocation and suppressing proinflammatory cytokines in insulin-sensitive tissues such as the pancreas (Passarelli and Machado, 2021). Adequate PPAR-γ expression is crucial for β-cell lipid homeostasis and insulin secretion. The marked reduction in G3 likely results from ROS accumulation and proinflammatory cytokine release following STZ-NI toxicity, both of which impair transcription. Partial restoration in G4 and G5 suggests recovery of transcriptional balance and insulin signaling via antioxidant and anti-inflammatory effects. Additionally, bioactive compounds from *B. diffusa* have been shown to activate PPAR-γ by modulating its ligand-binding domain, potentially contributing to the observed upregulation in G4 (Hoseinpoor *et al*., 2024). Silver nanoparticles may also enhance nuclear receptor activation and bioavailability. The synergy between phytochemicals and nanocarrier delivery systems could therefore provide a promising approach for reversing insulin resistance and restoring PPAR-γ activity in diabetic conditions.

RBP4 expression was markedly elevated in the STZ-NI alone group G3 (2.49 ± 0.43), approximately 2.5-fold higher than the control (1.0 ± 0.41). This comparison shows that the uncontrolled diabetic state in G3 exhibits a dramatic elevation in RBP4 expression compared with G1, indicating severe impairment of insulin signaling pathways. In contrast, the EBdAgNPs treatment G4 (1.35 ± 0.41) and standard treatment G5 (0.89 ± 0.40) resulted in notable downregulation. When comparing G3 with G4 and G5, both treatments clearly suppress the heightened RBP4 expression, with G5 reversing it to below control level and G4 reducing it substantially but not as strongly as G5.

These results suggest that hyperglycemia and insulin resistance significantly upregulate RBP4 expression, consistent with its role as an adipokine that impairs insulin signaling and enhances gluconeogenesis (Fan and Hu, 2024). Suppression of RBP4 in G4 and G5 demonstrates the potential of these interventions to counteract diabetic overexpression. Mechanistically, RBP4 interferes with insulin signaling by reducing phosphatidylinositol
3-kinase (PI3K) activity in muscle and increasing phosphoenolpyruvate carboxykinase (PEPCK) activity in pancreatic and liver tissues (Liu *et al*., 2022). STZ-NI-induced oxidative stress and β-cell destruction may activate retinol metabolism pathways, elevating RBP4 transcription. The downregulation observed with treatments may result from inhibition of the RA receptor or upstream enzymes such as retinaldehyde dehydrogenases, mediated by antioxidant or insulin-sensitizing compounds. Boeravinones, key phytoconstituents of *B. diffusa*, have been reported to reduce oxidative stress and normalize adipokine release (Dutta *et al*., 2022). In addition, silver nanoparticles can provide site-specific delivery, enhancing local anti-RA signaling bioactivity. This combined approach in G4 likely suppresses RBP4 overexpression by restoring metabolic balance, reducing inflammation and promoting insulin-mediated glucose uptake.

4.4.2 Assessment of Target Gene Expression in the Adipose Tissue of EBdAgNPs

Adipose tissue is essential in lipid metabolism, glucose homeostasis and systemic insulin sensitivity and is thus a target tissue in studies of obesity and type 2 diabetes. Gene expression profiling aimed at nuclear receptors such as the peroxisome proliferator activated receptors (PPARs) and metabolic indicators such as Retinol Binding Protein 4

(RBP4) yields crucial information regarding the molecular pathways governing adipogenesis and insulin resistance. This research measured the mRNA expression levels of PPAR-α, PPAR-γ and RBP4 in adipose tissue of rats with HFD and treatments involving either sibutramine or EBdAgNPs.

4.4.2.1 PPAR-α, PPAR-γ and RBP4 Expression in Experimental Rats

FIGURE 4.24

GENE EXPRESSION OF PPAR-α PPAR-γ AND RBP4 in HFD INDUCED RATS

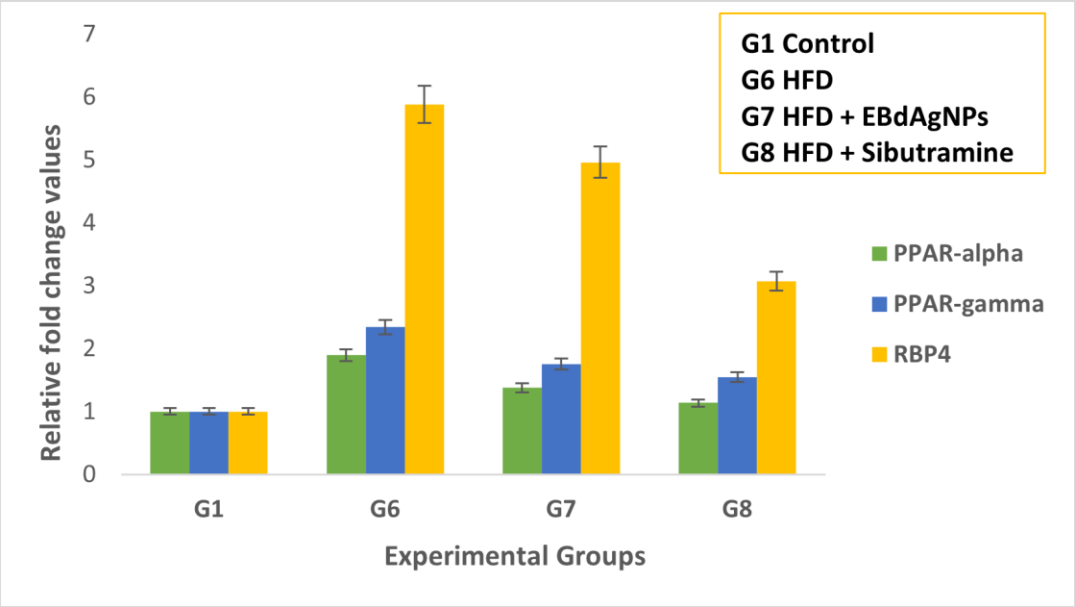

TABLE 4.11

OVERLAID FOLD CHANGE VALUES OF TARGET GENES IN ADIPOSE TISSUES OF HFD INDUCED RATS

TARGET GENE	PPAR-alpha	PPAR-gamma	RBP4
G1- Control	1 ± 0.05	1.0 ± 0.14	1.0 ± 0.38
G6 – HFD	1.90 ± 0.25	2.34 ± 0.06	5.88 ± 0.37
G7 – HFD+EBdAgNPs	1.38 ± 0.10	1.75 ± 0.04	4.96 ± 0.48
G8 – HFD+Sibutramine	1.14 ± 0.16	1.55 ± 0.14	3.07 ± 0.10

Relative fold change values of PPAR-α, PPAR-γ and RBP4 genes in control, HFD, HFD+ extract-treated and HFD+standard groups in rat adipose tissues determined by RT-qPCR. Values represent the mean ± SD from three independent experiments (N = 3).

Figure 4.24 and table 4.11 illustrates the variation in expression of PPAR-α among the groups was significant. G6 (HFD only) had highly increased expression (1.90 ± 0.25) over the control G1 (1 ± 0.05). This indicates that the adipose tissue of G6 shows a marked elevation when directly compared to G1, suggesting a strong lipid-overload response in HFD-fed rats. However, administration of EBdAgNPs G7 (1.38 ± 0.10) and sibutramine G8 (1.14 ± 0.16) reduced this expression toward levels seen in the control. When comparing G6 with the treatment groups, both G7 and G8 demonstrate a clear decline in PPAR-α expression, showing effective normalization following treatment.

PPAR-α is a transcription factor largely expressed in tissues with high mitochondrial β-oxidation activity, including the liver and brown adipose tissue. Its activation results in upregulation of genes responsible for fatty acid uptake and oxidation, thereby curbing lipid accumulation (Zheng and Cai, 2019). In rats fed HFD (G6), increased expression of PPAR-α might be a compensatory response to fat overfeeding by boosting lipid oxidation. Chronic activation, however, might interfere with the proper balance of lipids and cause metabolic dysregulation (Kakazu *et al*., 2025). Treatment with EBdAgNPs and sibutramine re-established PPAR-α levels to baseline, supporting normalization of lipid metabolic processes. EBdAgNPs may act on PPAR-α through bioactive phytochemicals present in *B. diffusa* that have been previously demonstrated to possess hypolipidemic activity (Atal *et al*., 2022). This concurs with the therapeutic goal of attenuating lipotoxicity in adipocytes and enhancing mitochondrial efficiency in lipid metabolism. Additionally, attenuated PPAR-α activation in treatment groups most likely indicates reduced fatty acid burden due to improved metabolic control and therefore less transcriptional activation required for oxidation-related genes, suggesting that both conventional (sibutramine) and novel (EBdAgNPs) treatments can alleviate adipose tissue stress via downregulation of PPAR-α-mediated pathways (Annunziata *et al*., 2022).

The expression of PPAR-γ gene followed a similar trend, as there was a very significant increase in G6 (2.34 ± 0.06) relative to G1 (1 ± 0.14). This comparison clearly shows that G6 exhibits more than double the expression observed in the control group, reflecting heightened adipogenic drive in the obese condition. This overexpression was significantly lowered in G7 (1.75 ± 0.04) and G8 (1.55 ± 0.14). A comparison between

G6 and the two treatment groups reveals that both interventions markedly reduce the elevated PPAR-γ expression, indicating a therapeutic reversal of adipogenesis activation.

PPAR-γ is the master regulator of adipogenesis and plays a major role in enhancing insulin sensitivity through regulation of glucose uptake-associated gene transcription, including GLUT4 (Chait and Hartigh, 2020). The increase in PPAR-γ observed in the obese phenotype (G6) corresponds with enhanced adipocyte differentiation, lipid storage, hypertrophic expansion of adipose tissue and systemic insulin resistance (Mohajan and Mohajan, 2024). The marked drop in PPAR-γ expression following EBdAgNPs treatment (G7) indicates the anti-adipogenic potential of the extract, supported by research showing that *B. diffusa* compounds can suppress adipogenesis and induce lipolysis (Sung *et al*., 2020). Similarly, sibutramine (G8) alleviated PPAR-γ overexpression, consistent with its known mechanism of reducing body fat via enhancement of central satiety and increased energy expenditure (Kounatidis *et al*., 2025). Modulation of this gene implies that both treatments may enhance insulin sensitivity by repressing excess adipogenic signaling, a key step in disrupting the cycle of inflammation, lipotoxicity and insulin resistance commonly seen in HFD-induced obesity (Wen *et al*., 2022). Downregulation of PPAR-γ would also lower pro-inflammatory cytokine production and improve adipose tissue structure.

Expression of RBP4 was most significantly increased in G6 (5.88 ± 0.37), with control G1 showing much lower expression (1 ± 0.38). A direct comparison indicates that G6 displays an exceptionally elevated RBP4 level, highlighting severe metabolic disturbance relative to G1. This expression was substantially downregulated in G7 (4.96 ± 0.48) and G8 (3.07 ± 0.10). When comparing G6 with these treatment groups, both show marked reductions, although EBdAgNPs (G7) demonstrates partial suppression compared to the stronger reduction observed in sibutramine (G8).

RBP4, an adipokine-secreted and liver-secreted hepatokine, is a well-known mediator of insulin resistance, diminishing insulin signaling by inhibiting PI3K activity and stimulating gluconeogenesis through PEPCK upregulation, thereby exacerbating hyperglycemia (Ren *et al*., 2022). The excessive RBP4 increase in HFD-fed rats reinforces its role in metabolic dysregulation and adipocyte dysfunction. Both

sibutramine and EBdAgNPs significantly suppressed RBP4 expression, although EBdAgNPs-treated rats (G7) retained slightly higher levels than sibutramine, indicating partial protection. The polyphenolic constituents in *B. diffusa* may downregulate RBP4 by enhancing antioxidant status, reducing adipose inflammation and indirectly normalizing insulin signaling (Dzitoyeva, 2024). Furthermore, HFD-induced oxidative stress and chronic inflammation can increase RBP4 expression via ROS-sensitive transcription factors like NF-κB, which may be modulated by the antioxidant effect of EBdAgNPs (Kumar *et al*., 2022). Overall, the suppression of RBP4 expression aligns with the antidiabetic potential of EBdAgNPs in improving glucose homeostasis and reducing insulin resistance.